PAUL SCHERRER INSTITUT

Andreas Suter :: Paul Scherrer Institute

Low Energy μSR, Thin Films and Interfaces

Muon Advanced School 2019

Acknowledgments

LEM-Team:

Thomas Prokscha (Head)
Zaher Salman
Andreas Suter
Hans-Peter Weber (Technician)

Elvezio Morenzoni (Head until 2008)

Contributors:

Ted Forgan (Moderator Cryo, LowTemp insert)

Initial Financial Support (muE4 Beamline, and LEM setup)

BMBF (via the Technical University of Braunschweig (J. Litterst) and the University of Konstanz (G. Schatz)), the UK EPSRC (via the University of Birmingham (T. Forgan)), and from the University of Zurich (H. Keller) and the Leiden University (G. J. Nieuwenhuys)

PAUL SCHERRER INSTITUT PSI

Outline

- **Low Energy Muons Basics**
  - PSI Overview
  - Low Energy μ^+ Production
  - Low Energy μ^+ Spectrometer at PSI
  - Implantation of Low Energy μ^+ in Matter – Stopping Profiles

- **Applications of Low Energy μ^+ – LE-µSR, Thin Films and Interfaces**
  - Semiconductors & Insulators
  - Magnetism
  - Superconductivity
  - Polymer Physics
  - Particle Physics Aspects

Paul Scherrer Institut

← Basel   Germany ↑   Aarau/Bern ↓   Zürich →

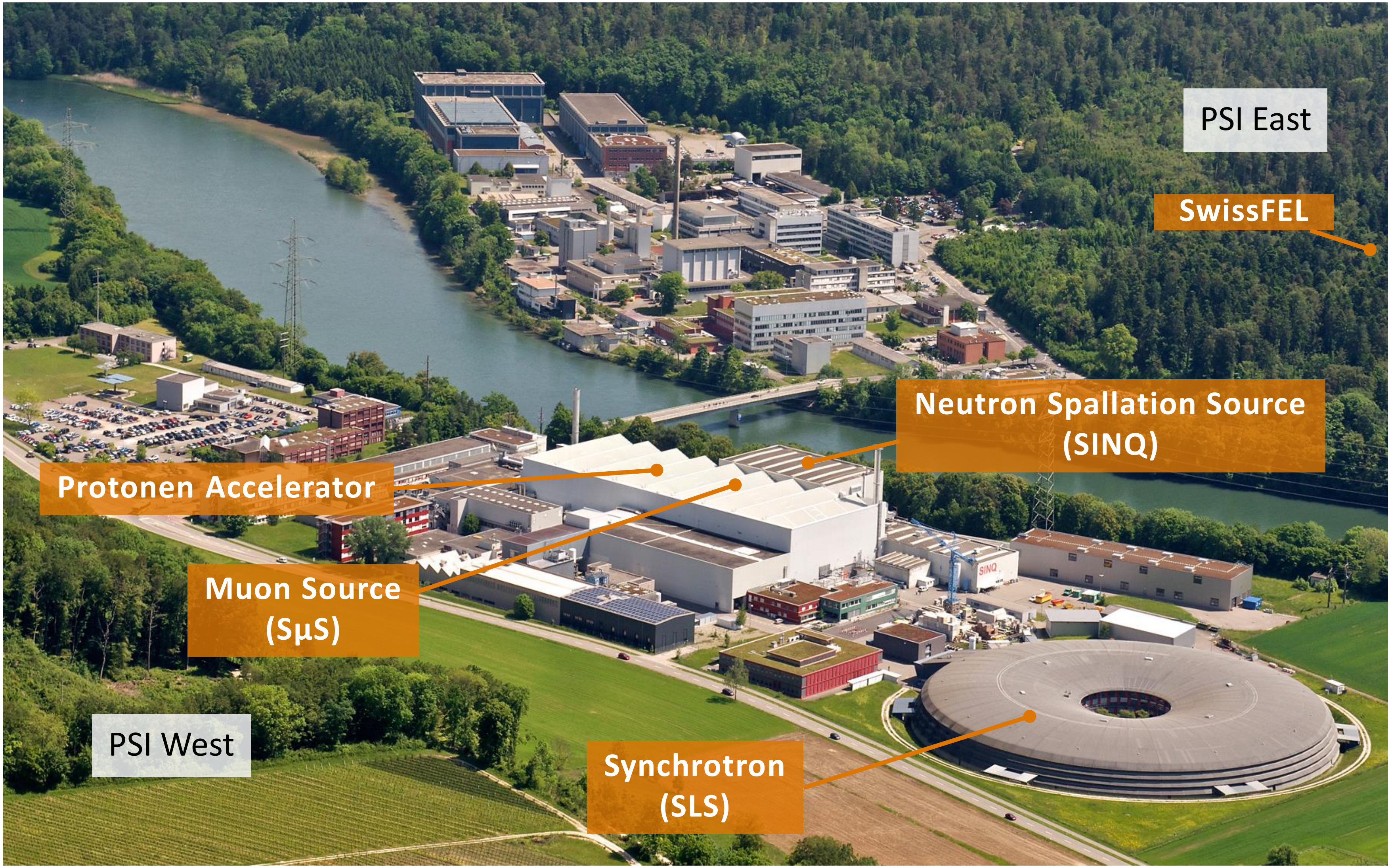

Large-Scale Project SwissFEL

Proton Accelerator (Overview)

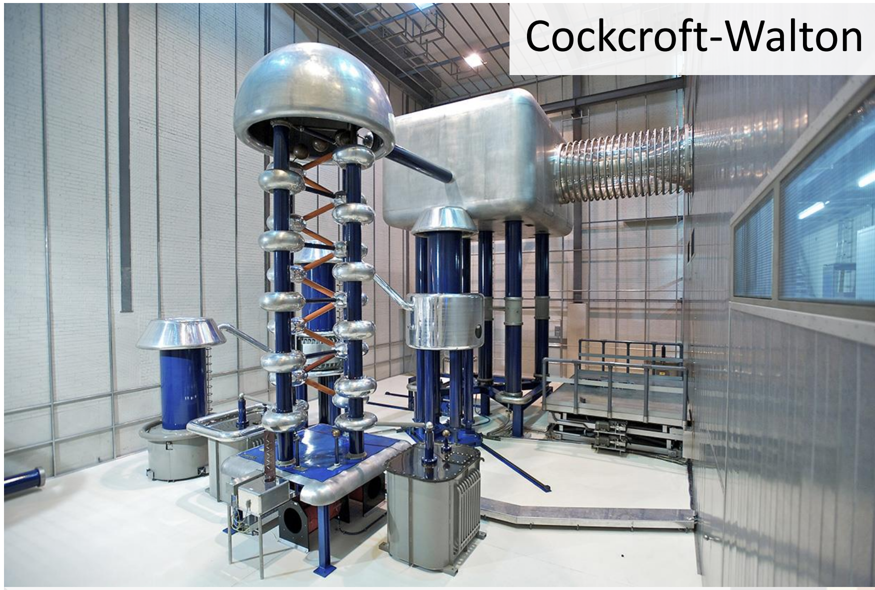

A proton energy of 870 keV is obtained from the 60 keV extraction voltage at the ion source and the 810 keV DC acceleration of the Cockcroft-Walton accelerator

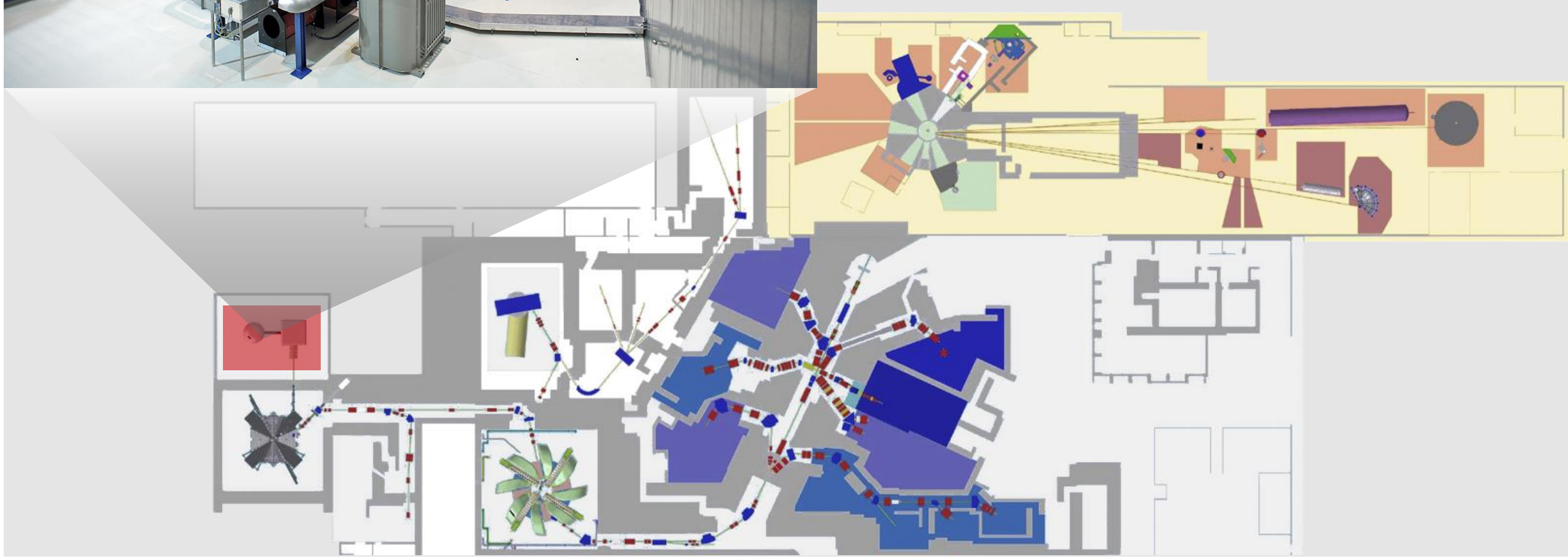

Proton Accelerator (Overview)

Injektor 2 (1st Cylcotron)

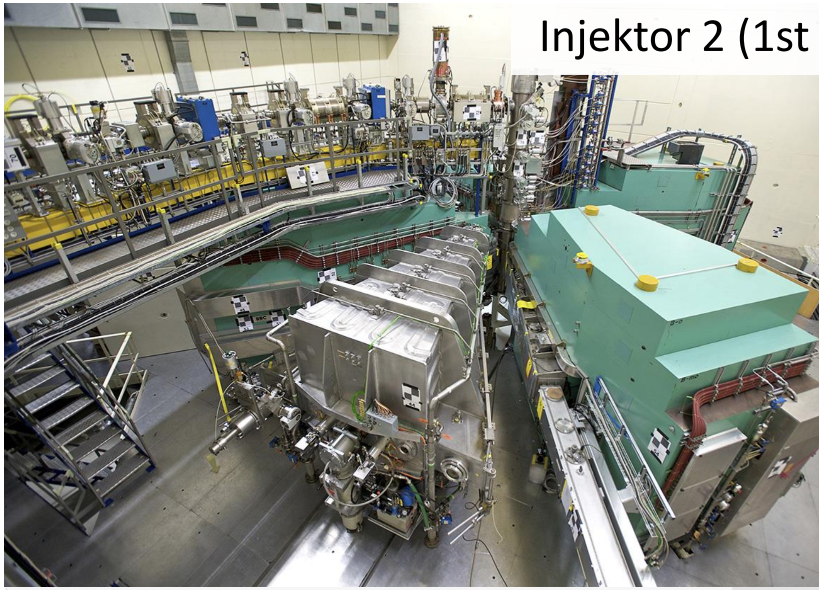

Injection Energy	870 keV (4.3% of light speed)
Extraction Energy	72 MeV (37.1% of light speed)
Energy spread (FWHM)	ca. 0.2 %
Beam Emittance	ca. 2 pi mm x mrad
Beam Current	2.5 mA DC
Accelerator Frequency	50.63 MHz
Time Between Pulses	19.75 ns
Bunch Width	ca. 0.3 ns
Magneticfield (Stiffness T x m, middle)	0.36 (1.25, 0.33 T)
Mass of Sektor Magnets	4 x 180.000 kg
Radius at Injection	400 mm
Radius at Extraction	3500 mm
Mass of Resonators	3 x 5.000 kg + 1 x 3.000 kg

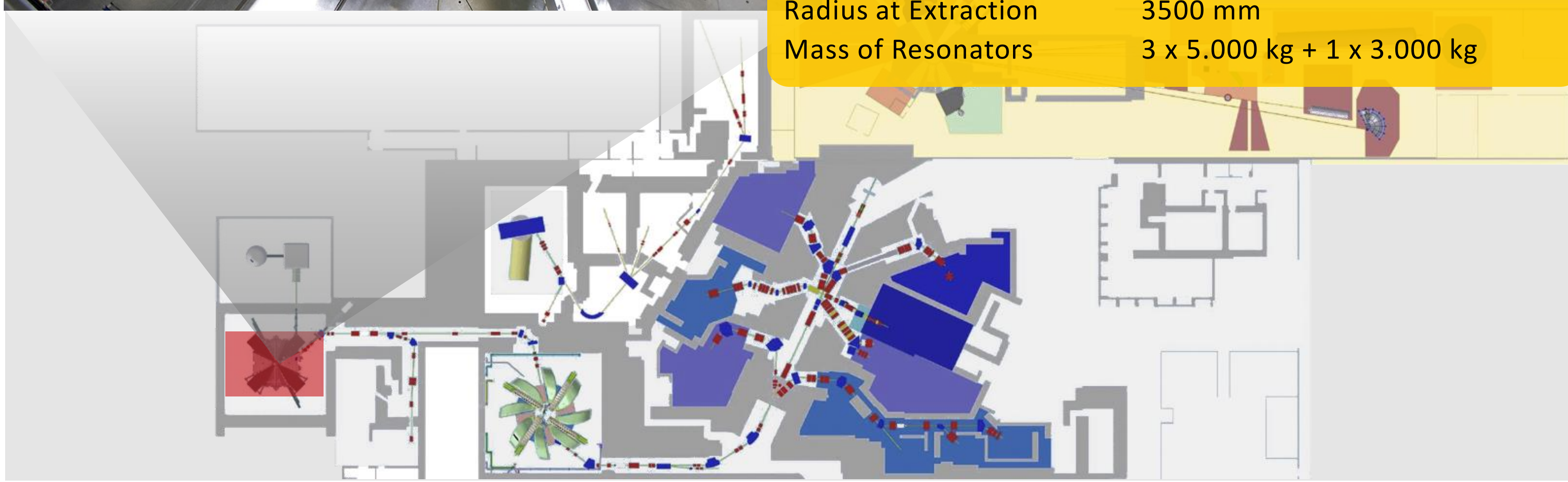

Proton Accelerator (Overview)

Main Cyclotron

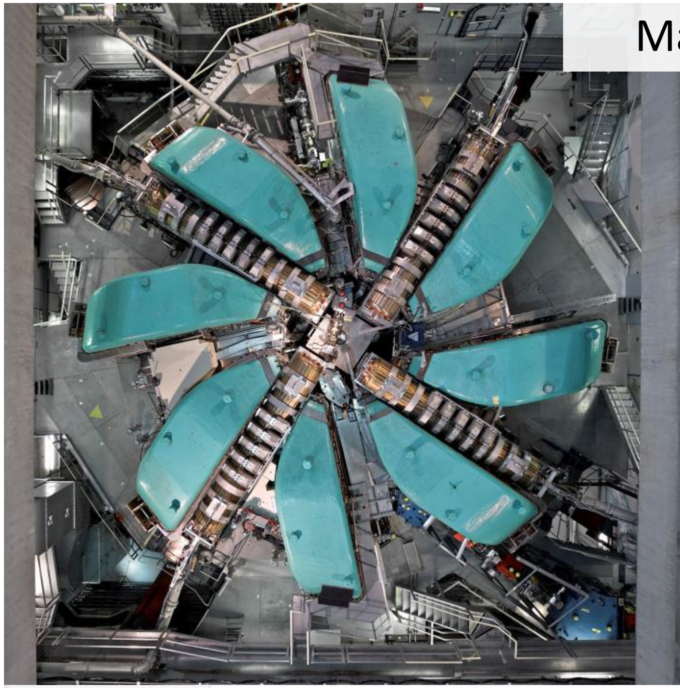

Injection Energy	72 MeV
Extraction Energy	590 MeV
Extraction Momentum	1.2 Gev/c
Energy spread (FWHM)	ca. 0.2 %
Beam Emittance	ca. 2 pi mm x mrad
Beam Current	2.2 mA DC
Accelerator Frequency	50.63 MHz
Time Between Pulses	19.75 ns
Bunch Width	ca. 0.3 ns
Extraction Losses	ca. 0.03 %

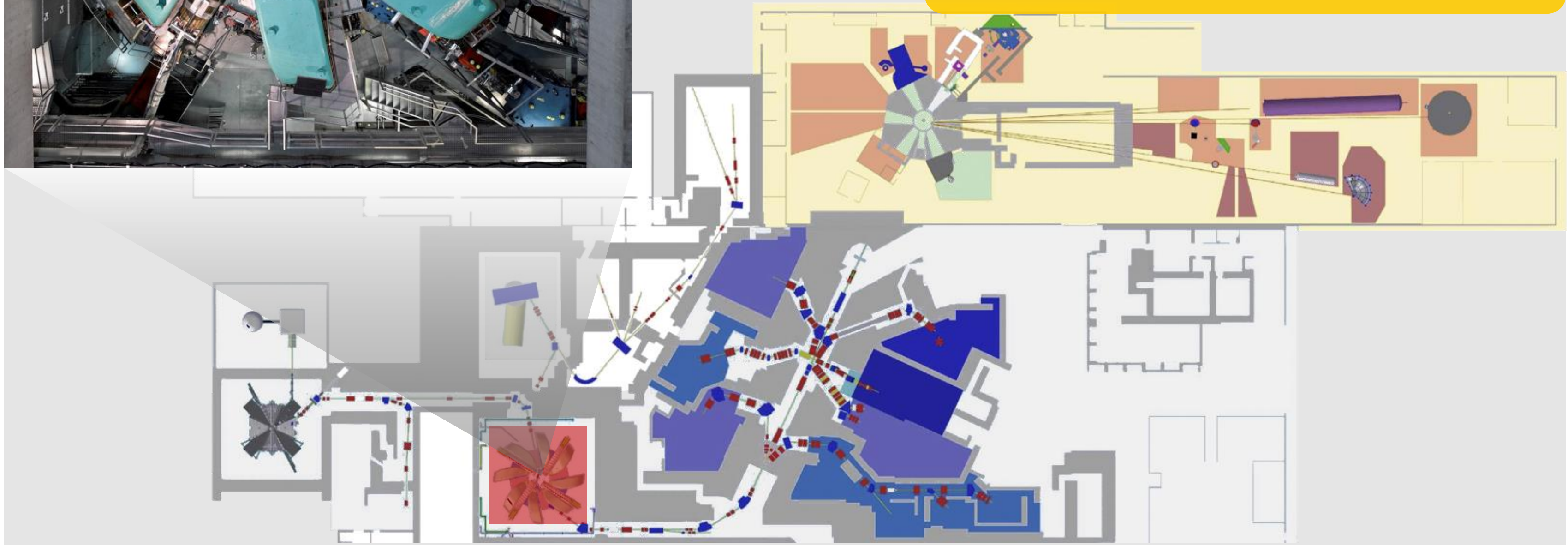

Beam Power of Accelerators World Wide

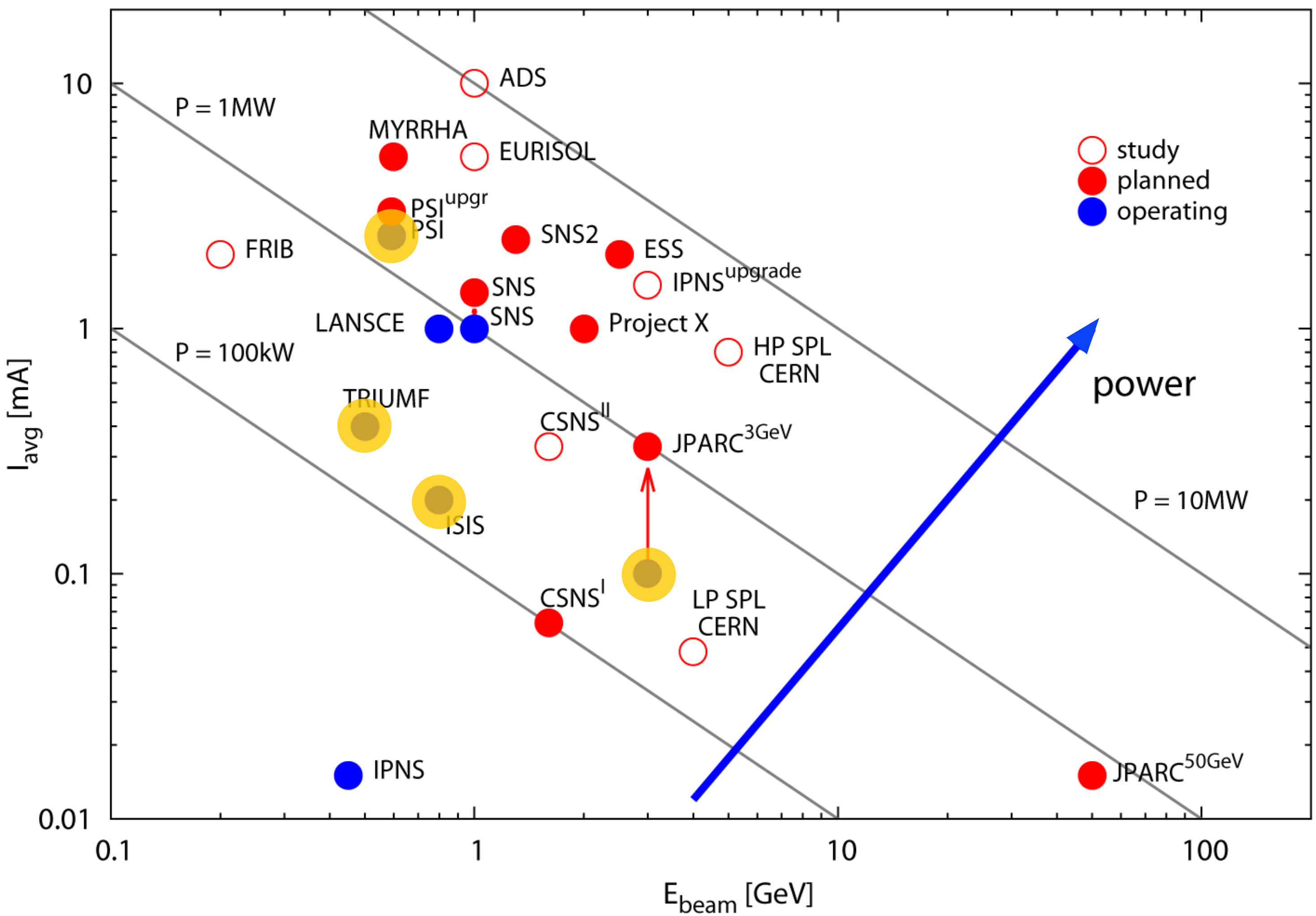

PSI

Proton Accelerator (Overview)

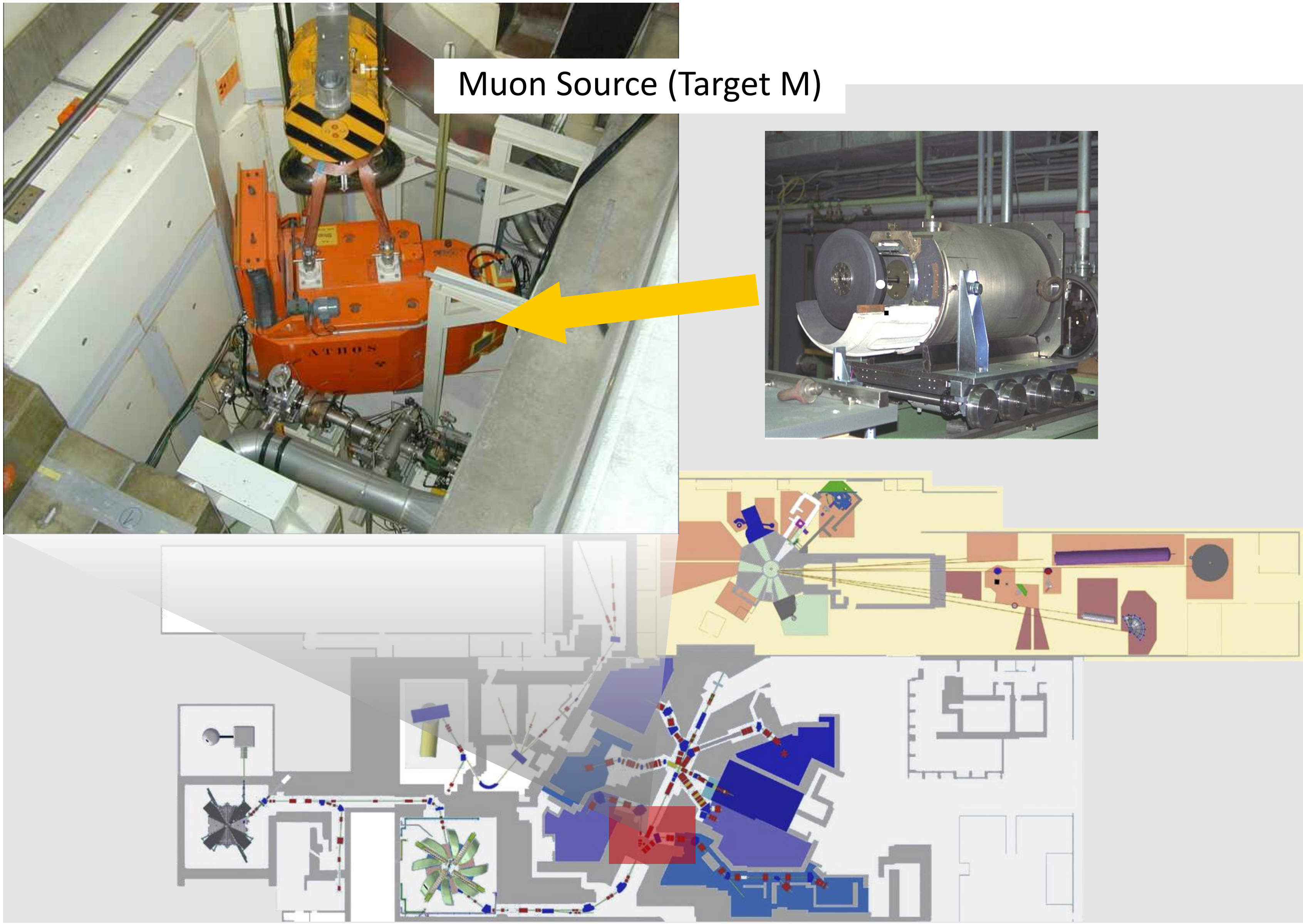

PAUL SCHERRER INSTITUT

Proton Accelerator (Overview)

Muon Source (Target E)

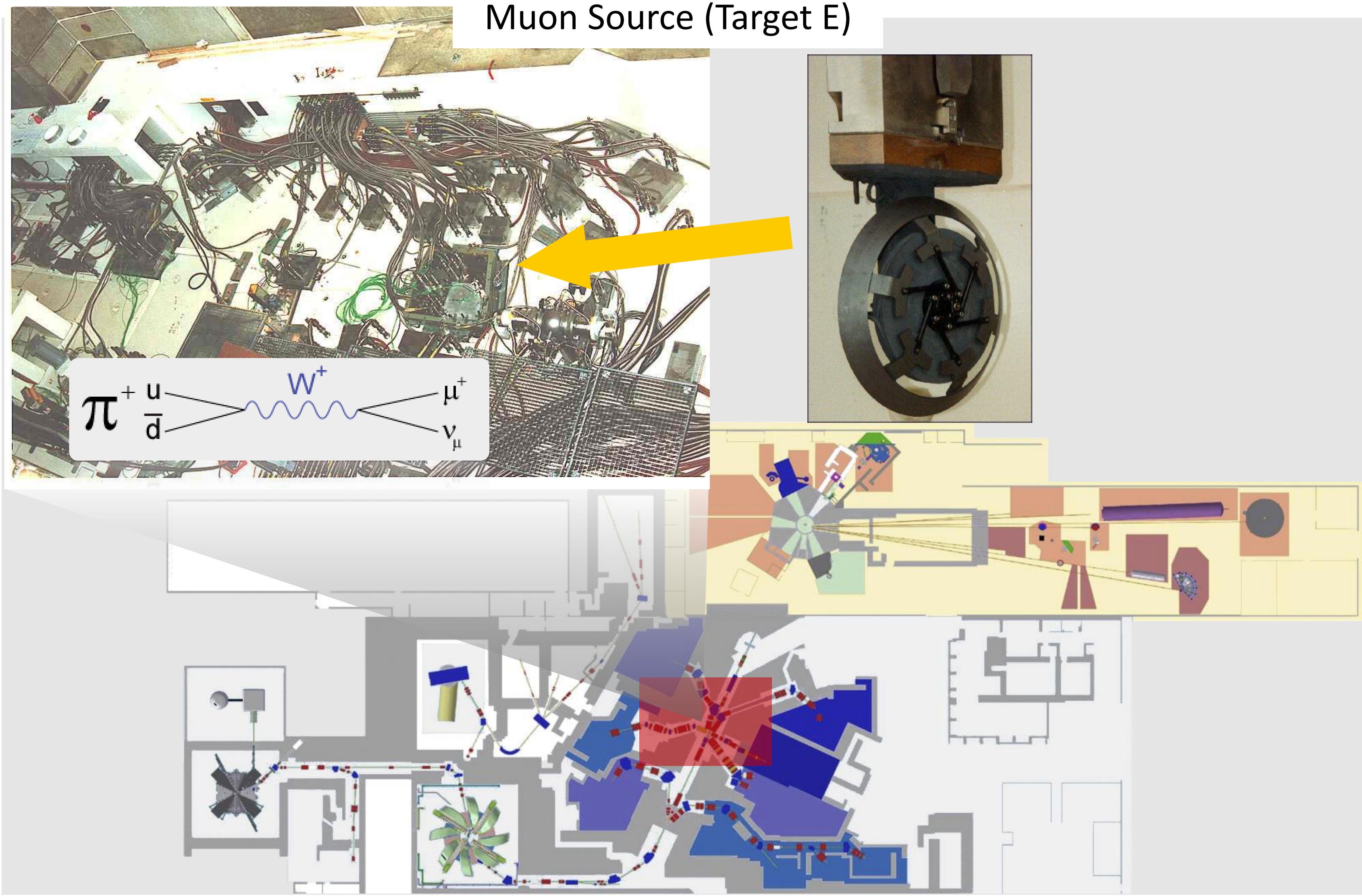

PAUL SCHERRER INSTITUT

Proton Accelerator (Overview)

Neutron Spalation Source (SINQ)

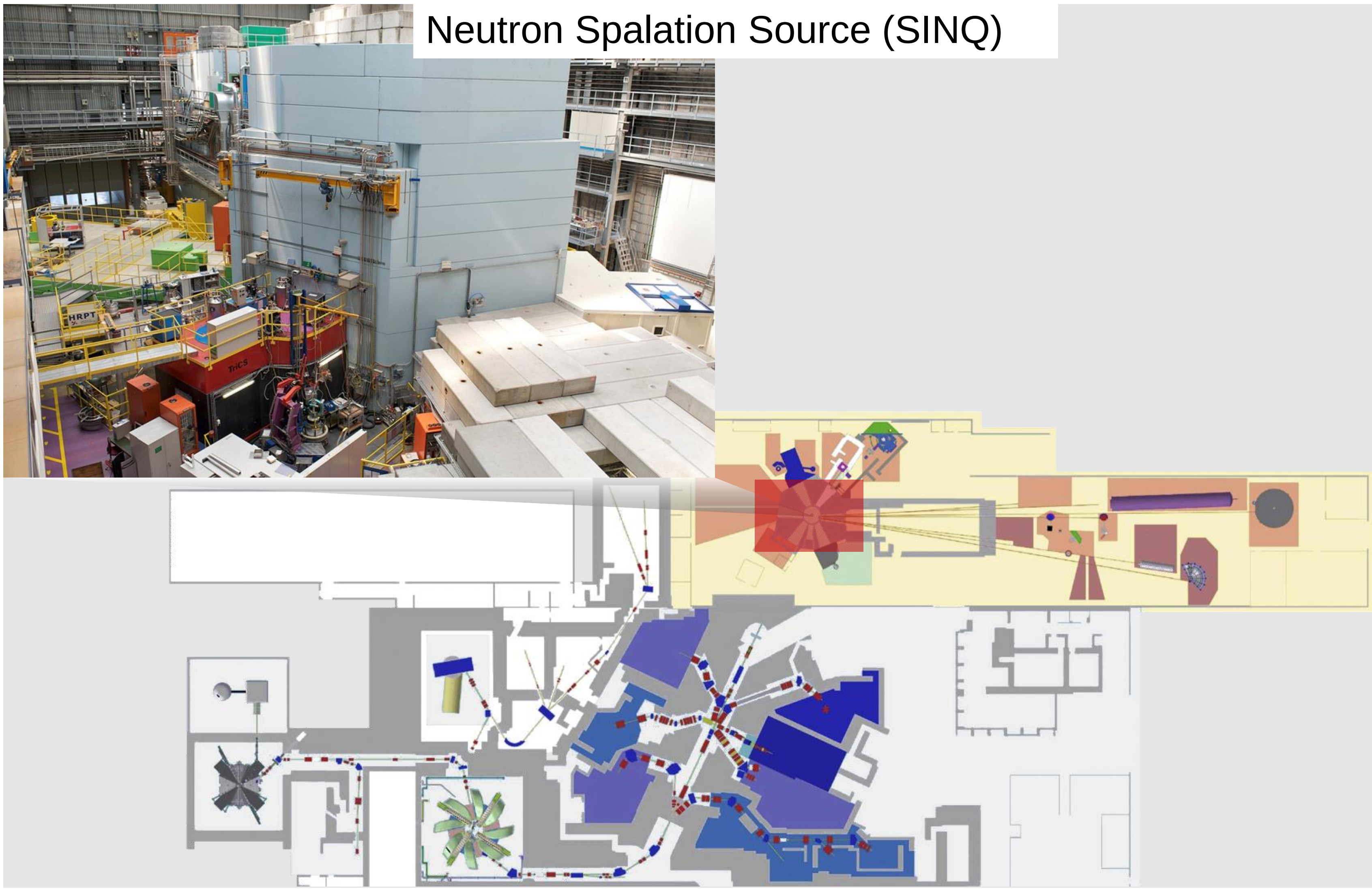

Muon Instruments at PSI:
SμS (Swiss Muon Source)

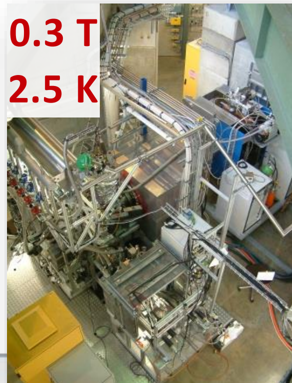

0.3 T
2.5 K

LEM

Low Energy Muon Instrument

Muon Energy: **0.5-30 keV**

0.5 T
0.25 K

DOLLY

Muon Energy: **4.2 MeV** (μ^+)

GPD

General Purpose Decay Channel Instrument (for Pressure Studies)

Muon Energy: **5-60 MeV** (μ^+/ μ^-)

0.5 T
0.3 K
2.8 GPa

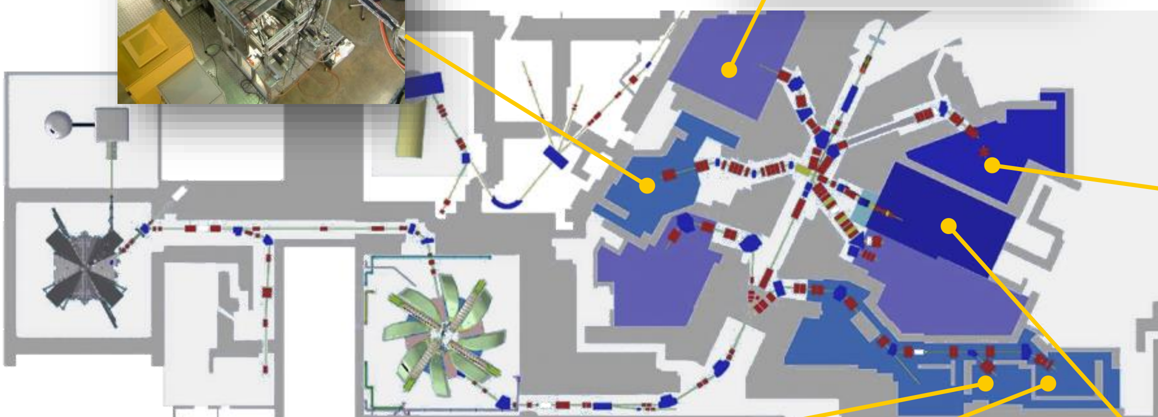

HAL-9500

High Field and Low Temperature

9.5 T
< 20mK

GPS

General Purpose Surface Muon Instrument

Shared Surface Muon Beam
Muon on Request (MORE)
Muon Energy: **4.2 MeV** (μ^+)

0.6 T
1.6 K

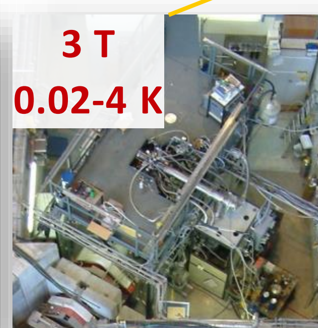

3 T
0.02-4 K

LTF

Low Temperature Facility
Retired Dec. 2018
Will be replaced by FLAME in 2021

Muon Production – Example: Target E at PSI

- Rotating Graphite Target (1 Hz)
- Radiation Cooled, T_{avg} = 1700K
- Thickness t=40 mm; h=6 mm; ∅ 450 mm
- Radiation Losses 30%

$p + C \rightarrow \pi^{+} \pi^{-}$ p n ...

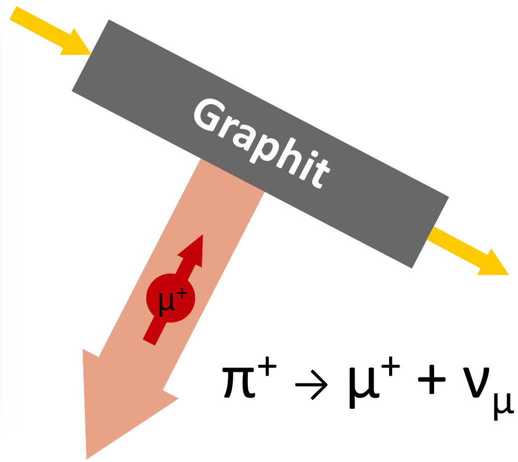

$\pi^{+} \rightarrow \mu^{+} + \nu_{\mu}$

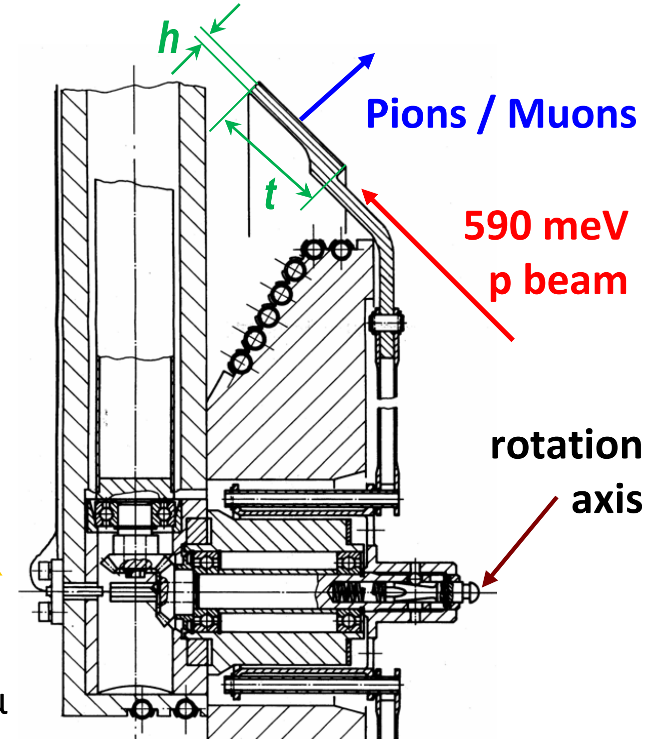

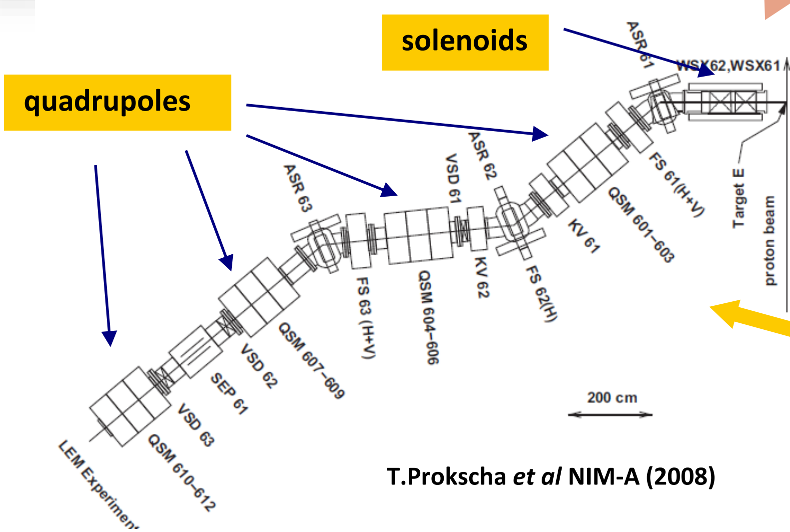

T.Prokscha *et al* NIM-A (2008)

2200 μA ≈ 1.4·10^{16} p/sec @ 590MeV →
≈ 10^{7} – 10^{8} μ^{+}/sec,
≈ 100% polarized
Surface Muons: ≈ 4 MeV

μE4 beamline at PSI: 4 · 10^{8} μ^{+}/sec

Different Muon Energies for Different Studies

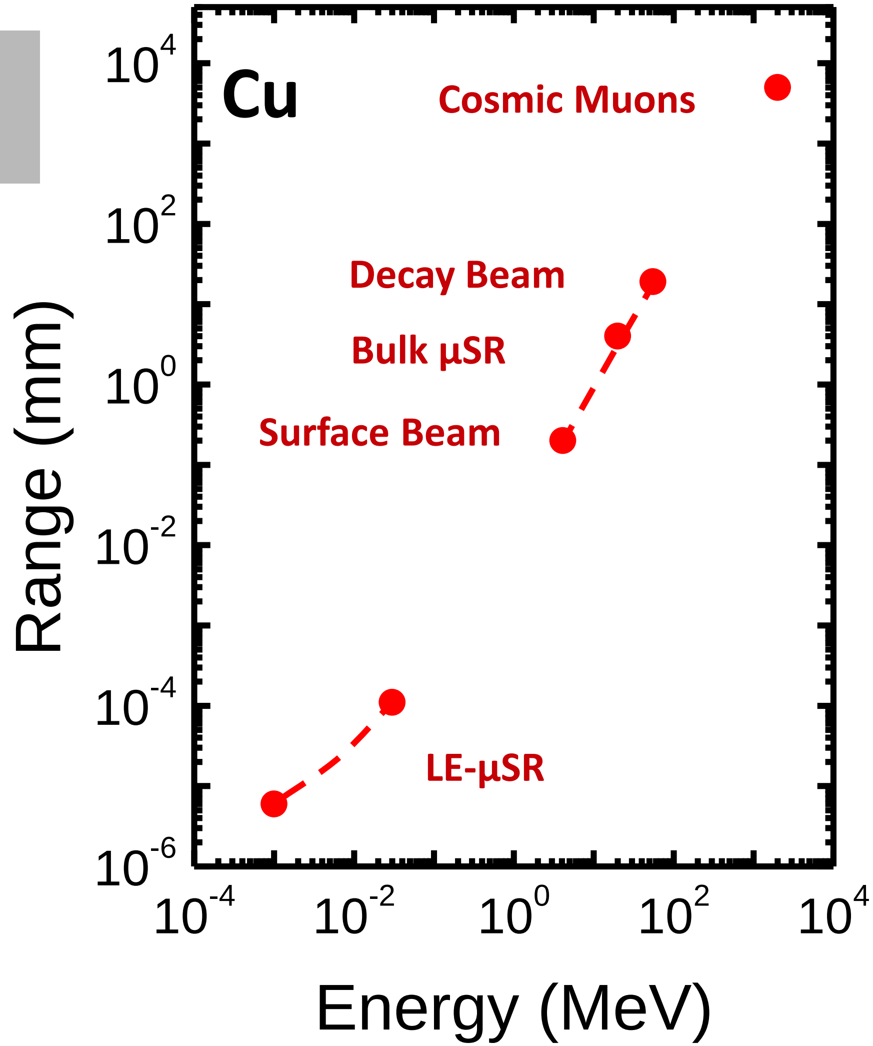

Bulk µSR:

- ''normal'' samples (sub-nm)
- bulk samples in pressure cells or containers (e.g. liquids)

LE-µSR:

- depth-dependent investigations (≈ 5 – 300nm)

Production of Low Energy μ^+ – First Attempts

- ~~By means of magnetic/electrical fields?~~

Not possible since the phase space (x,y,z,p_x,p_y,p_z) behaves like an incompressible liquid.

- Degrader approach, i.e. place material into a surface muon beam.

Highest low energy muon yield for LiF:
$\approx 10^{-7}$

Why is it so bad?
Can we do better?

YES!!
Otherwise I wouldn't be here

All Tragets at 150°C

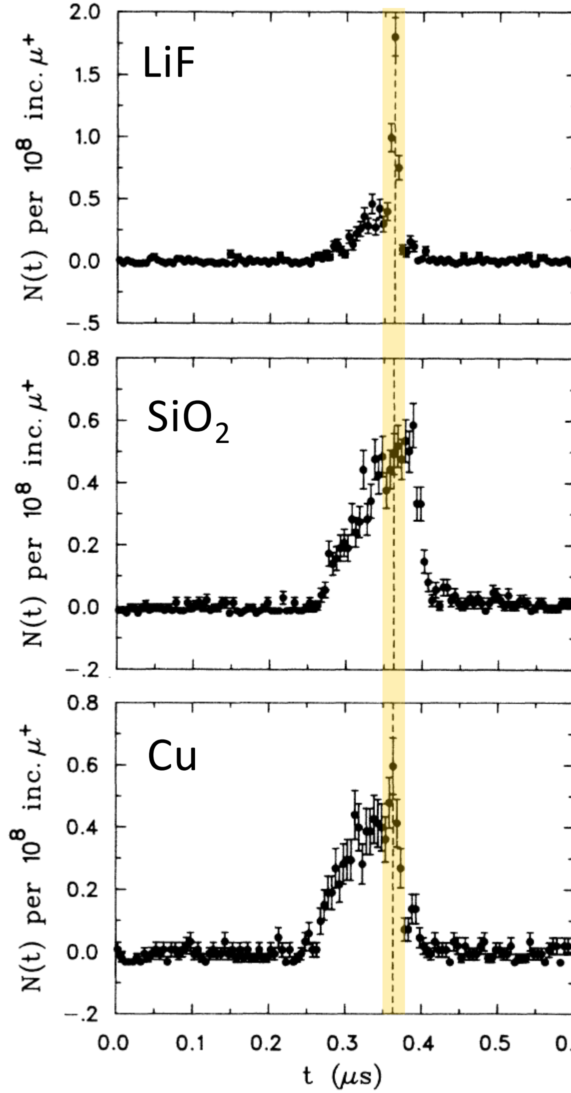

D.R. Harshman, *et al.* PRL **56**, 2850 (86).

Generation of Thermal μ^+ at a Pulsed Muon Beam
J-PARC (RIKEN-RAL)

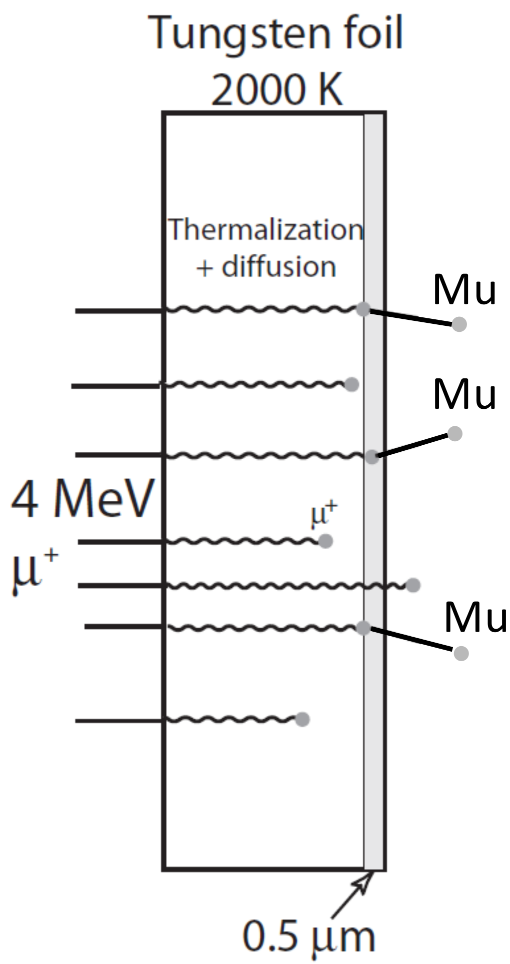

K. Nagamine, *et al.*, PRL **74**, 4811 (1995).
P. Bakule, *et al.*, Nucl. Instr Meth. B **266**, 335 (2008).

Generation of Thermal μ^+ at a Pulsed Muon Beam

J-PARC (RIKEN-RAL)

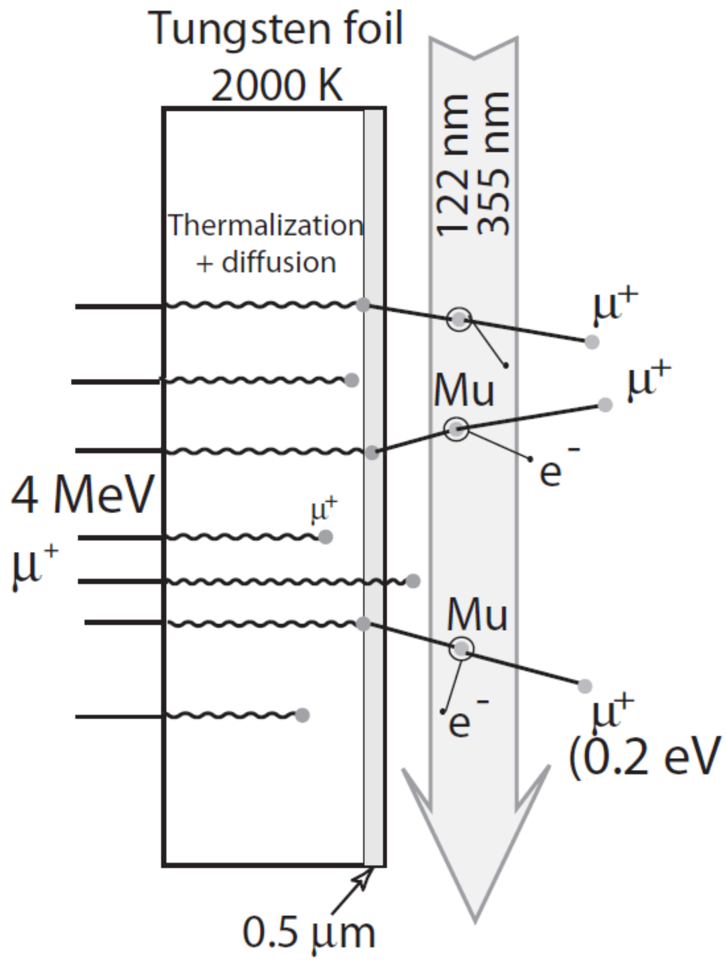

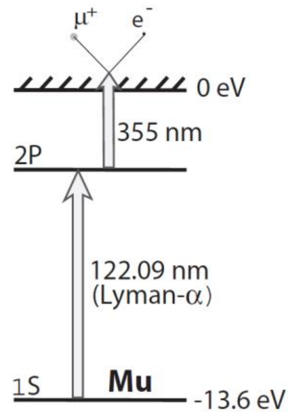

Advantage:

- high LE-μ^+ yield

Disadvantage:

- Only ½ of the asymmetry
- Tricky Laser system

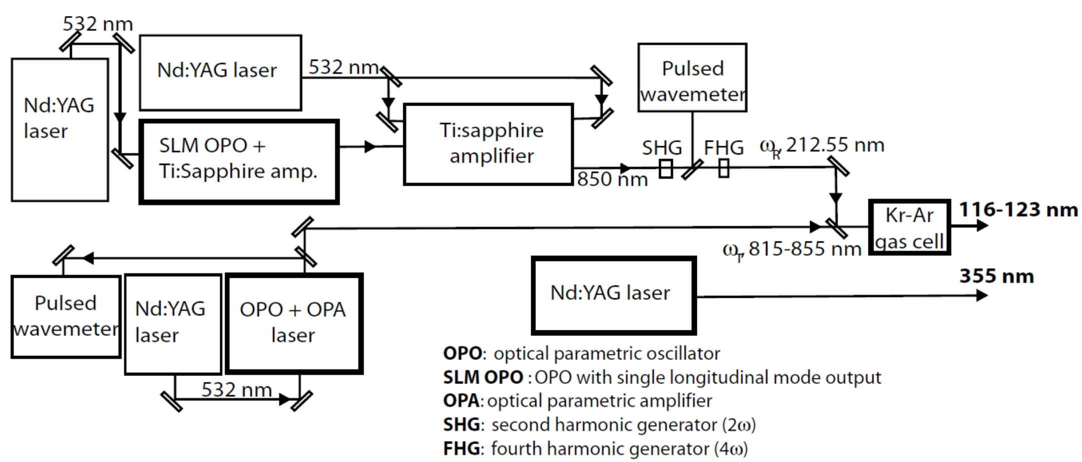

Schematic diagram of the pulsed laser system used at RIKEN – RAL for resonant ionization of muonium.

K. Nagamine, *et al.*, PRL **74**, 4811 (1995).
P. Bakule, *et al.*, Nucl. Instr Meth. B **266**, 335 (2008).

Generation of Slow Positive Muons from Solid Rare-Gas Moderators

Generation of slow positive muons from solid rare-gas moderators

D. R. Harshman and A. P. Mills, Jr.
AT&T Bell Laboratories, Murray Hill, New Jersey 07974

J. L. Beveridge, K. R. Kendall, G. D. Morris, M. Senba, and J. B. Warren
TRIUMF, University of British Columbia, Vancouver, British Columbia, V6T 2A3, Canada

A. S. Rupaal and J. H. Turner
Western Washington University, Bellingham, Washington 98225
(Received 27 April 1987)

We observe the emission of slow positive muons (μ^+) from solid neon, argon, krypton, and xenon moderators exposed to a 4.2-MeV incident μ^+ beam. The time-of-flight spectra for all of the targets studied exhibit a narrow distribution with no delayed component. Energy spectra obtained from the time-of-flight data indicate a maximum below ~10 eV with a tail extending to higher energies. The data suggest a slowly thermalizing muon emission mechanism, implying a long diffusion length for low-energy μ^+ in these solids. Of the targets measured, argon was observed to produce the highest yield ($\sim 10^{-5}$ slow μ^+ per incident μ^+), providing a useful flux for further experimentation.

PRB **36R**, 8850 (87).

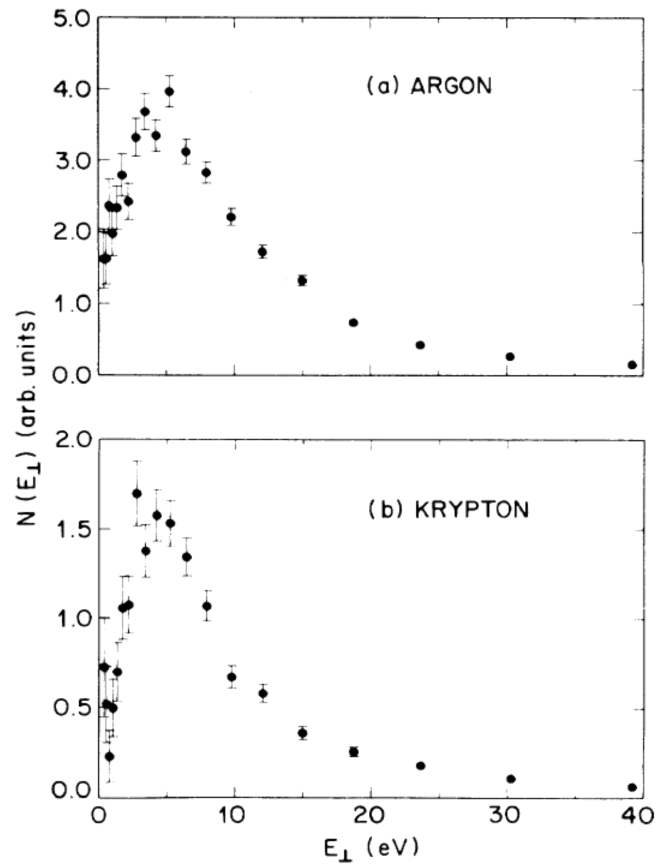

Generation of Polarized Epithermal μ^+

„Surface“
Muons
~ 4 MeV
~ 100% pol.

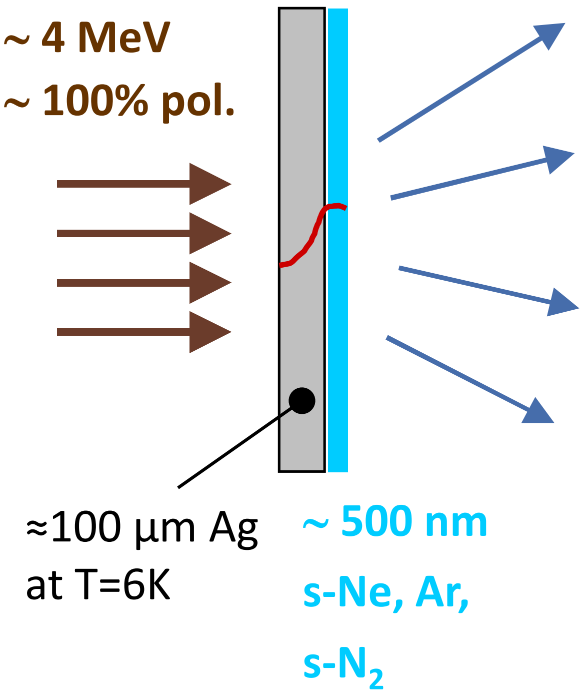

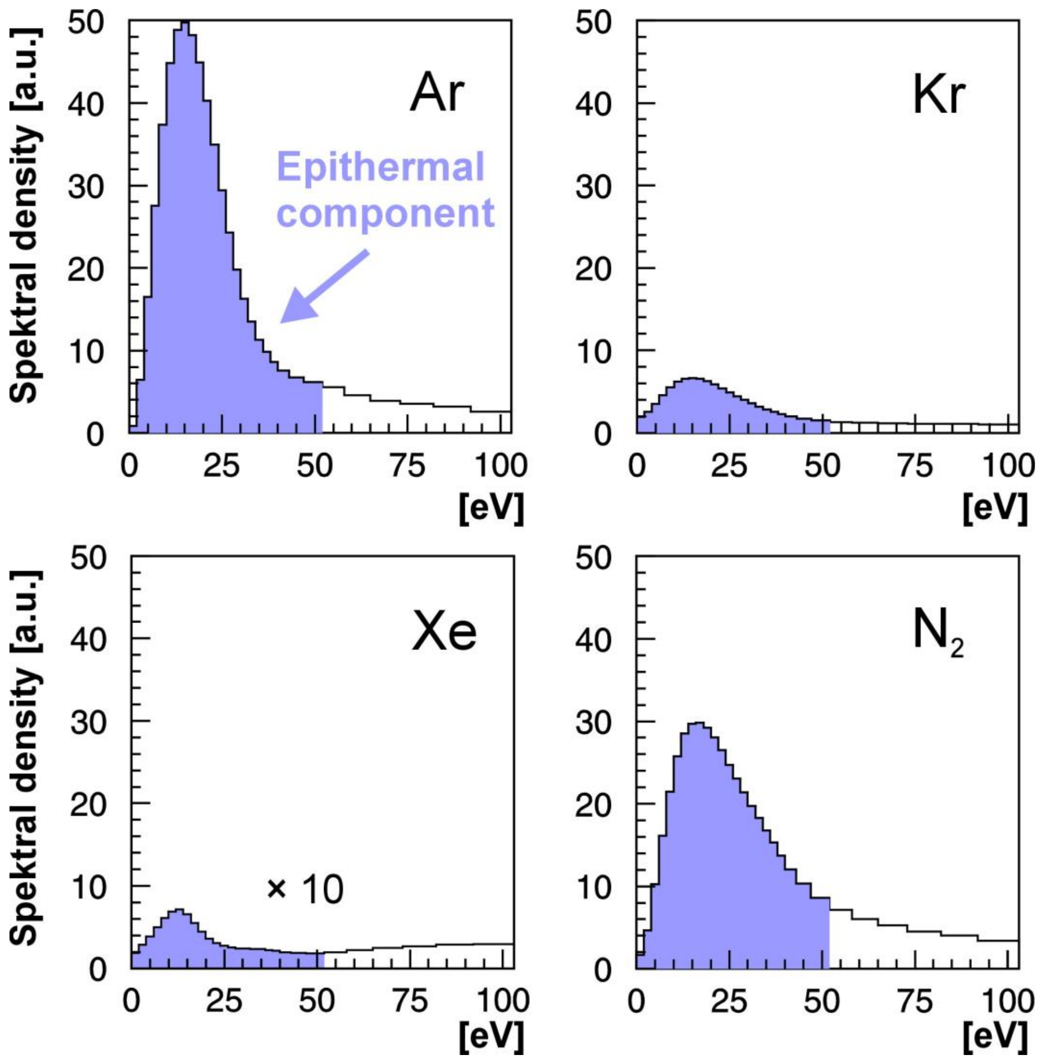

motivated by experiments for positron moderation

T. Prokscha et al., Appl. Surf. Sci. **172**, 235 (2001).
T. Prokscha et al., Phys. Rev. **A58**, 3739 (1998).
E. Morenzoni et al,. J. Appl. Phys. **81**, 3340 (1997).
D. Harshmann et al., Phys. Rev. **B36**, 8850 (1987).

Characteristics of Epithermal μ^+

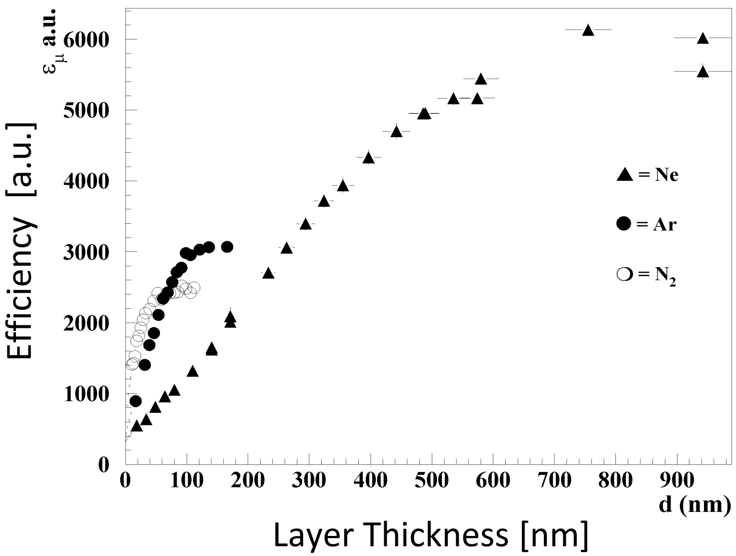

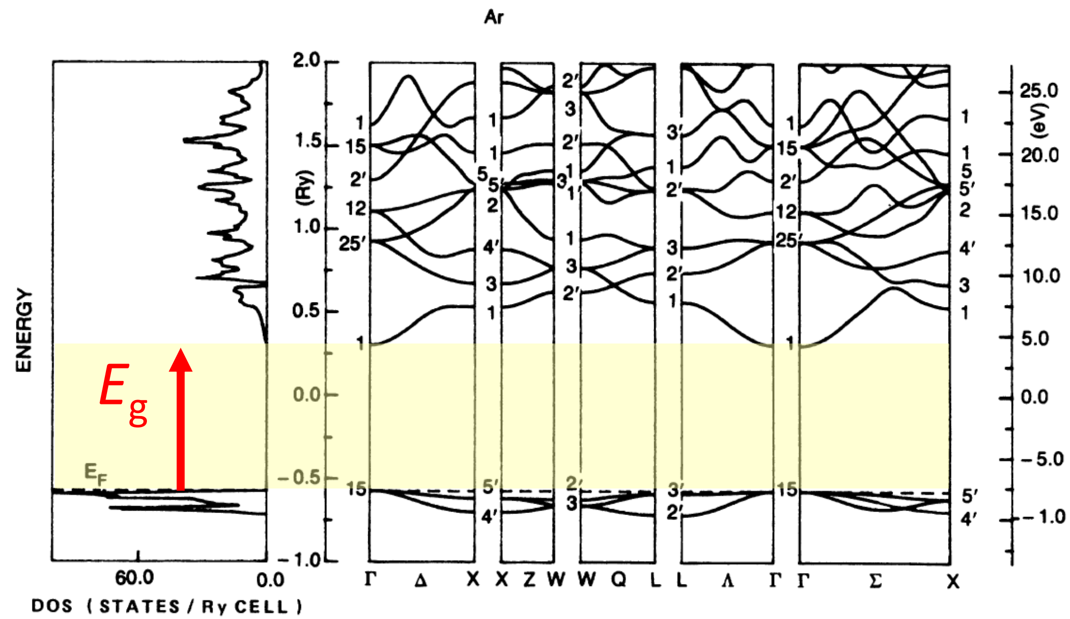

FIG. 3. The band structure and density of states for solid argon.

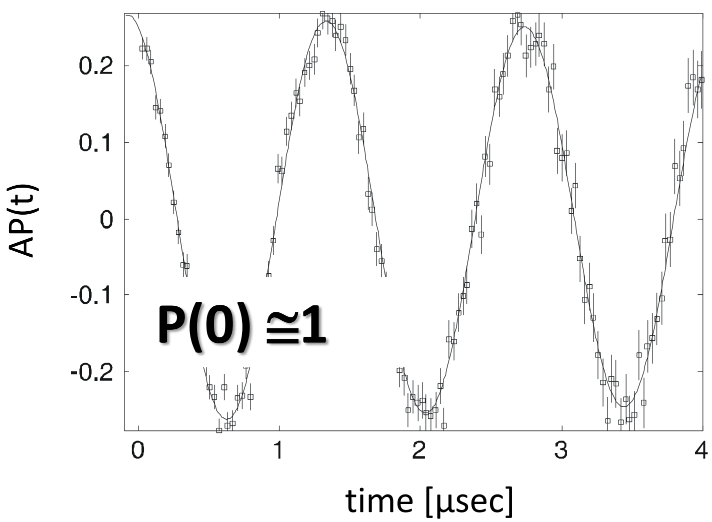

- suppression of electronic energy loss for $E<E_g$ ($E_g \approx$ 10-20eV)
- large escape depth $L \approx$ 50-200nm
- moderation efficiency:

$$\varepsilon_+ = N_{\rm epith}/N_{\rm 4MeV} \simeq (1-F_{\rm Mu})L/\Delta R \simeq 10^{-5}\ldots10^{-4}$$

- no loss of polarization during the moderation

E. Morenzoni, *et al.* Phys.Rev.Lett. **72**, 2793 (1994).

PAUL SCHERRER INSTITUT

Low Energy μ^+ Beam and Setup for LE-μSR

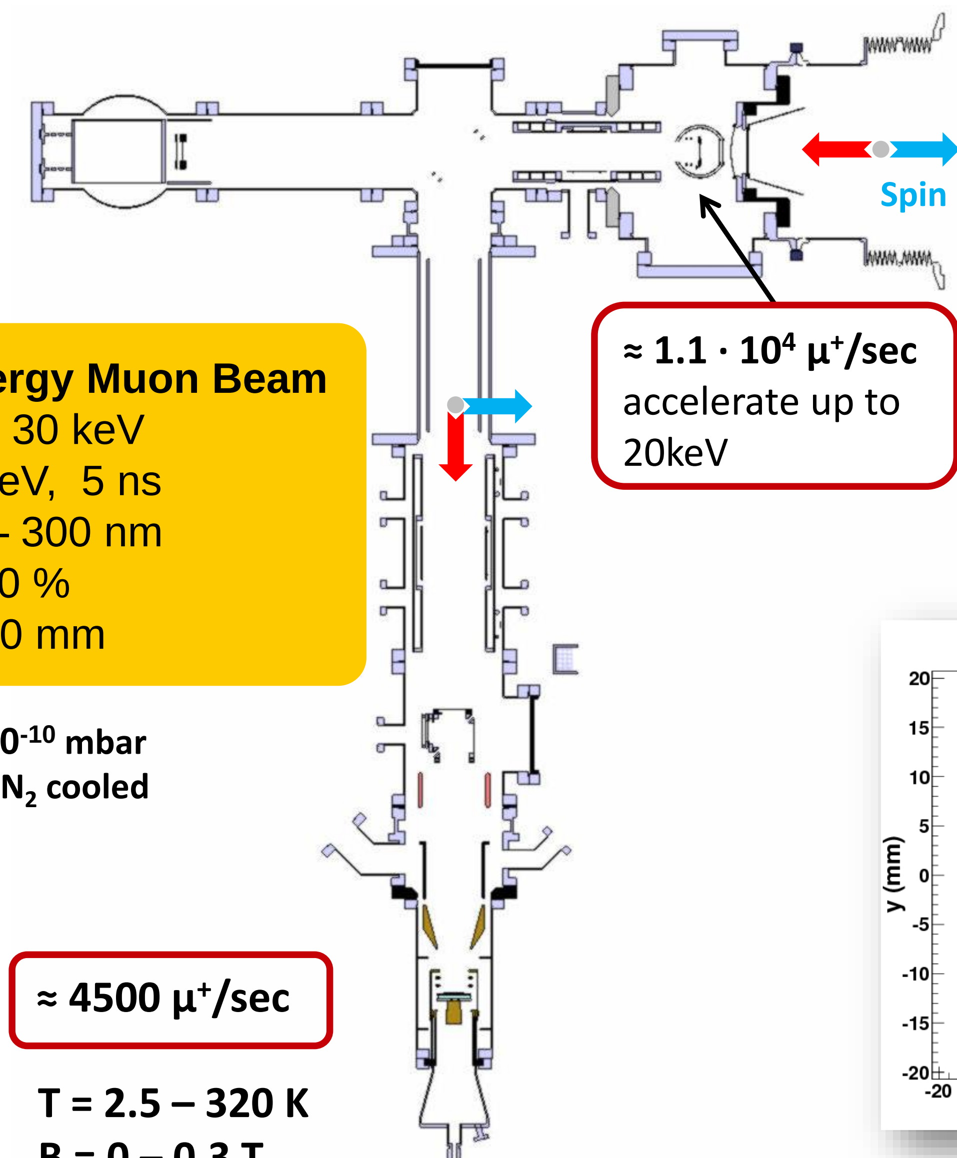

Surface μ^+ beam ≈ 4MeV

≈ $1.7 \cdot 10^8$ μ^+/sec

≈ $1.1 \cdot 10^4$ μ^+/sec
accelerate up to 20keV

Polarized Low Energy Muon Beam

Energy:	0.5 - 30 keV
ΔE, Δt:	400 eV, 5 ns
Depth:	≈ 1 – 300 nm
Polarization:	≈ 100 %
Beam Spot:	10-20 mm

UHV chambers, 10^{-9} – 10^{-10} mbar
All transport elements LN_2 cooled

≈ 4500 μ^+/sec

T = 2.5 – 320 K
B = 0 – 0.3 T

Beamspot at the sample position

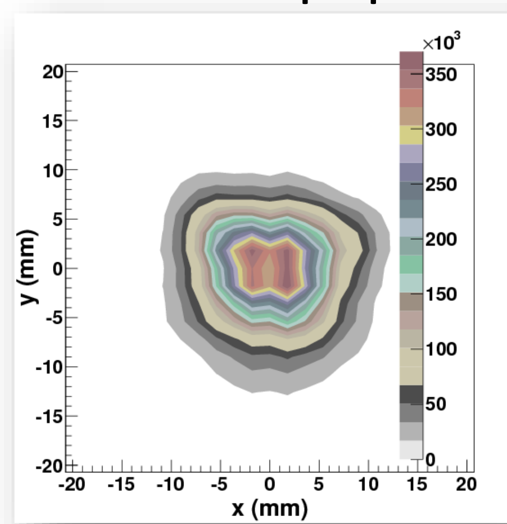

Low Energy μ⁺ Beam and Setup for LE-μSR

Muon Spin
Muon Momentum

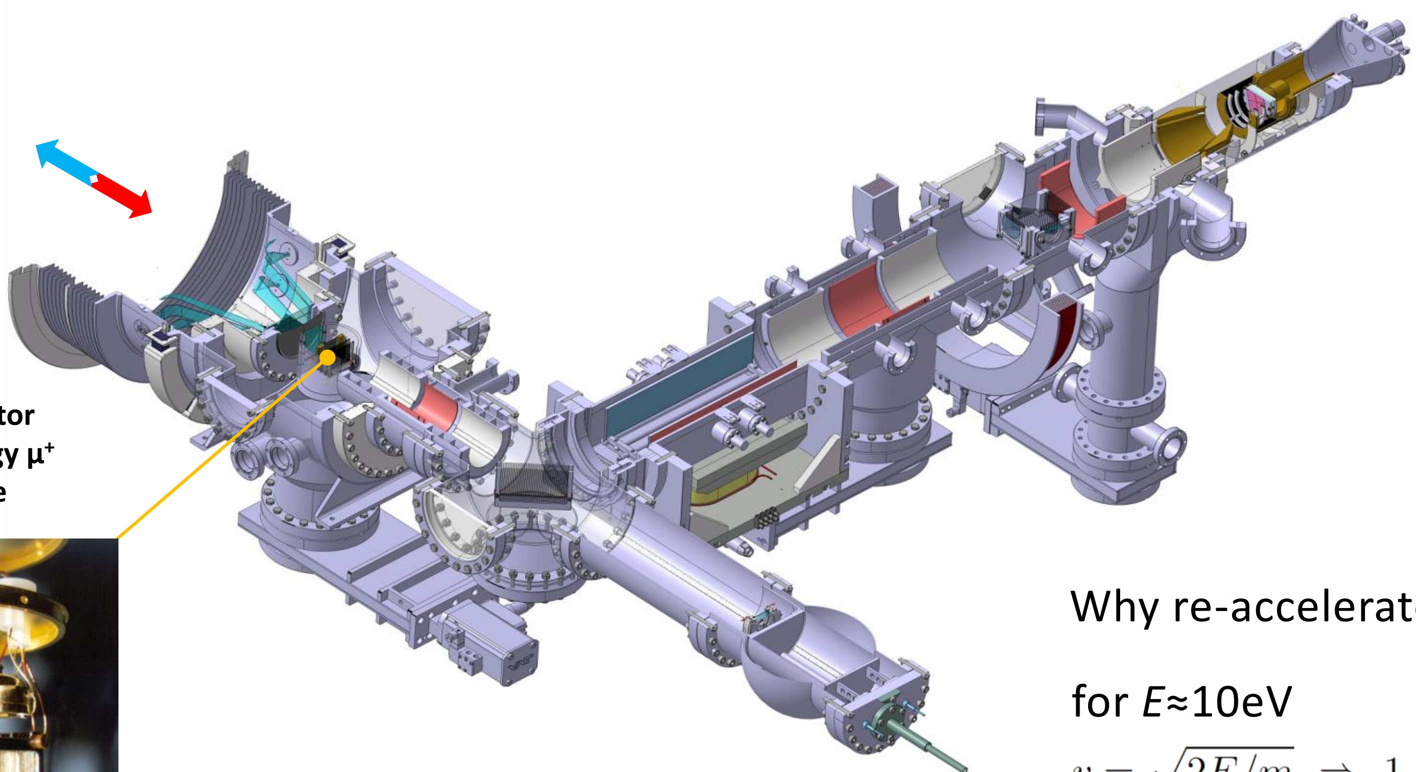

Moderator low energy μ^+ source

Typical re-acceleration voltage at the moderator: 15kV

Why re-accelerate slow μ^+?

for $E \approx 10$eV

$$v = \sqrt{2E/m} \;\Rightarrow\; 1.3 \cdot 10^5\,(\mathrm{m/s})$$

$$\ell_\dagger = v \cdot (5\tau_\mu) \simeq 1.4\,\mathrm{m}$$

↓

No μ^+ left

Low Energy μ^+ Beam and Setup for LE-μSR

Muon Spin
Muon Momentum

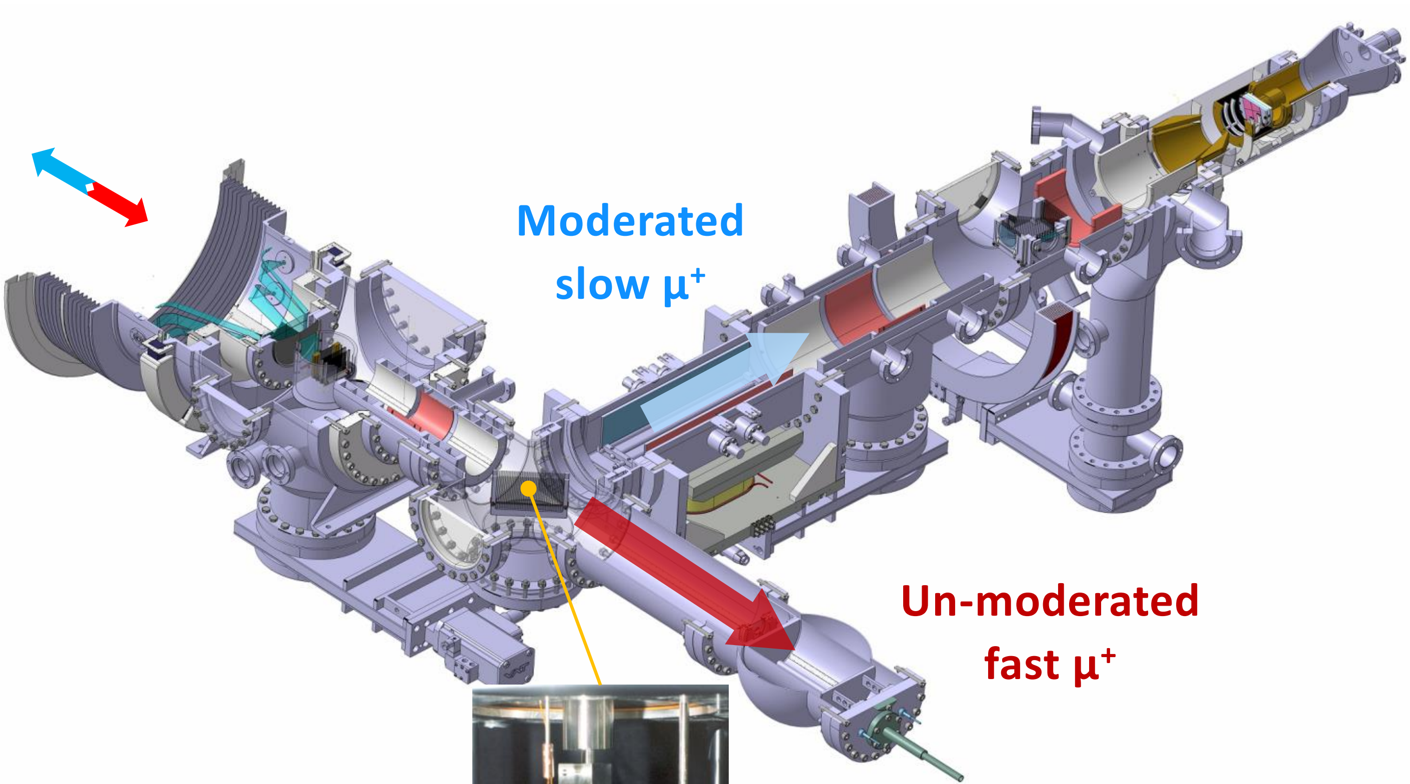

Mirror
energy filter

Mirror at the same high voltage as the moderator. Typically 15kV

PAUL SCHERRER INSTITUT

Low Energy μ^+ Beam and Setup for LE-μSR

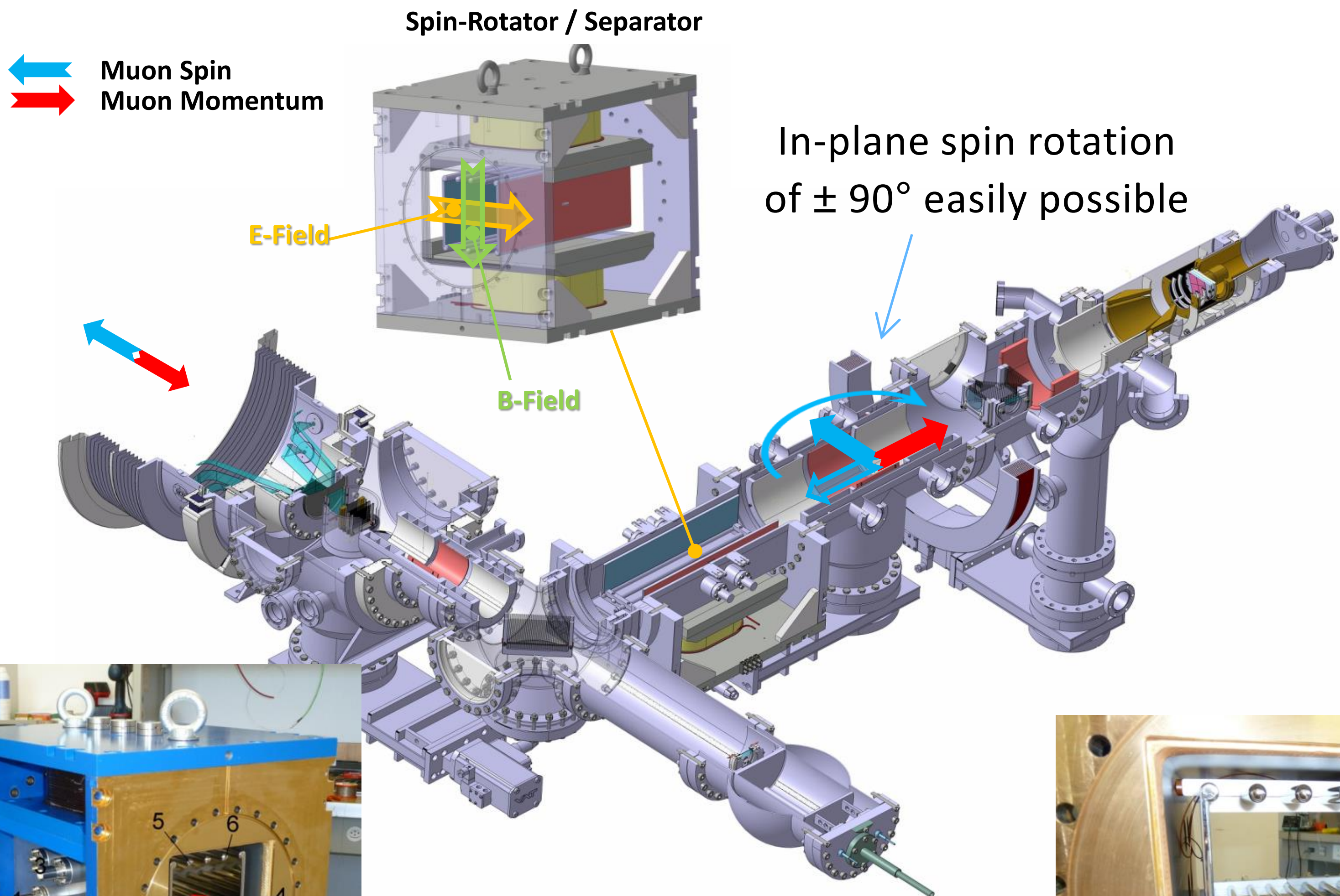

Low Energy μ^+ Beam and Setup for LE-μSR

Muon Spin
Muon Momentum

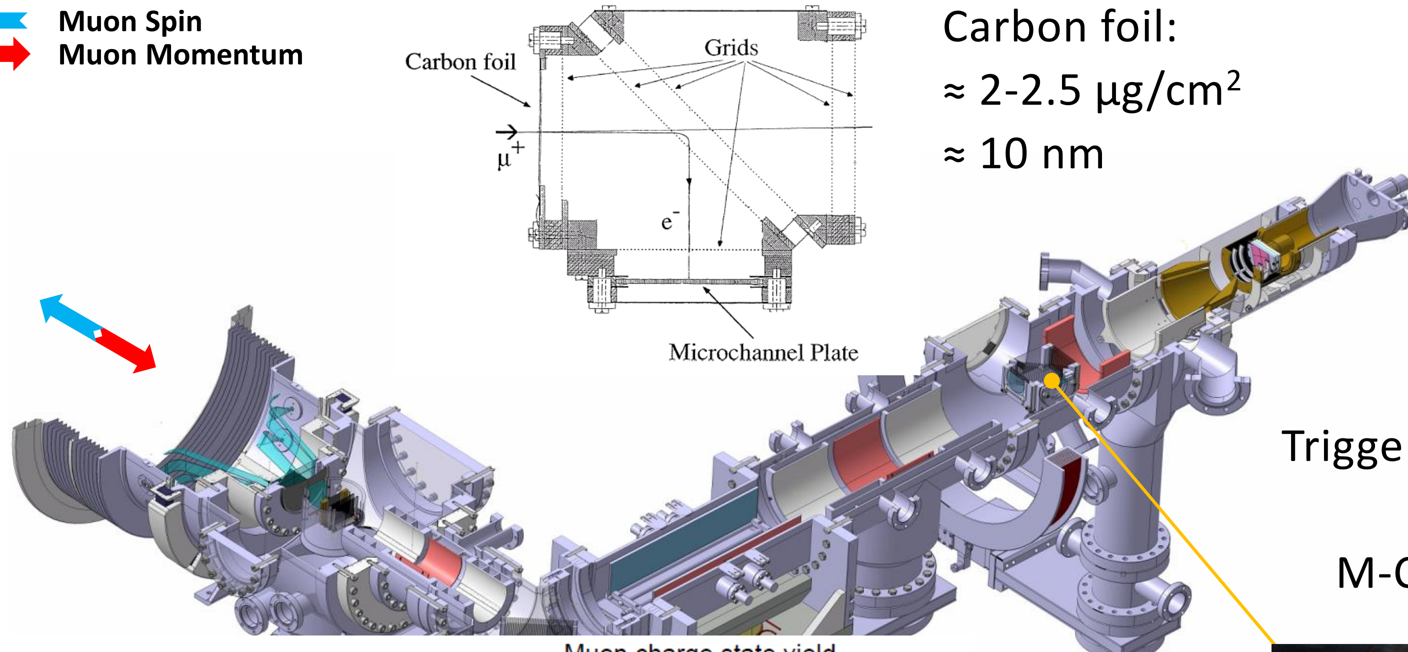

Carbon foil:
≈ 2-2.5 µg/cm^2
≈ 10 nm

Trigger Detector
or
M-Counter

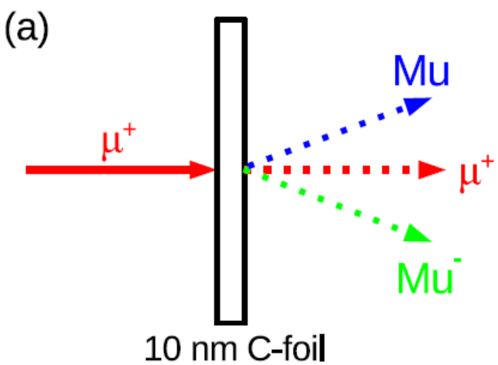

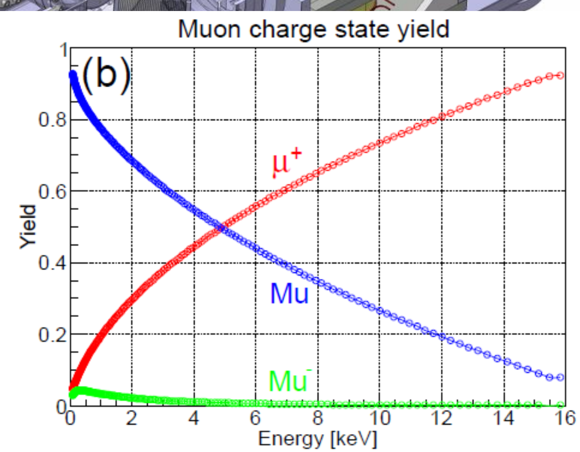

Trigger implantation time

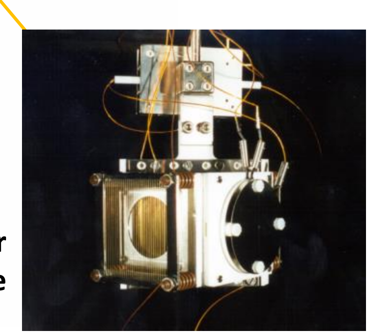

A. Hofer, PhD Thesis (98)
K.S. Khaw, *et al.*, JINST **10**, P10025 (15).

Low Energy μ⁺ Beam and Setup for LE-μSR

Muon Spin
Muon Momentum

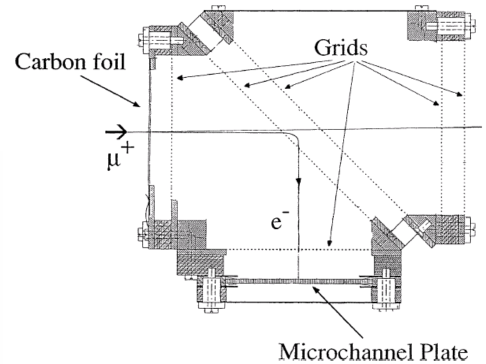

Carbon foil:
≈ 2-2.5 μg/cm^2
≈ 10 nm

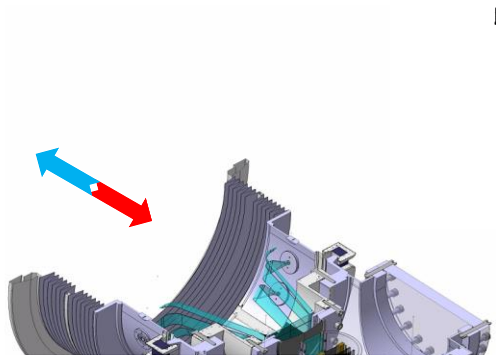

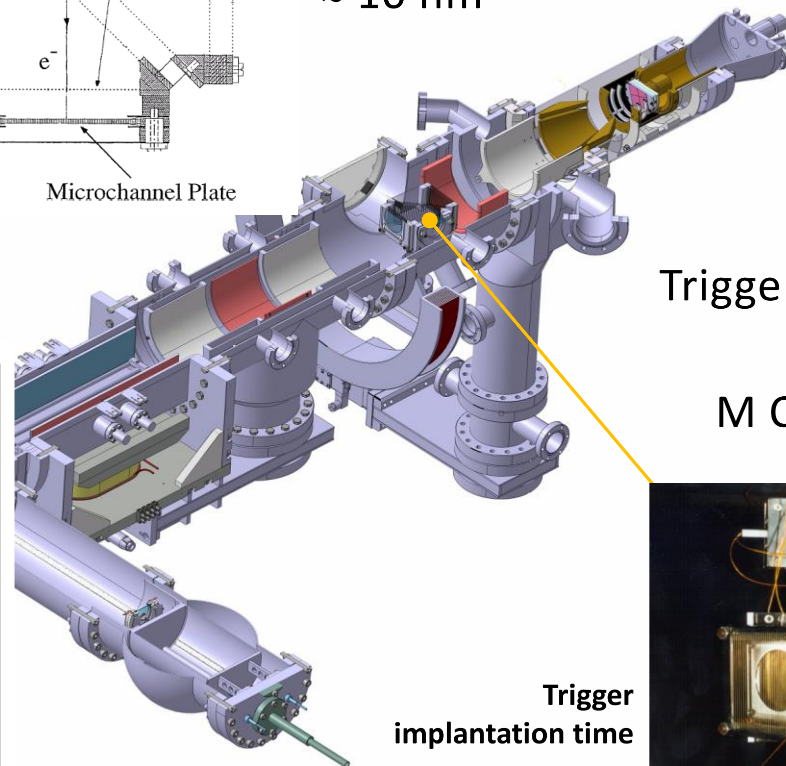

Trigger Detector
of
M Counter

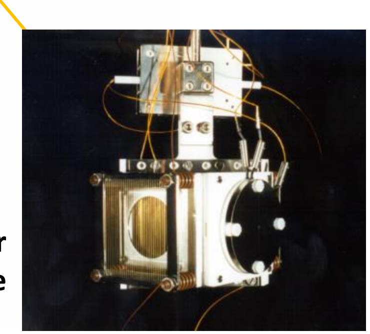

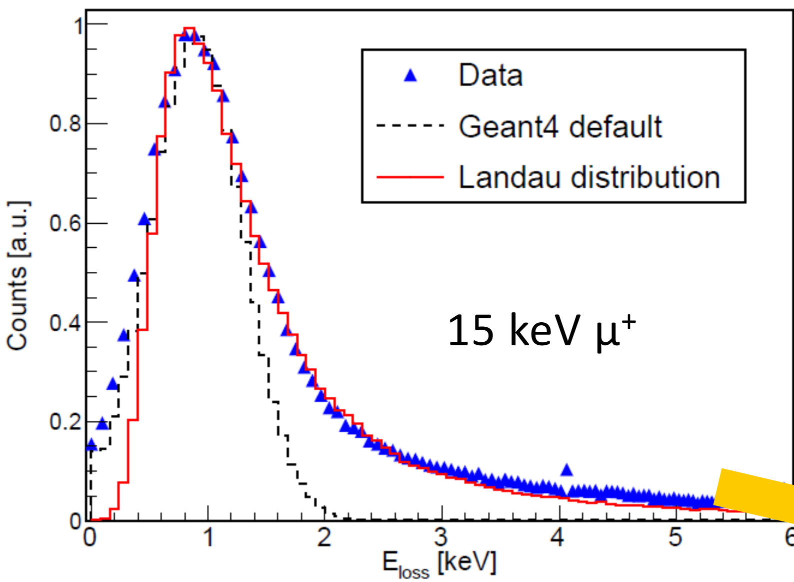

A. Hofer, PhD Thesis (98)
K.S. Khaw, *et al.*, JINST **10**, P10025 (15).

This energy loss distribution is limiting the frequency resolution of LEM to ≤ 50 MHz

Low Energy μ^+ Beam and Setup for LE-μSR

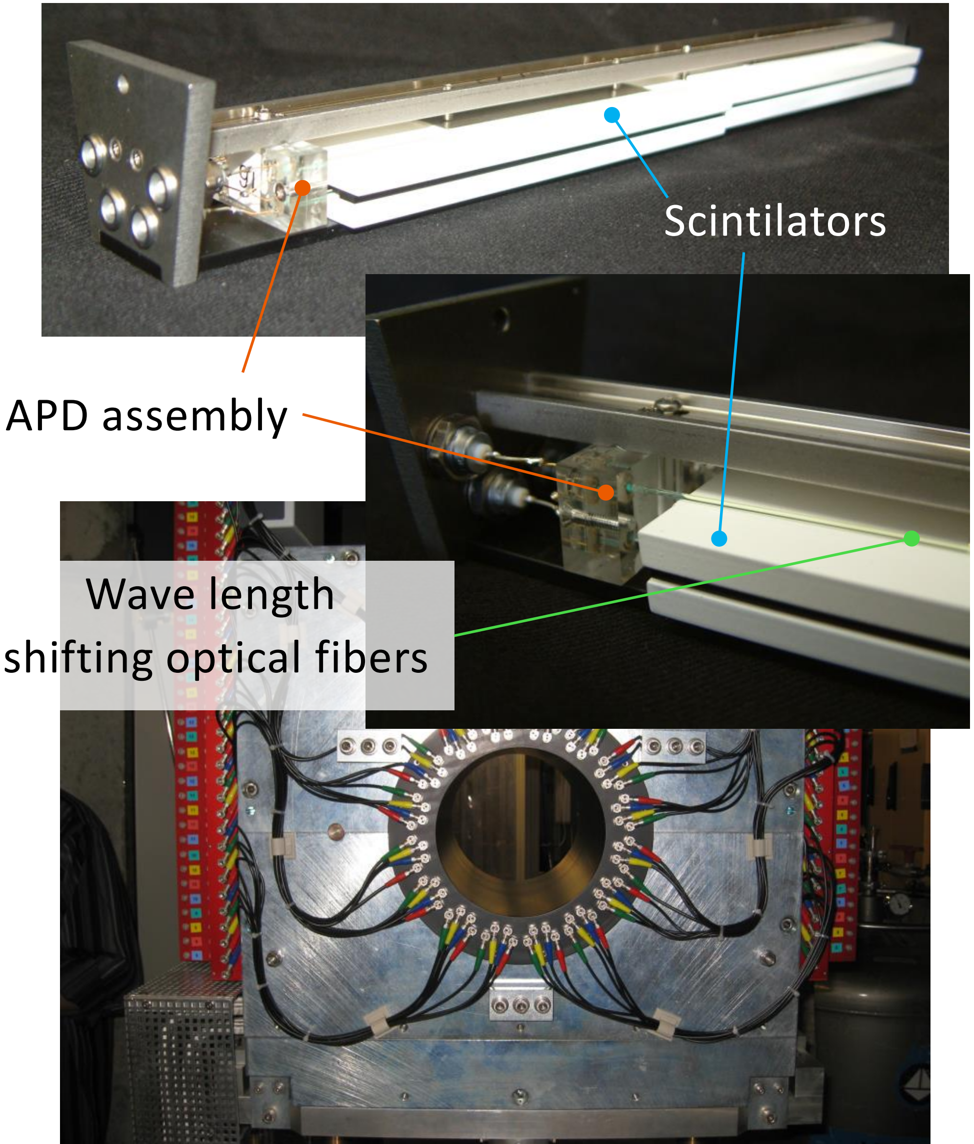

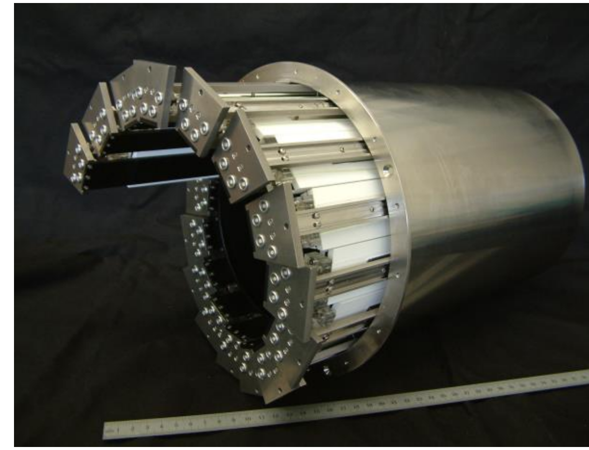

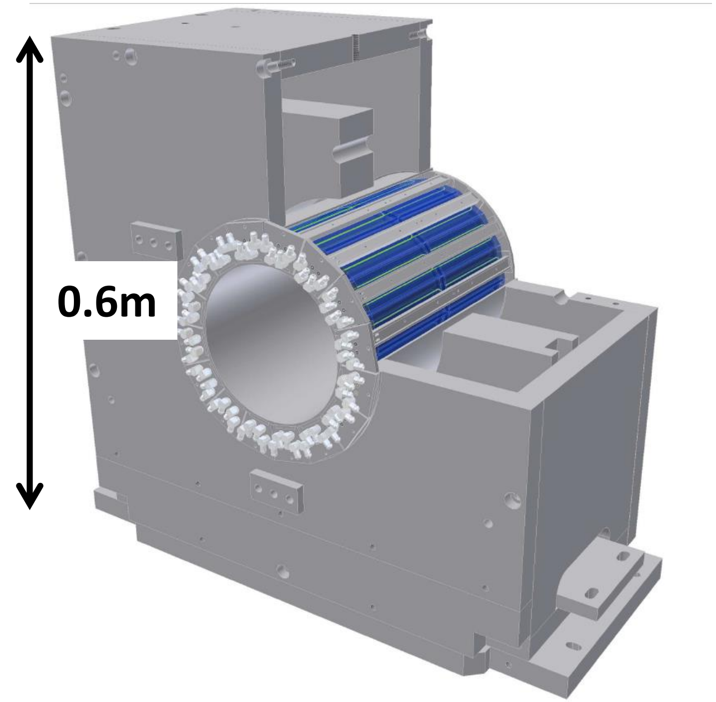

A. Stoykov, R. Scheuermann, *et al.*, Physica B **404**, 986 (09).
See also https://www.psi.ch/en/lmu/position-sensitive-detection-psd-of-muons-and-positrons

t_0 at a Quasi Continuous Muon Source

Surface Muons

Prompt peak due to relativistic e^+ firing M- and positron-counter almost instantly

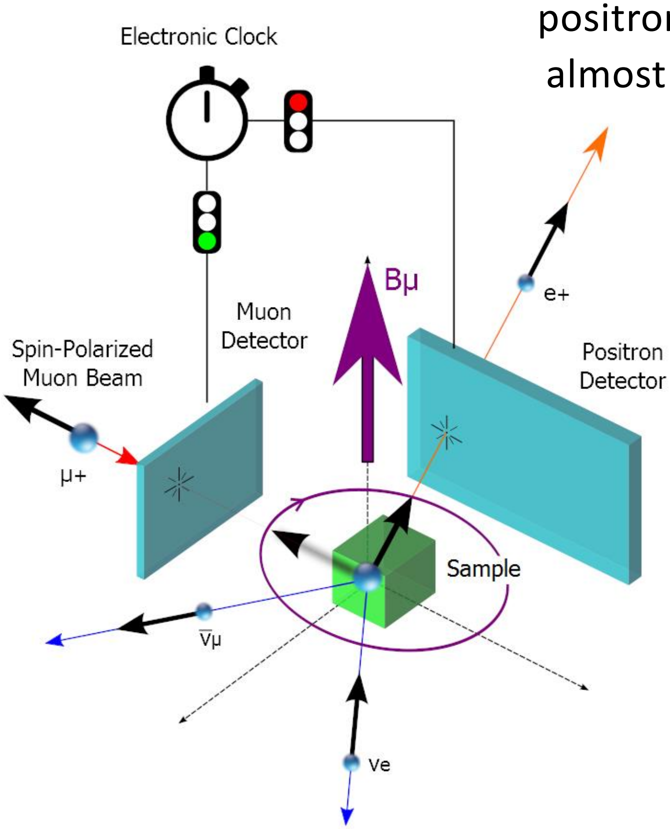

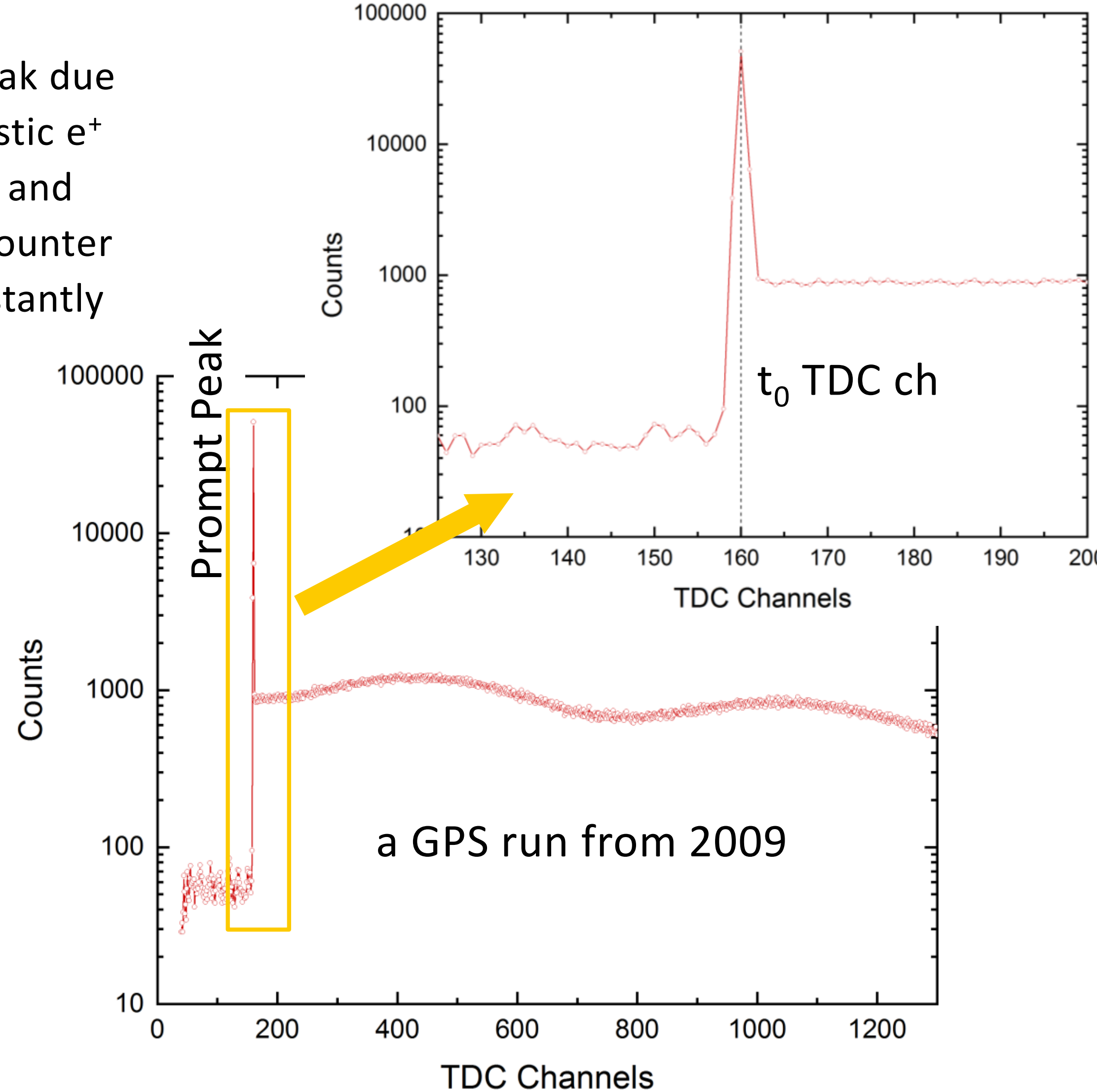

t_0 at a Quasi Continuous Muon Source – LEM

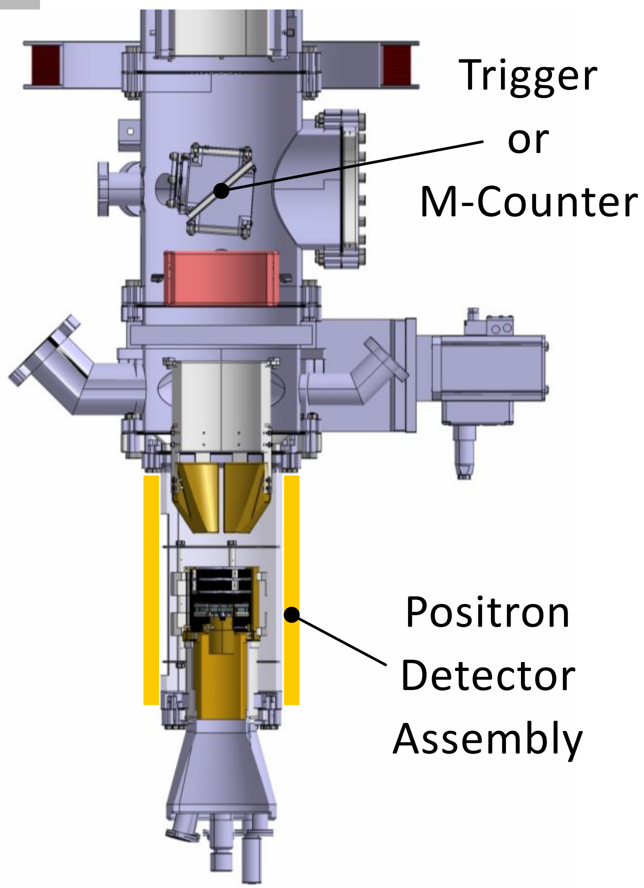

Where is the prompt peak, and hence the t_0 TDC channel?

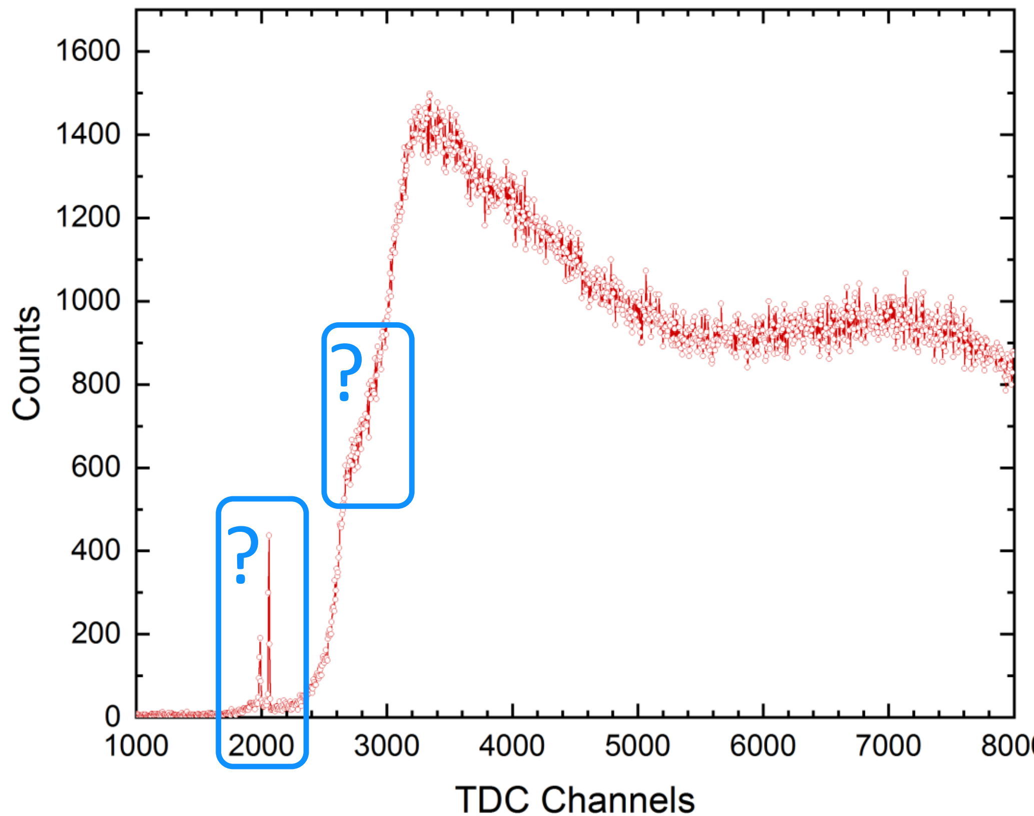

Example: 7.5kV Transport settings, i.e. very slow low-energy μ^+

t_0 at a Quasi Continuous Muon Source – LEM

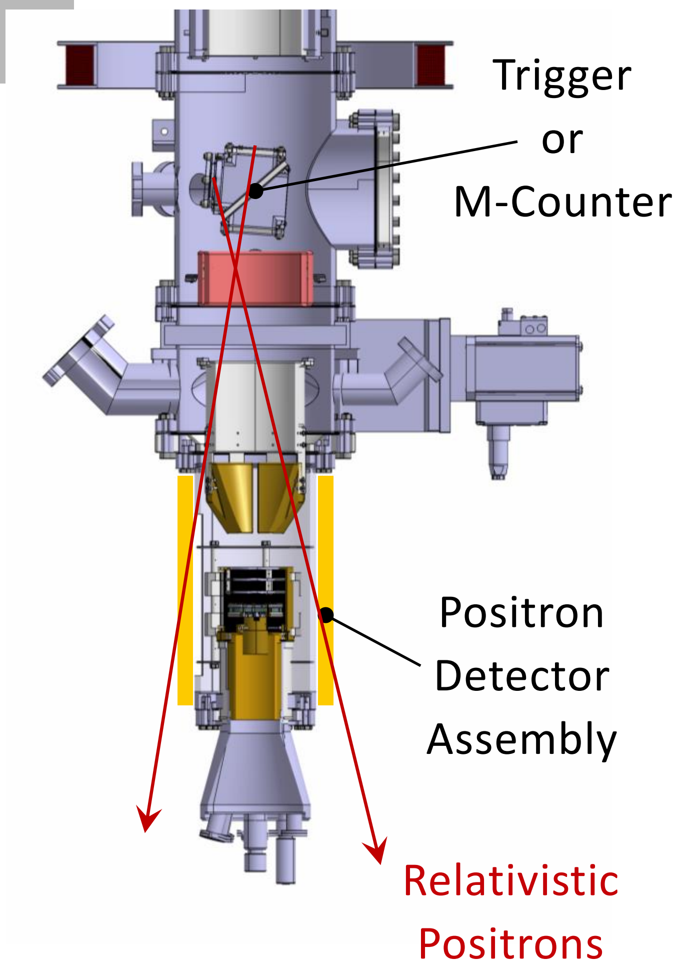

**Where is the prompt peak,
and hence the t_0 TDC channel?**

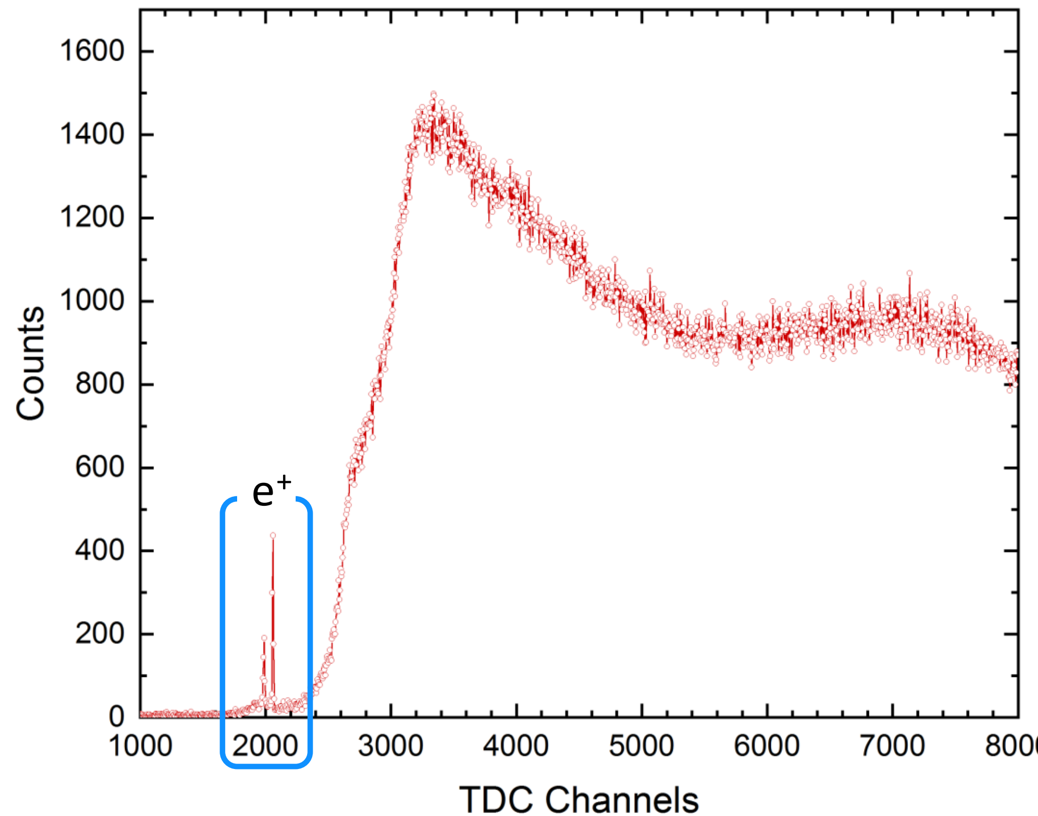

Example: 7.5kV Transport settings, i.e.
very slow low-energy μ^+

t_0 at a Quasi Continuous Muon Source – LEM

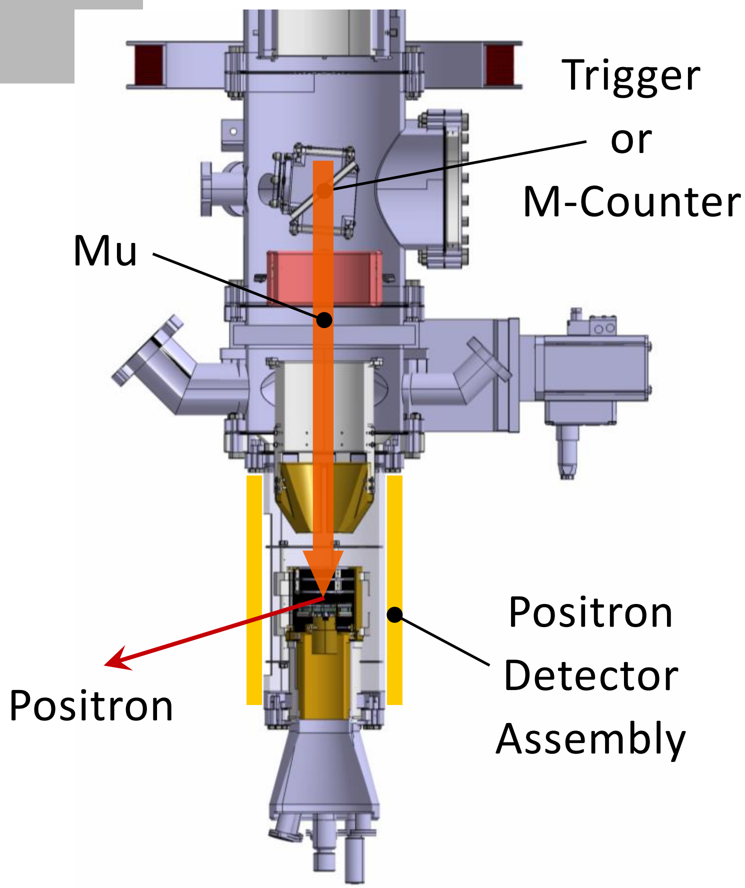

Where is the prompt peak, and hence the t_0 TDC channel?

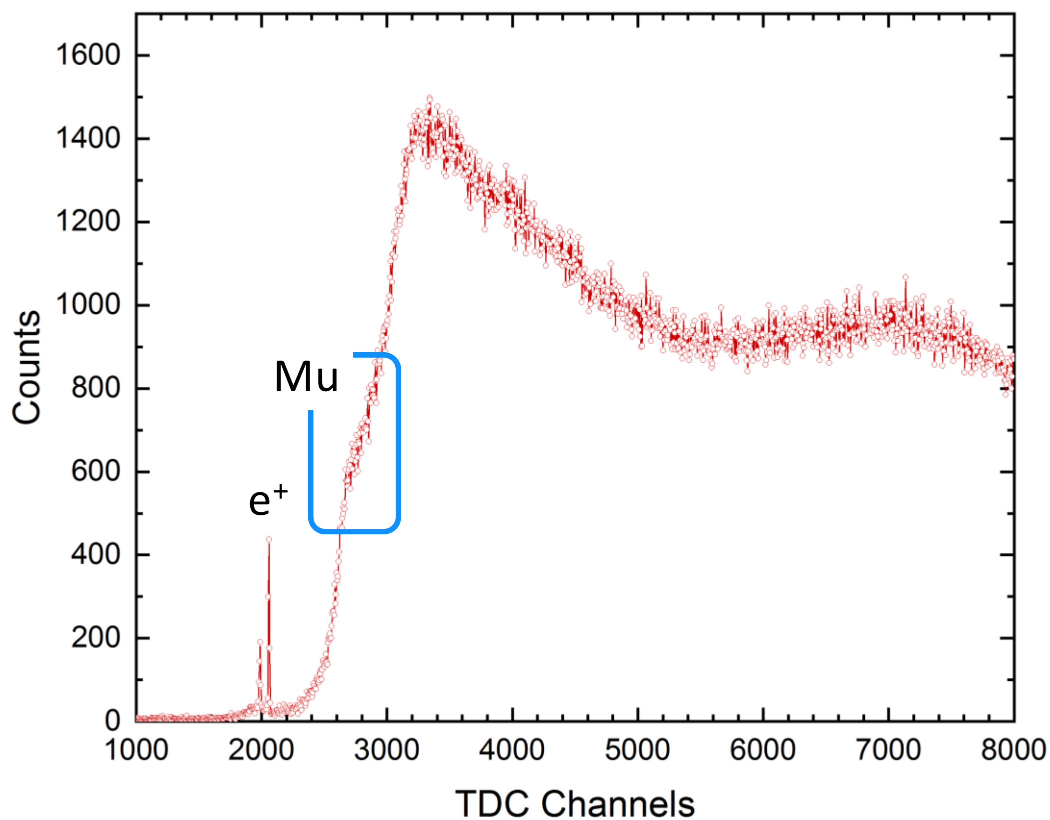

Example: 7.5kV Transport settings, i.e. very slow low-energy μ^+

t_0 at a Quasi Continuous Muon Source – LEM

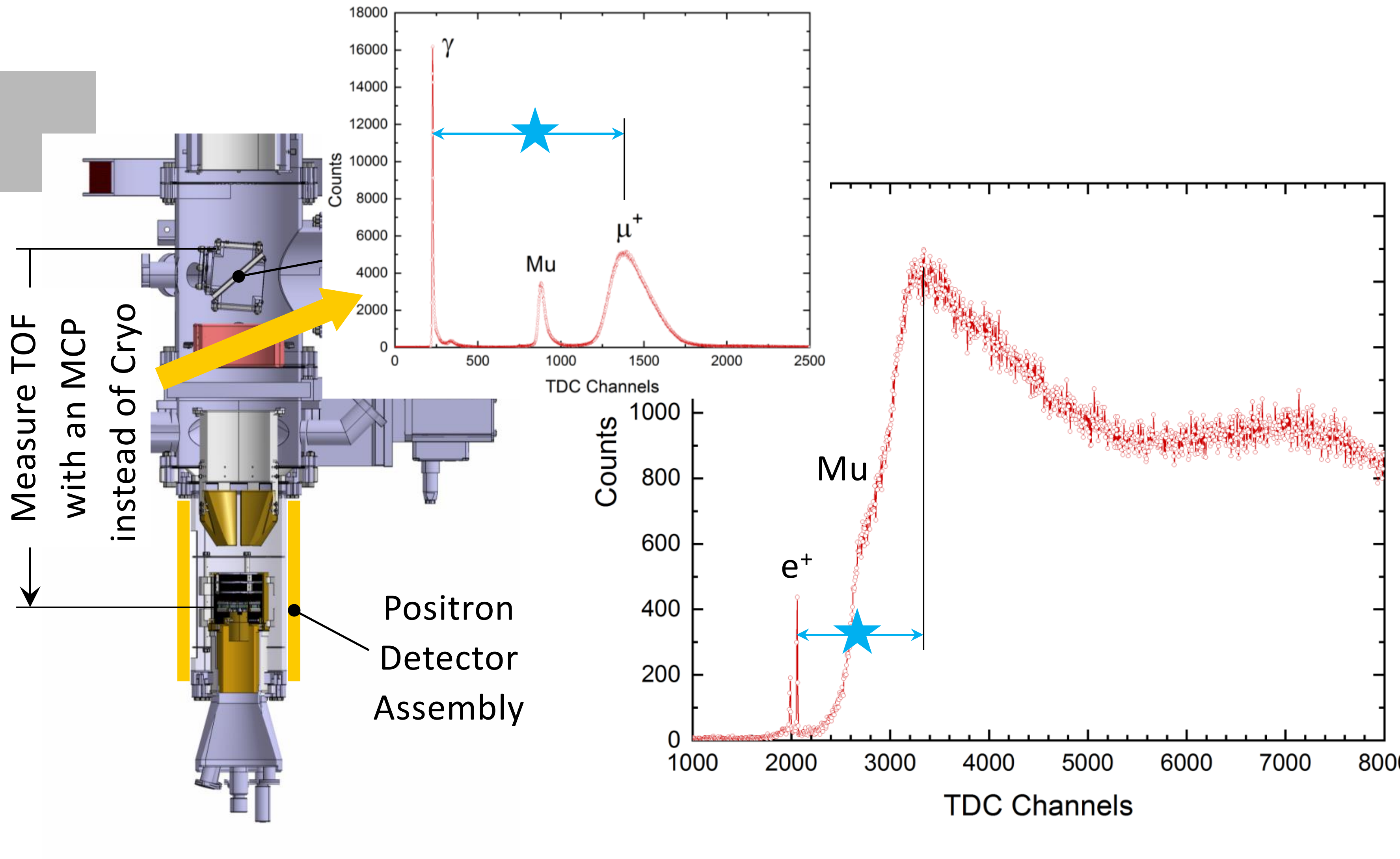

Example: 7.5kV Transport settings, i.e. very slow low-energy μ^+

LEM Cryos – Konti Cryos

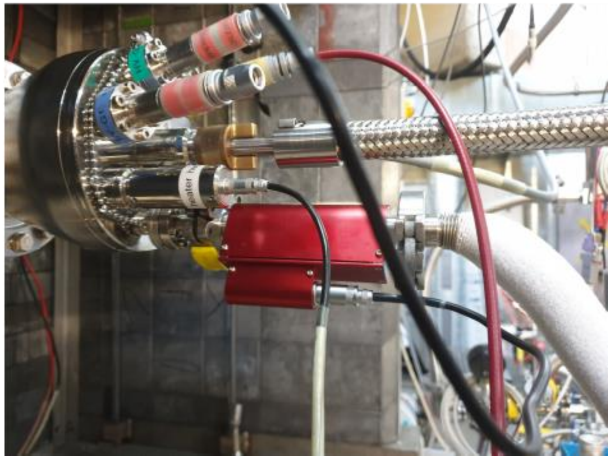

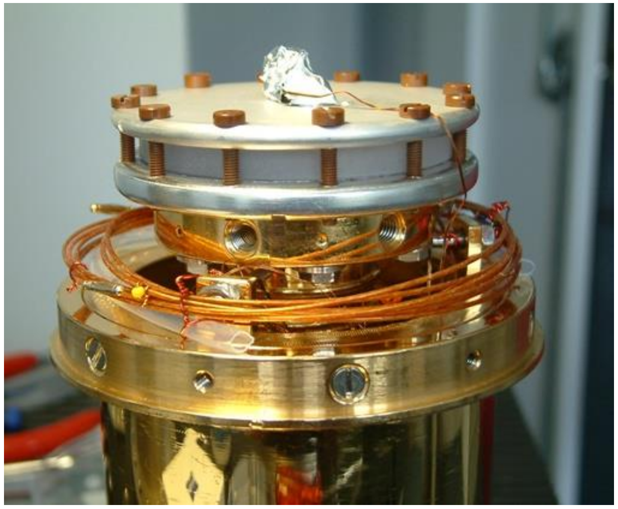

Konti flow cryostats, 4 - 320 K at sample plate

Konti-1: for special experiments (current injection, illumination with LEDs) and tests

Konti-2: normal user operation

Konti-3: normal user operation,

application of electric fields, current injection

Konti-4: normal user operation

LEM Cryos – LowTemp Cryo

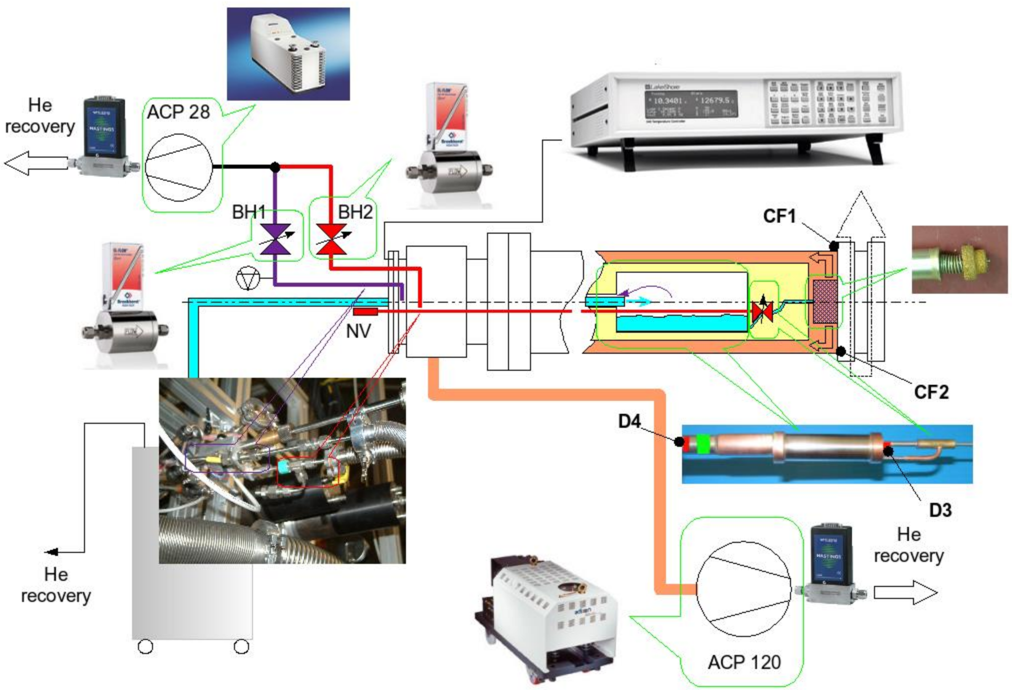

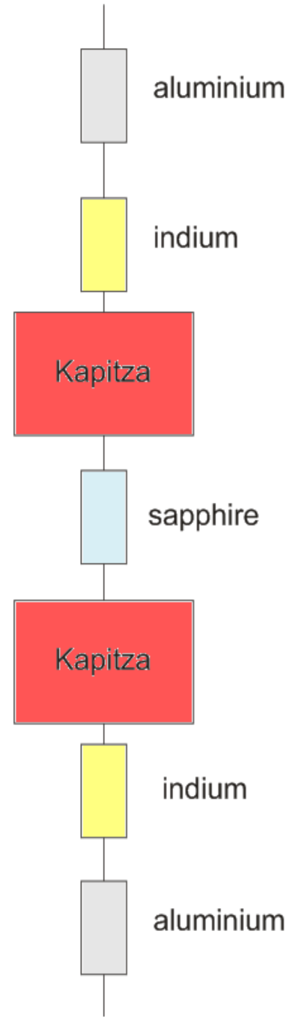

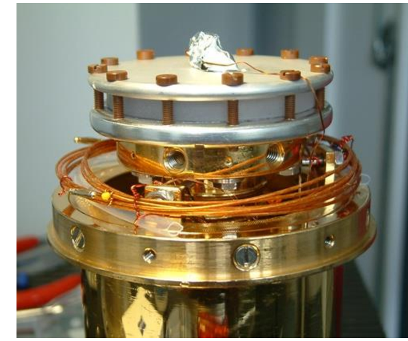

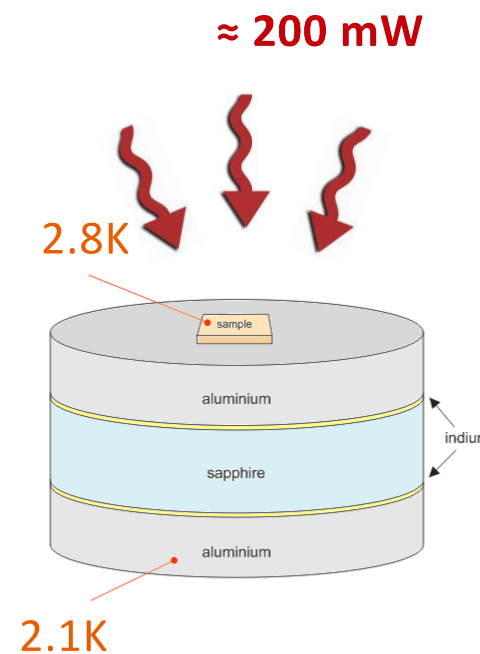

PAUL SCHERRER INSTITUT

LEM Cryos – LowTemp Cryo

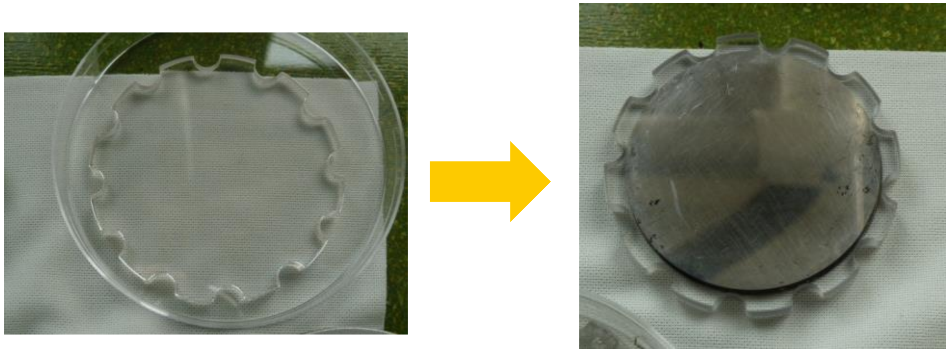

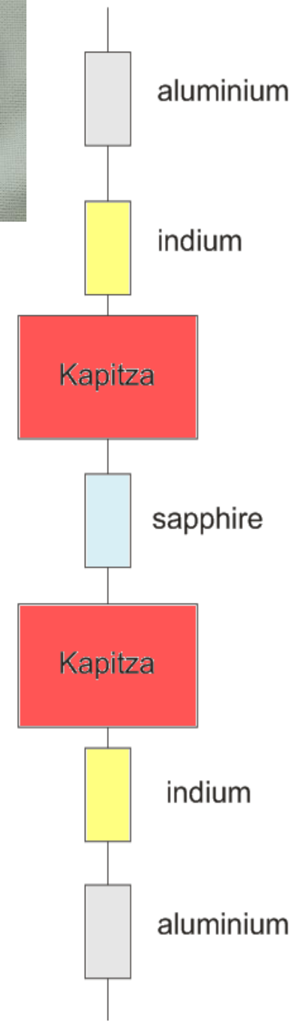

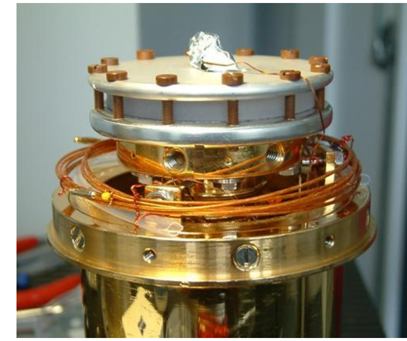

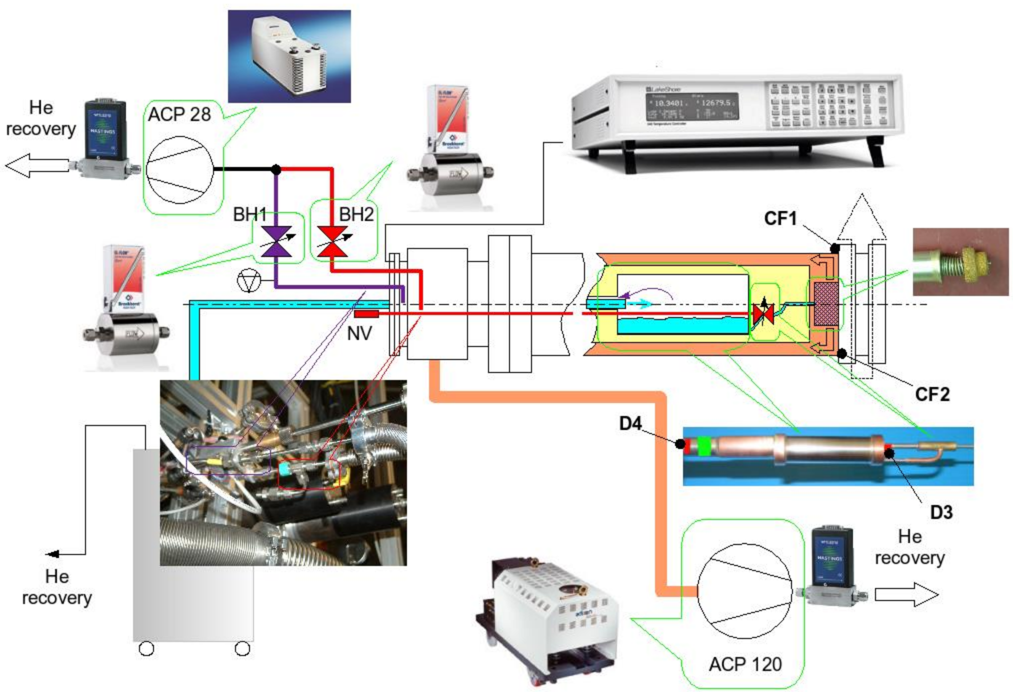

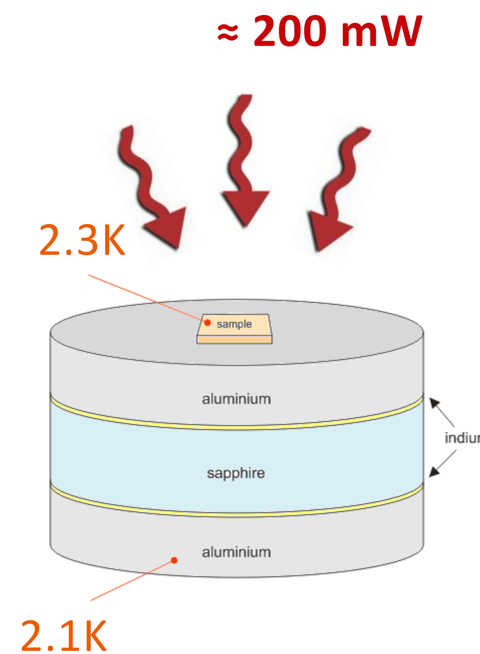

PAUL SCHERRER INSTITUT

LEM – Oven

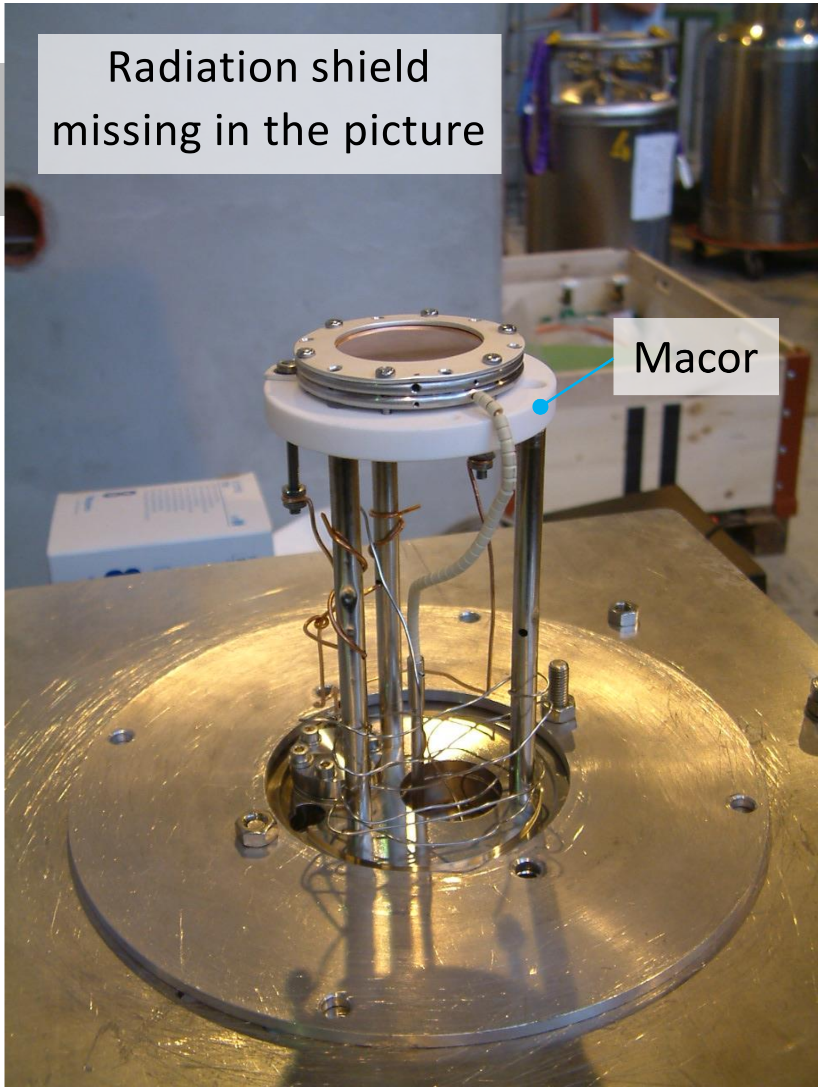

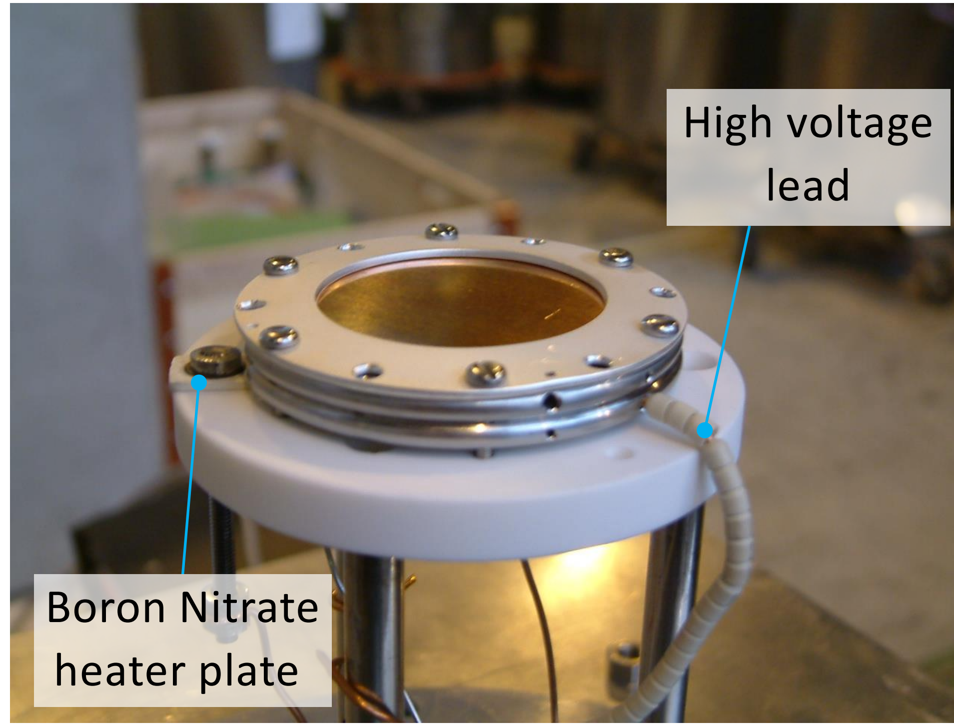

RT – 150 °C with +-10 kV at sample
T > 150 °C high voltage might get tricky due to electron emission

LEM Cryo with Positron Detectors

Side Half View

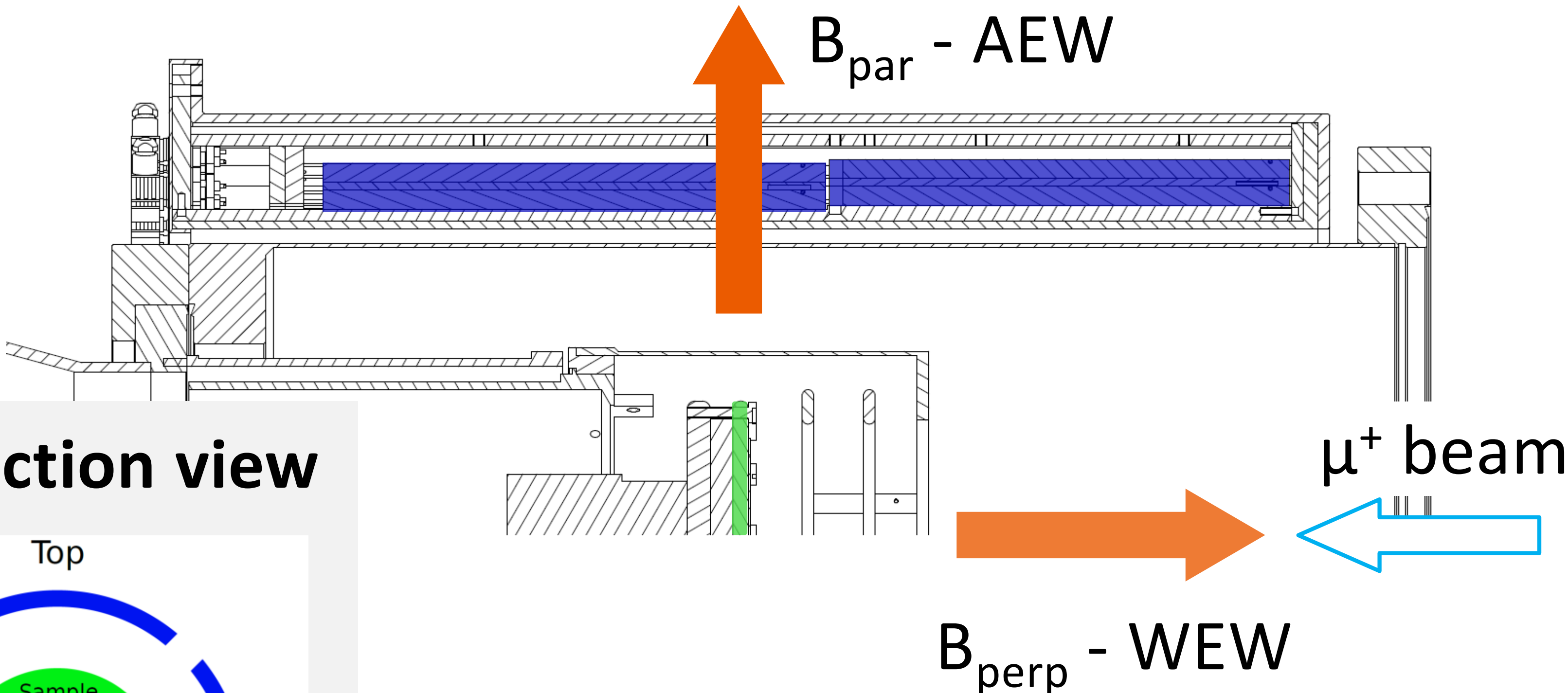

μ+ direction view

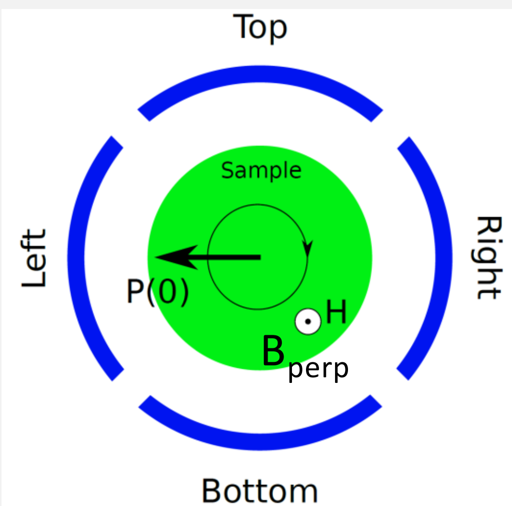

μ+ Spin Out-of-Plane (TF/ZF)

μ+ Spin anti-/parallel WEW (LF)

WEW Magnet with APD Positron Spectrometer

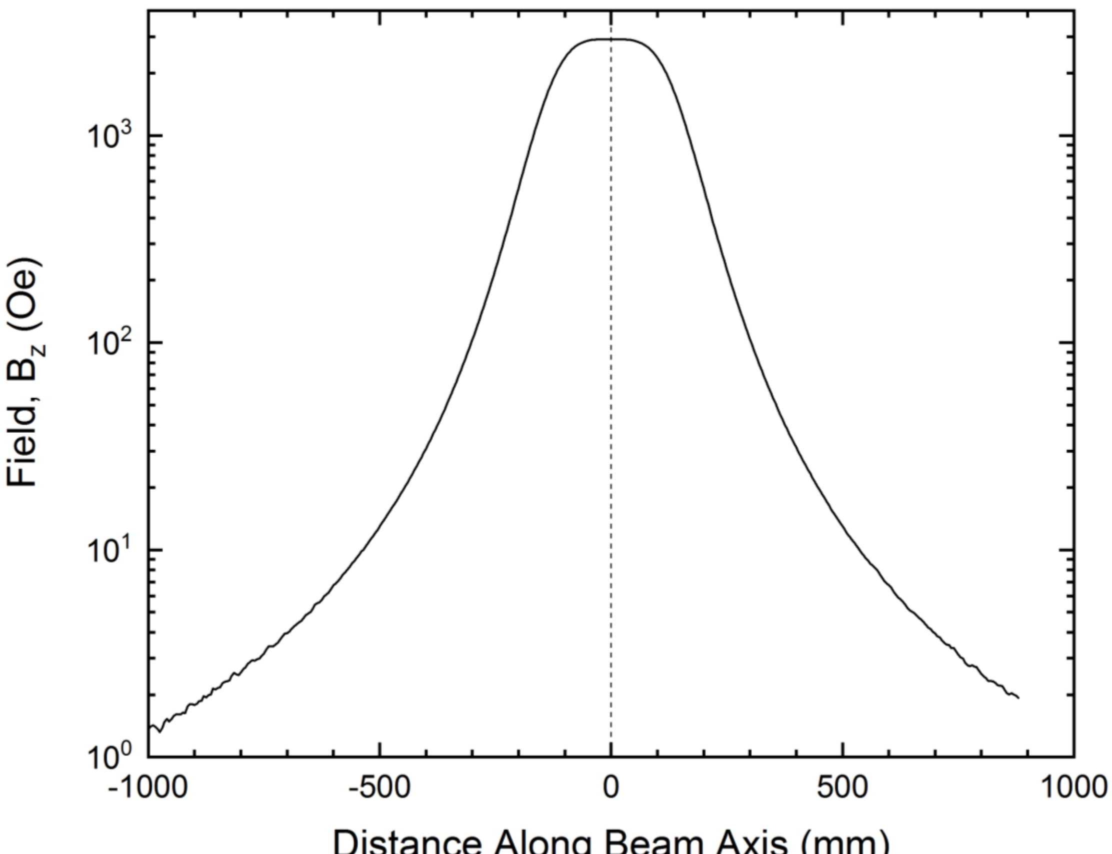

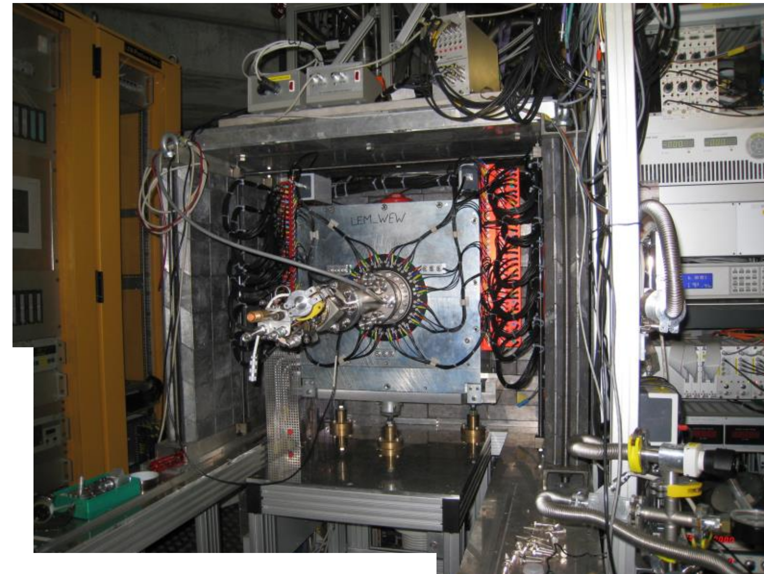

I_{max} = 550 A (0.32 T)

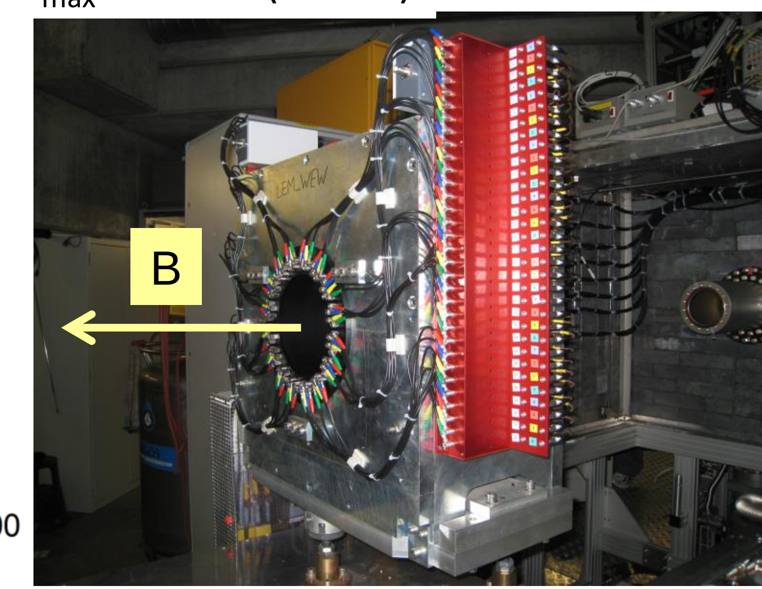

PAUL SCHERRER INSTITUT

WEW Magnet with APD Positron Spectrometer

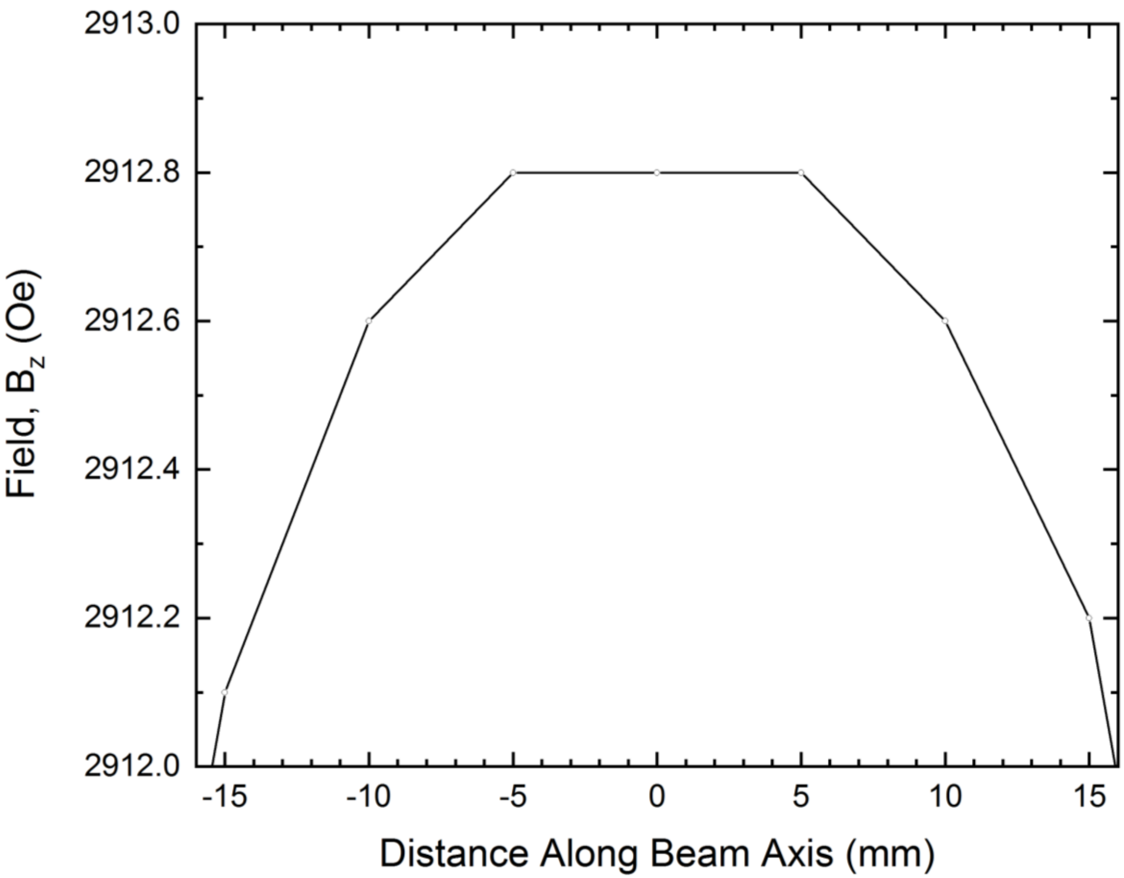

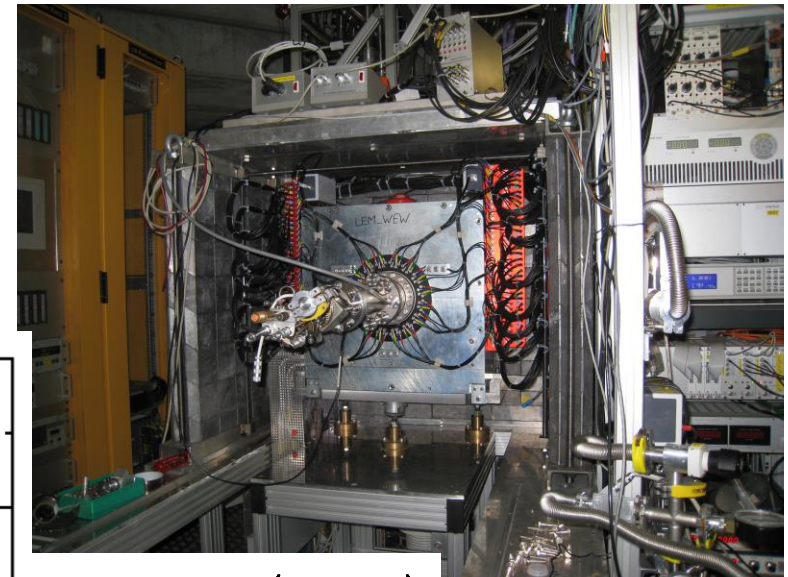

I_{max} = 550 A (0.32 T)

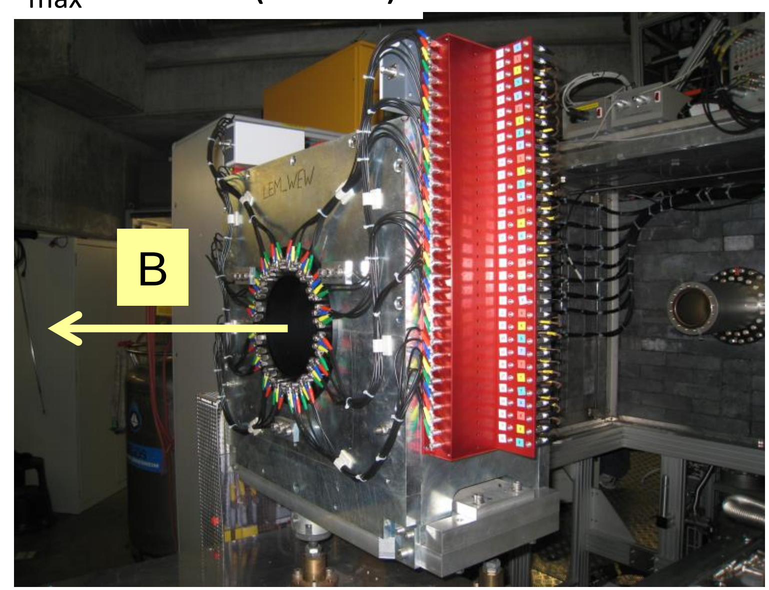

AWE Magnet (B parallel)

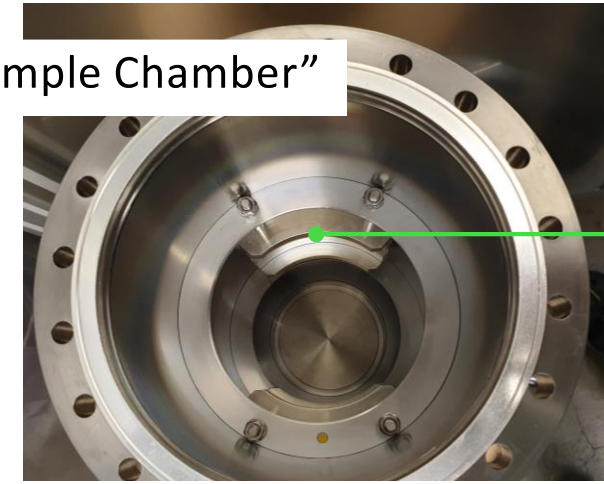

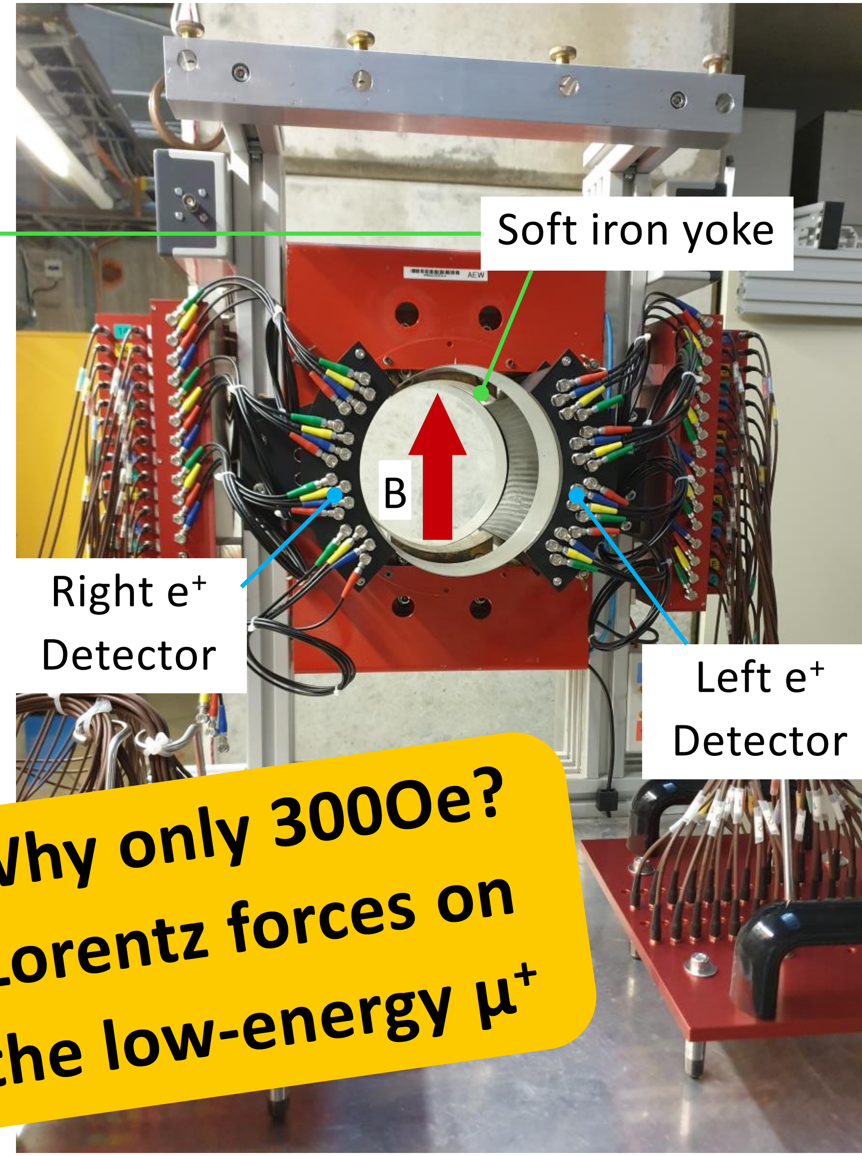

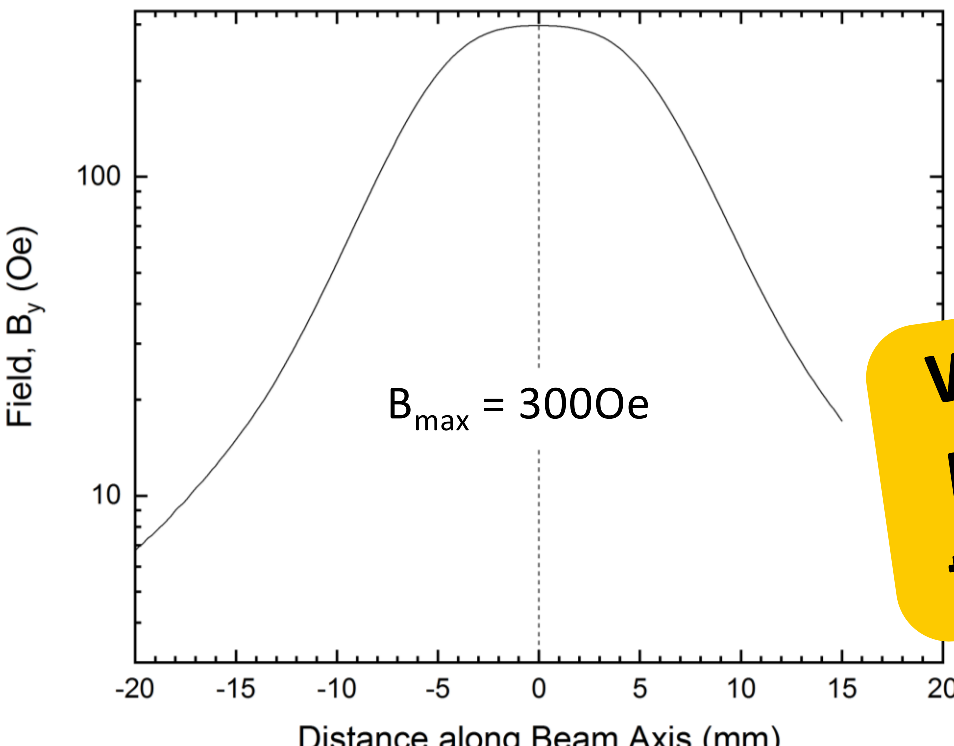

Why only 300Oe? Lorentz forces on the low-energy μ^+

LEM – Sample Plates

Sample plates:
- Ag coated pure aluminum
- Ni coated pure aluminum

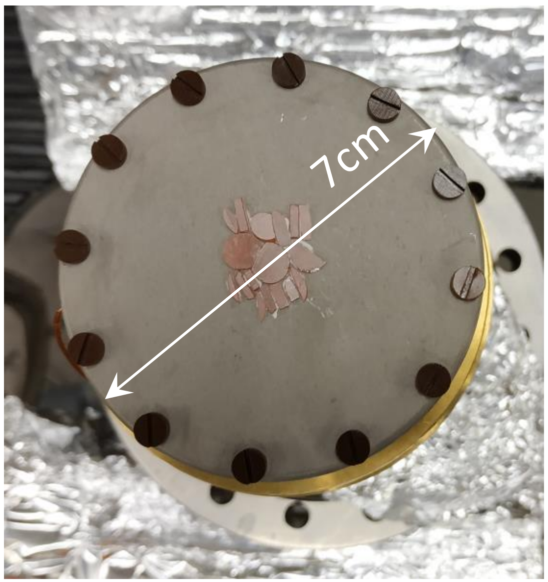

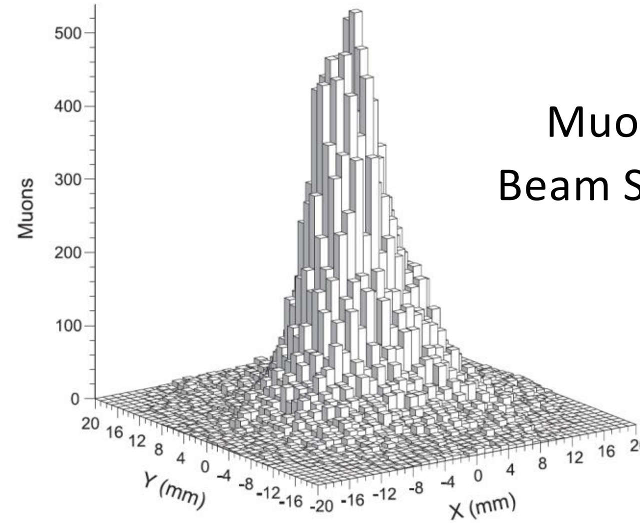

Muon
Beam Spot

Sample size dependent
Muon fraction

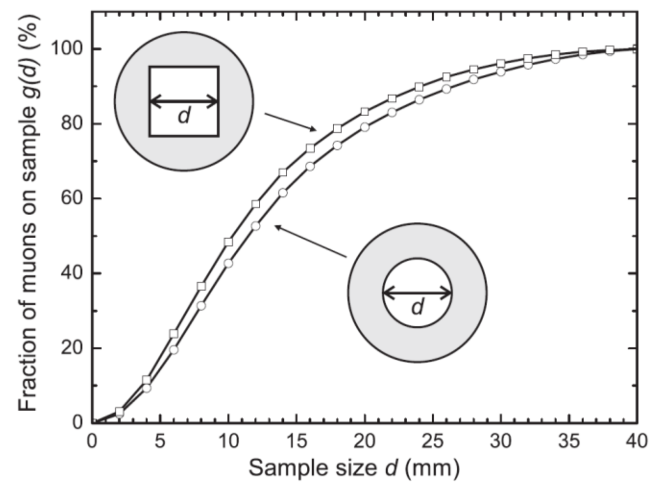

How do we deal
with the background?

LEM – Sample Plates

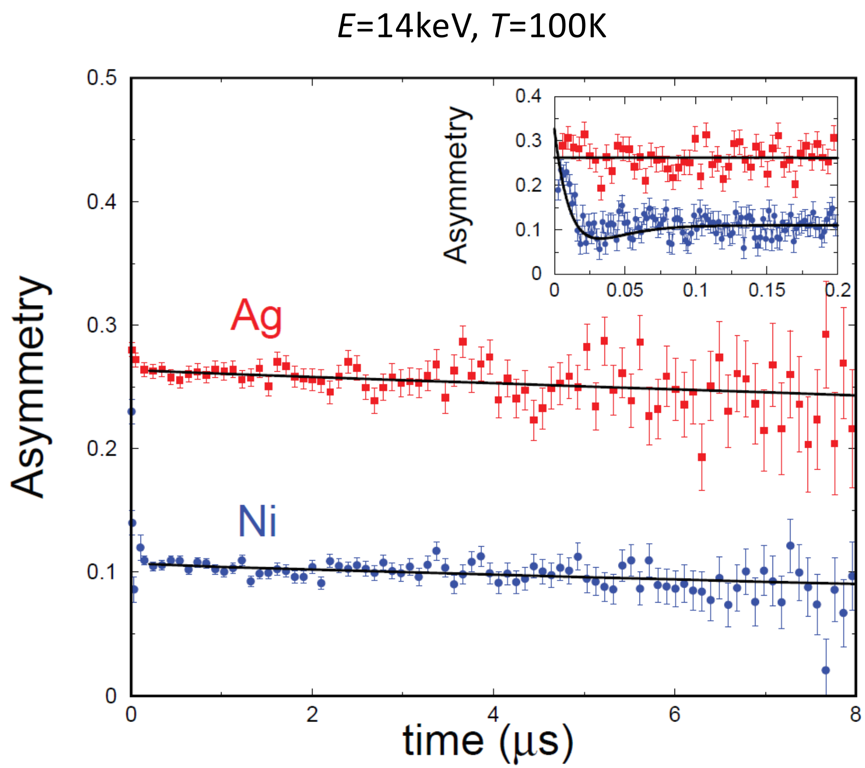

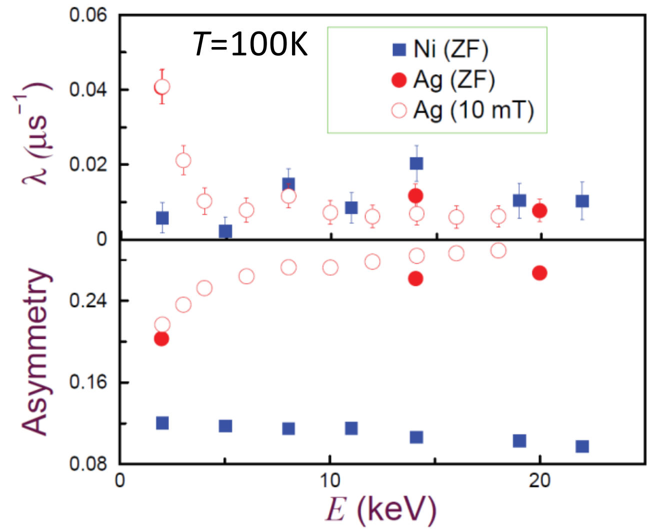

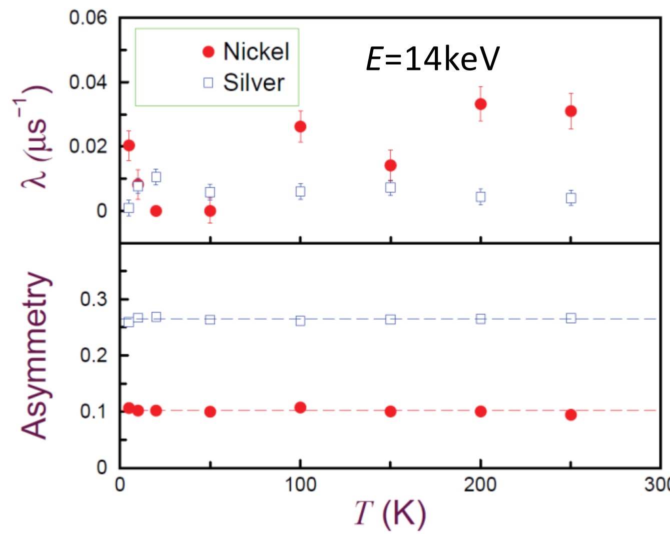

Ni coated sample plates act as passive veto system of low-energy μ^+ missing the sample

H. Saadaoui, *et al.* Physics Procedia **30,** 164 (12).

Low Energy μ^+ Stopping Profiles

Calculated by the Monte Carlo code TRIM.SP

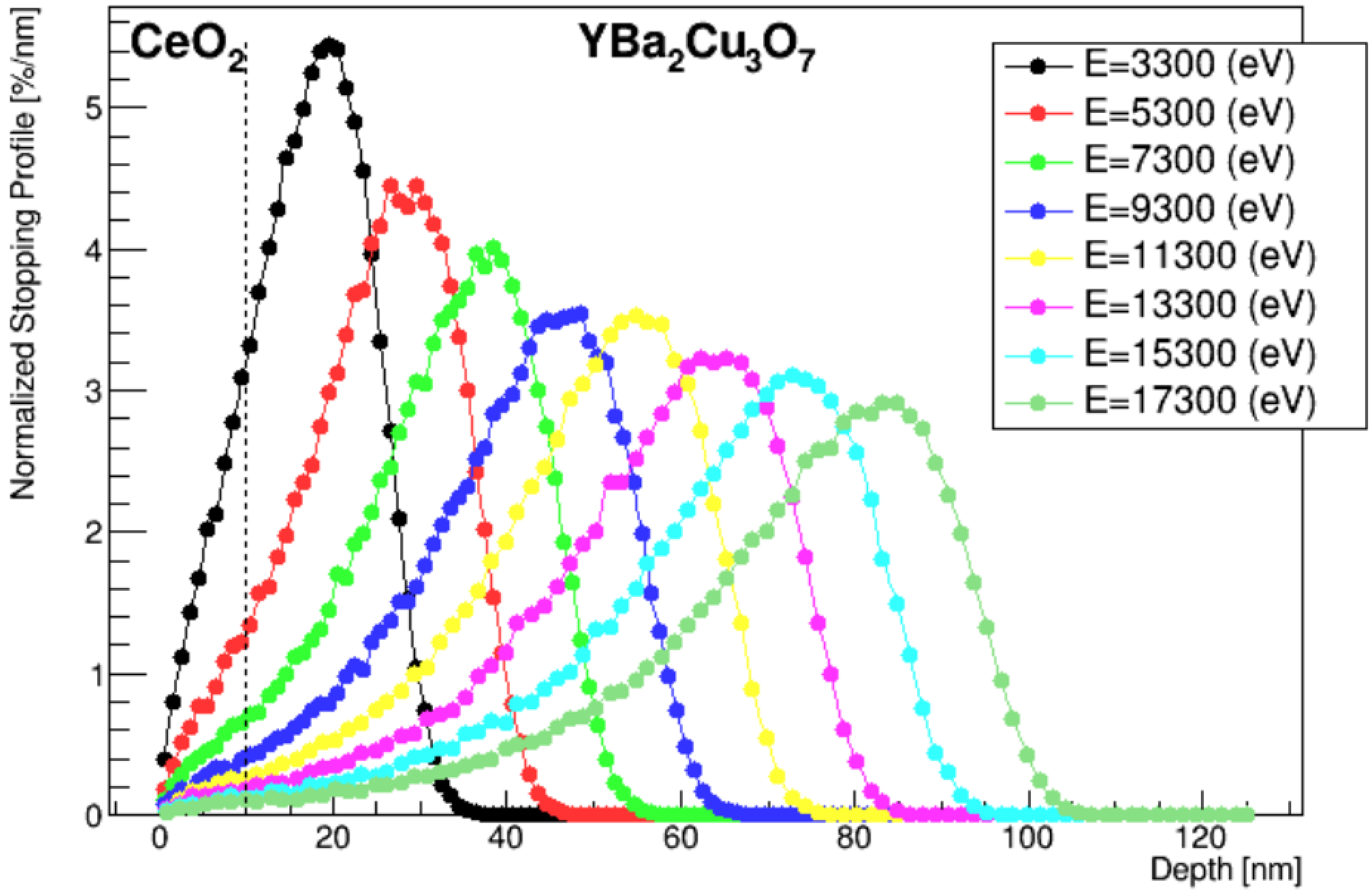

Ref. TRIM.SP: W. Eckstein "Computer Simulation of Ion-Solid Interactions", Springer (1991).

Particles Stopping in Matter

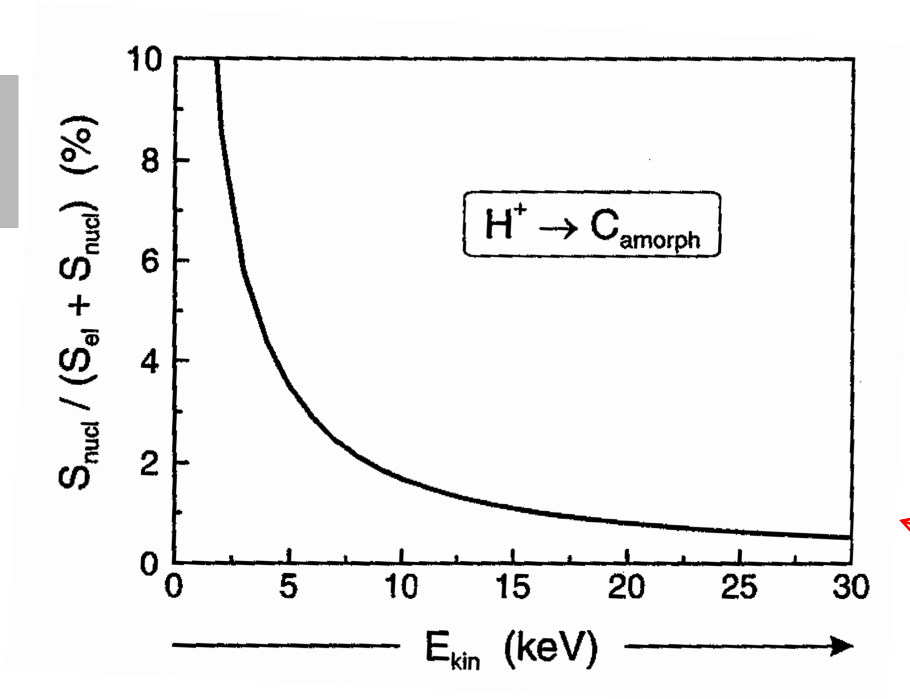

Energy loss of particles in matter: Stopping Power

$$S = -\frac{dE}{dx}$$

$$S = S_{\mathrm{el}} + S_{\mathrm{nucl}}$$

Nuclear Energy Loss
mainly important at
very low implantation energies

W. Eckstein, “Computer Simulation of Ion-Solid Interactions”, Springer (1991).
J.F. Ziegler, J.P. Biersack, M.D. Ziegler, “SRIM - The Stopping and Range of Ions in Matter”, Lulu Press Co.

Particles Stopping in Matter

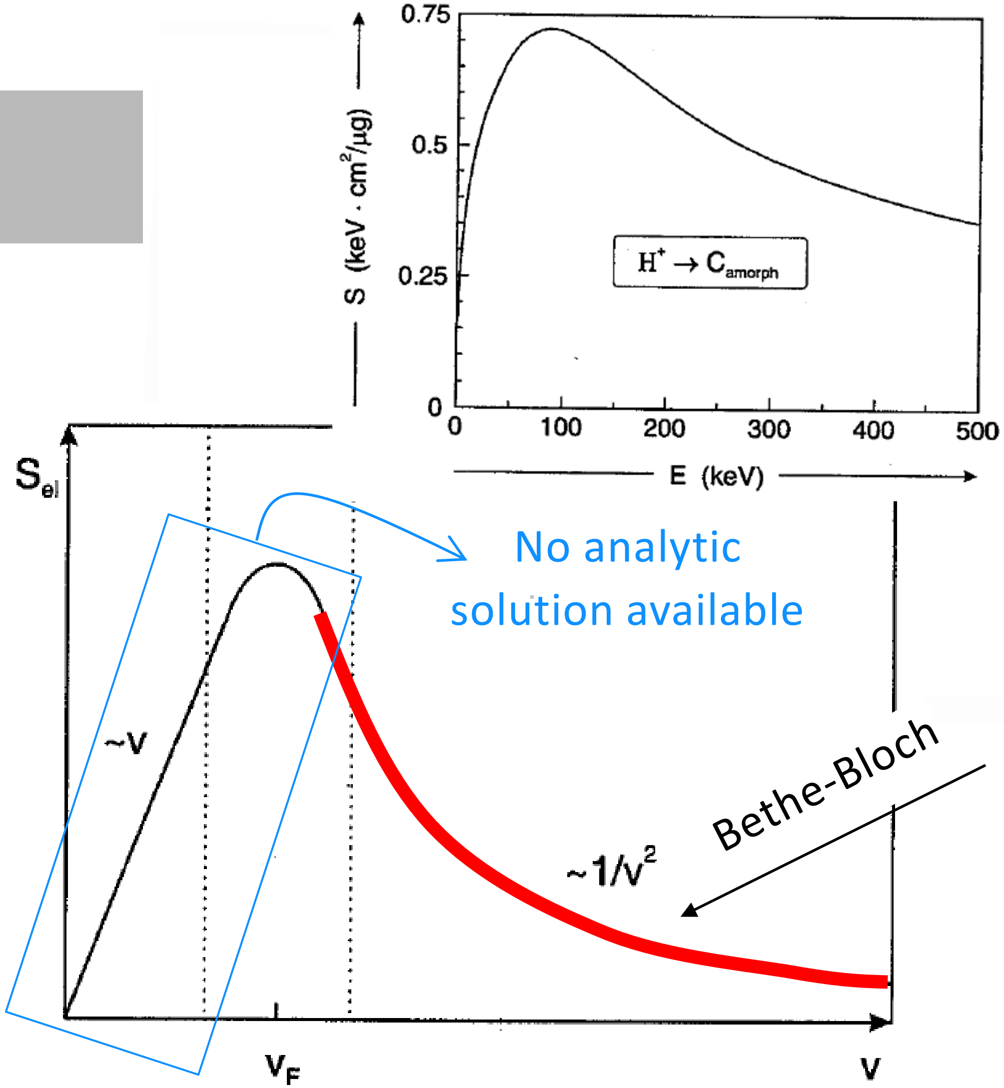

Energy loss of particles in matter: Stopping Power

$$S = -\frac{dE}{dx}$$

$$S = S_{\mathrm{el}} + S_{\mathrm{nucl}}$$

$$v \gg v_{\mathrm{F}}$$

$$S = \left(\frac{e^2}{4\pi\epsilon_0}\right)^2 \ln\left[\frac{2m_e v^2}{E_{\mathrm{I}}}\right] \frac{4\pi n z^2}{m_e v^2}$$

z : charge of the projectile

v : speed of the projectile

n : electron mean density of the target

m_e : electron mass

E_{I} : average ionisation energy of the traget material

W. Eckstein, "Computer Simulation of Ion-Solid Interactions", Springer (1991).
J.F. Ziegler, J.P. Biersack, M.D. Ziegler, "SRIM - The Stopping and Range of Ions in Matter", Lulu Press Co.

TRIM.SP, SRIM – check Monte Carlo Codes

Idea:

- Experimental fact: in fused quartz implanted μ^+ form almost 100% muonium, Mu, at almost all implantation energies.
- Grow sample on SiO_2, and do the following:

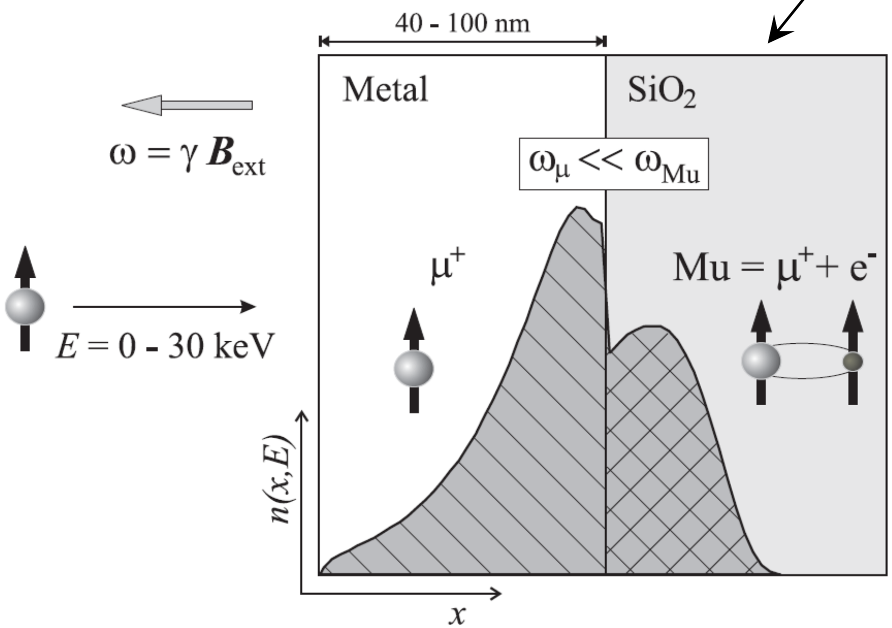

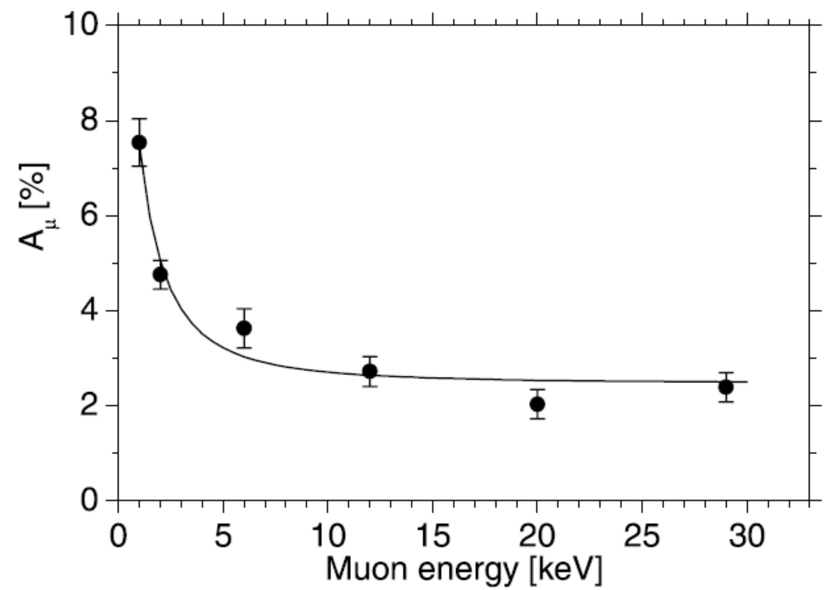

E. Morenzoni, *et al.* NIM **B 192**, 254 (02).

TRIM.SP, SRIM – check Monte Carlo Codes

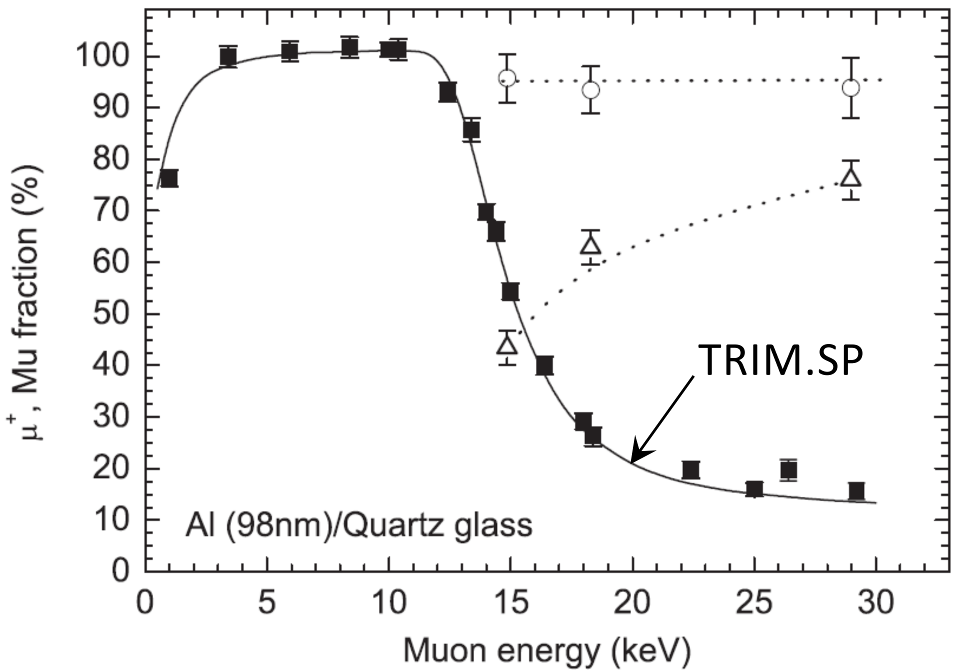

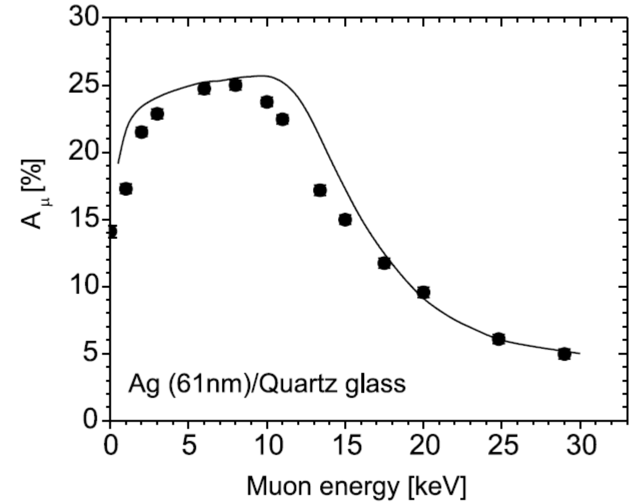

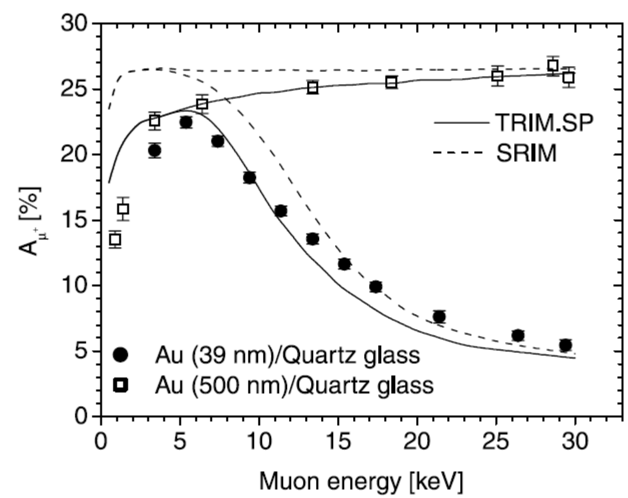

E. Morenzoni, *et al.* NIM **B 192**, 254 (02).

LE-μSR Studies
Selected Examples

Meissner Effect within the London Theory

1st London Eq.: $$\frac{\mathrm{d}\mathbf{j}}{\mathrm{d}t} = \frac{n_S e^2}{m}\mathbf{E}$$

2nd London Eq.: $$\nabla \wedge \mathbf{j} = -\frac{n_S e^2}{mc}\mathbf{B}$$

$$\nabla \wedge \mathbf{B} = \frac{4\pi}{c}\mathbf{j}$$

$$\nabla \wedge \nabla \wedge \mathbf{B} = 4\pi \frac{n_S e^2}{mc^2}\mathbf{B} = \frac{1}{\lambda_L^2}\mathbf{B}$$

Boundaries:
Half plane
+
$B(0) = B_0$

$$B_z(z) = B_0 \exp(-z/\lambda_L)$$

Boundaries:
film with
thickness $2t$
+
$B(0) = B_0 = B(2t)$

$$B_z(z) = B_0 \frac{\cosh\left[(t-z)/\lambda_L\right]}{\cosh(t/\lambda_L)}$$

Measure Meissner Screening with LEM - Principle

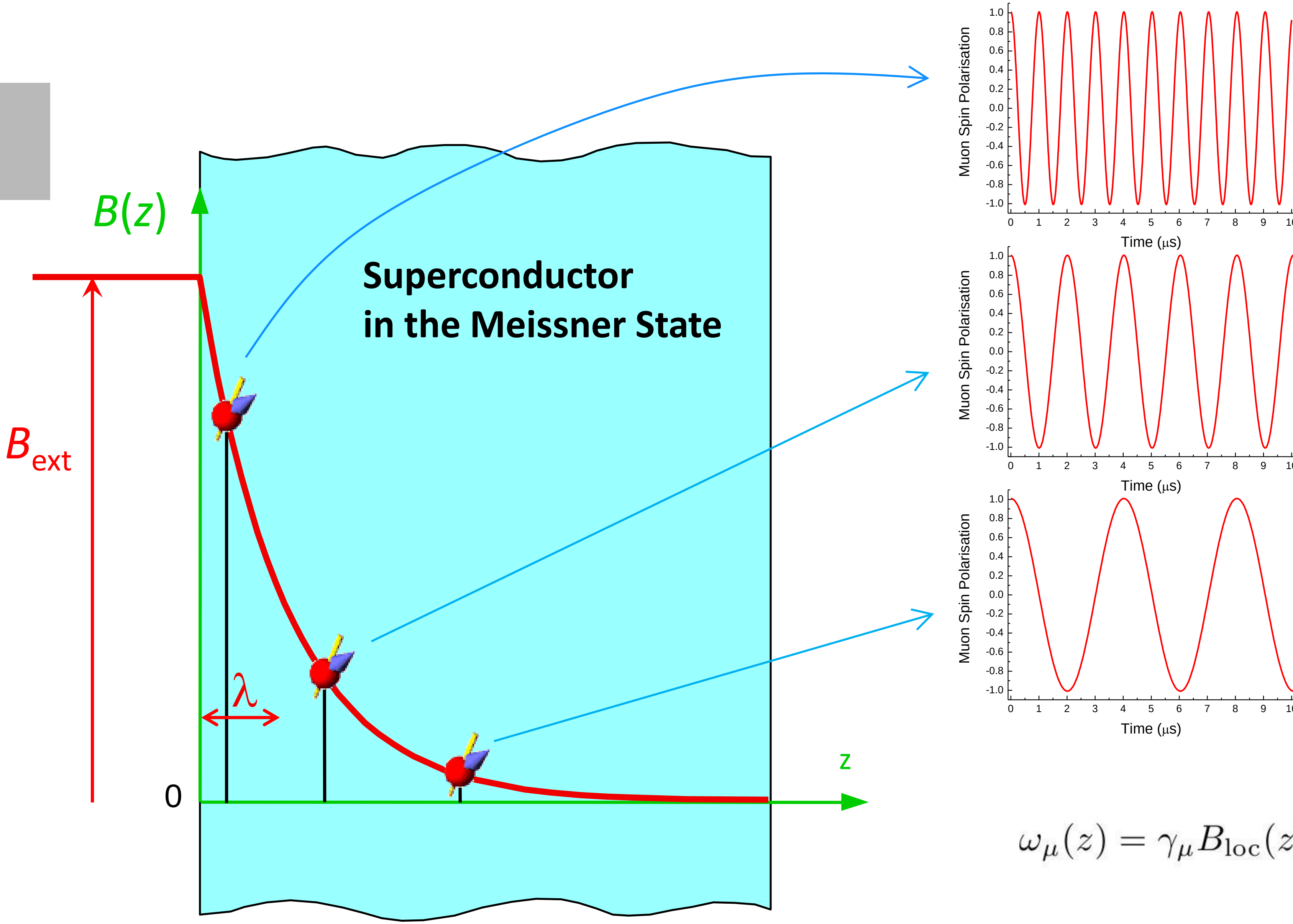

$$\omega_\mu(z) = \gamma_\mu B_{\rm loc}(z)$$

Measure Meissner Screening with LEM YBCO as an Example

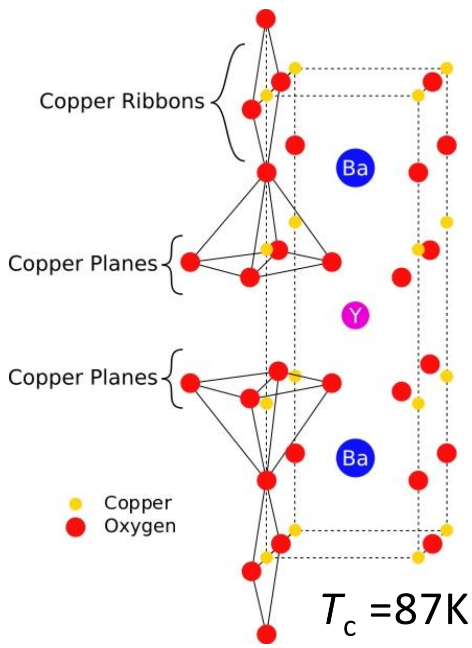

T_c =87K

Measuring Protocol:

1. Zero Field Cooling to base temperature
2. Apply a field and correct the beam steering
3. Perform an energy scan
4. Warmup to $T>T_c$ (field untouched)
5. Preform another energy scan

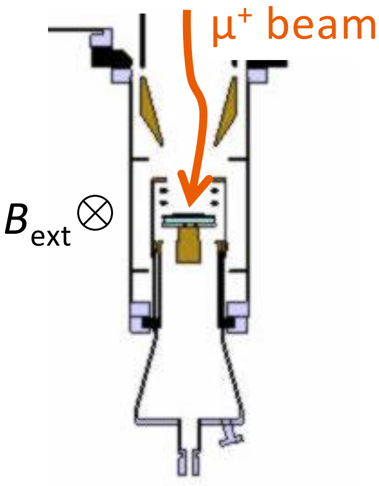

Measure Meissner Screening with LEM
YBCO as an Example

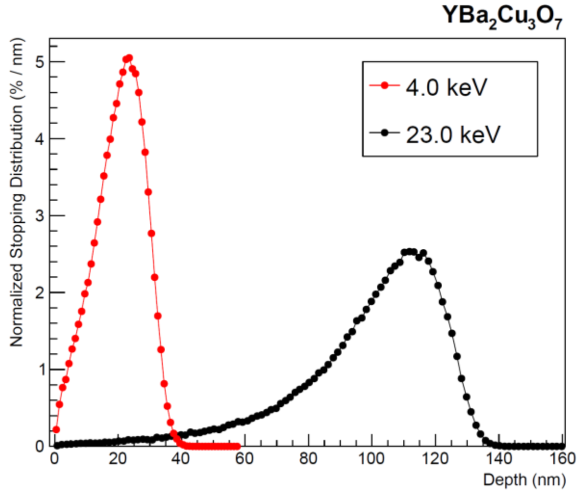

Fit function:

$$P(t) = \cos(\gamma_\mu B t + \phi) \exp\left[-(\sigma t)^2/2\right]$$

E=4keV

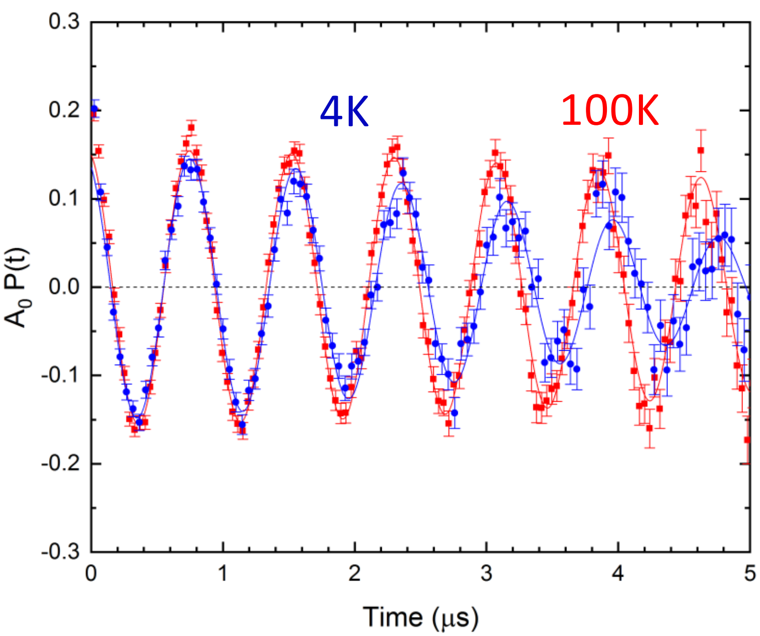

E=23keV

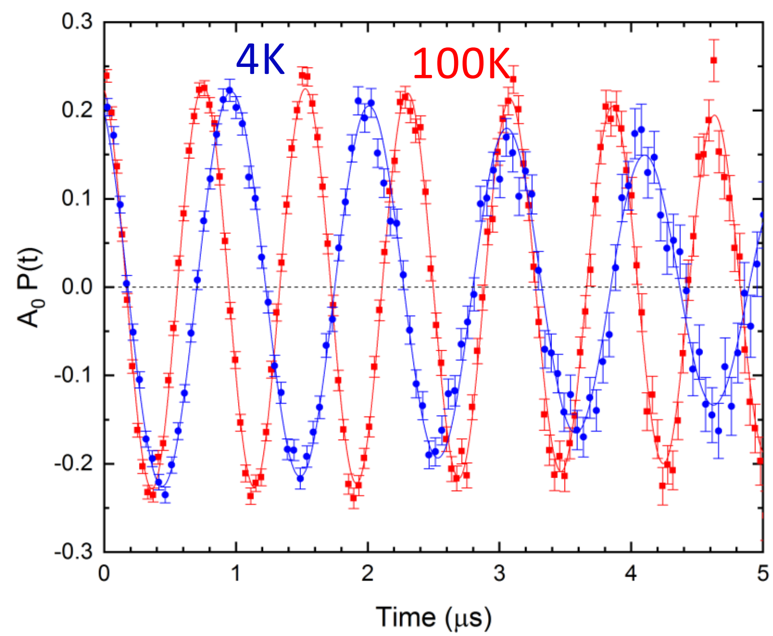

Measure Meissner Screening with LEM YBCO as an Example

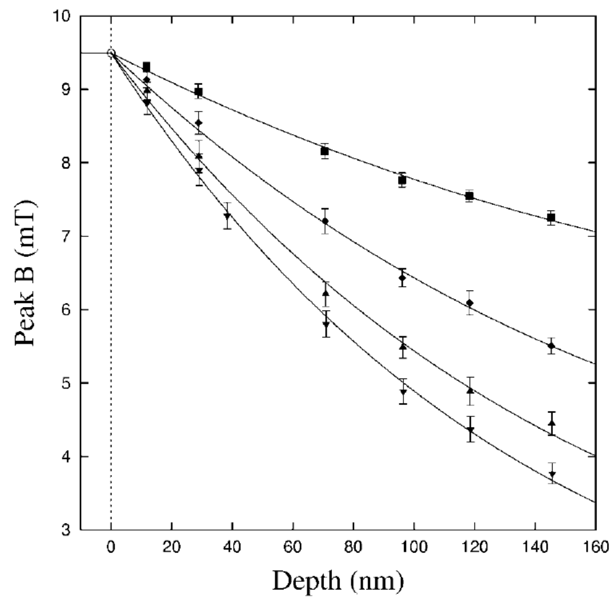

FIG. 3. Values of field versus depth for various values of sample temperature (▼) 20 K, (▲) 50 K, (◆) 70 K, and (■) 80 K. The solid lines represent fits of Eq. (5) to the data with λ_L as the free parameter. The implantation depth has been corrected by a fixed amount z_0 mainly to allow for the slight surface roughness of the sample. The thickness $2t$ was not corrected, because z_0 is comparable with the error in the thickness and small changes in $2t$ have a negligible effect on the fit parameters.

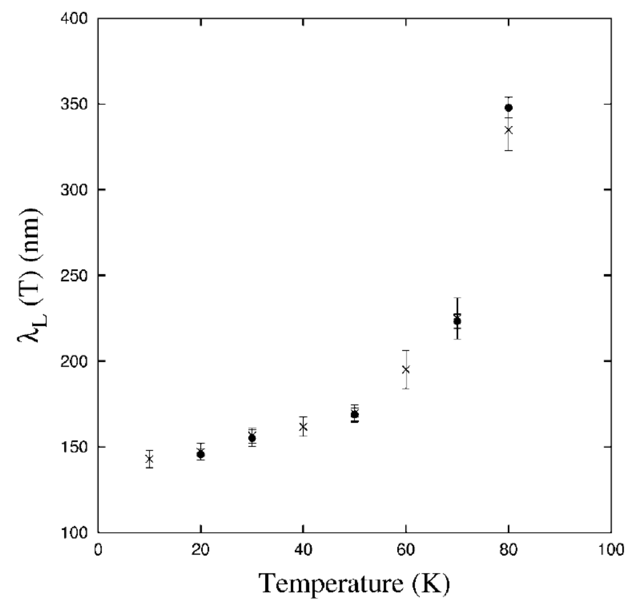

FIG. 4. The temperature dependence of the penetration depth λ_L arising from supercurrents in the basal plane of our YBCO sample. (●) Values derived from the fits in Fig. 3. (×) Data from the field distributions observed in the mixed state of the same sample [25]. Excellent agreement is seen between the two techniques.

T.J. Jackson, *et al.* PRL **84**, 4958 (00).

Measure Meissner Screening with LEM YBCO as an Example – Dead Layer

$$B(z) = B_0 \frac{\cosh[(t - z)/\lambda_L)]}{\cosh(t/\lambda_L)}. \qquad (5)$$

This is the form taken by Eq. (3) for a film of thickness $2t$, with flux penetrating from both surfaces. The value of z in Eq. (5) has been corrected by a small quantity z_0, corresponding to a "dead layer." This may partly be due to

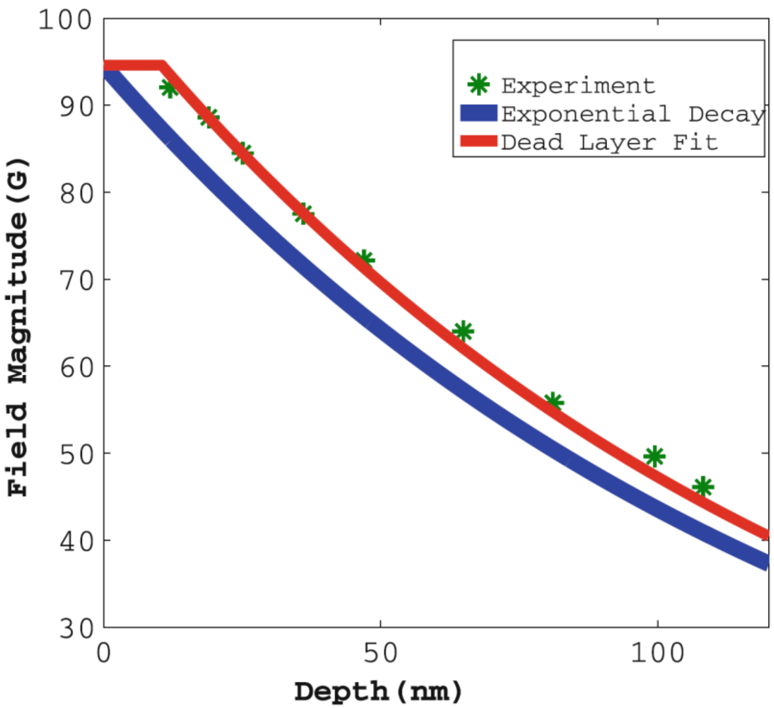

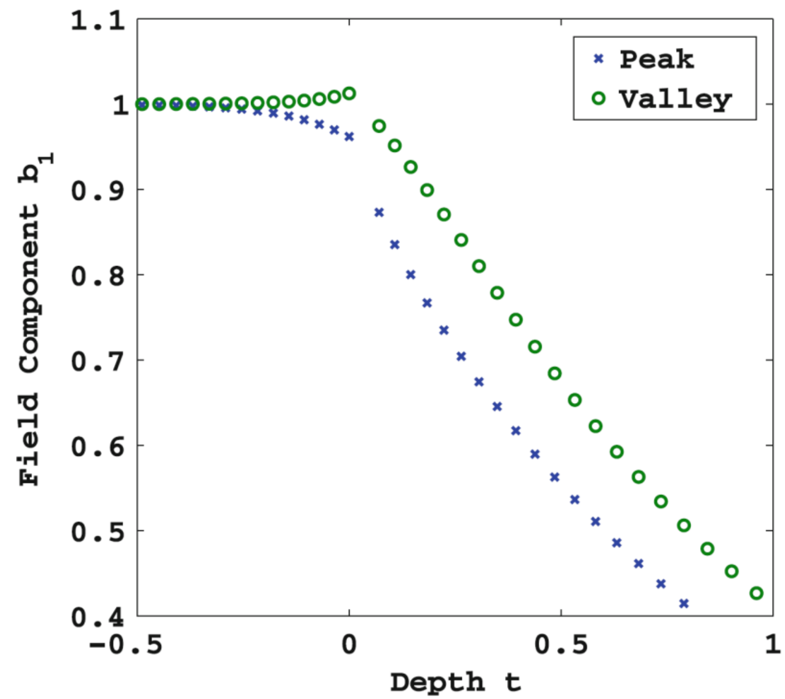

Surface roughness on the scale λ has the largest impact on the $B(z)$ variation close to the interface (≈ λ/10).

Measurements on indium, which has a self-assembling surface, show that the dead layer is 0.

M. Lindstrom, *et al.*, J. Eng. Math. DOI 10.1007/s10665-013-9640-y

Measure Meissner Screening with LEM YBCO as an Example – Anisotropy

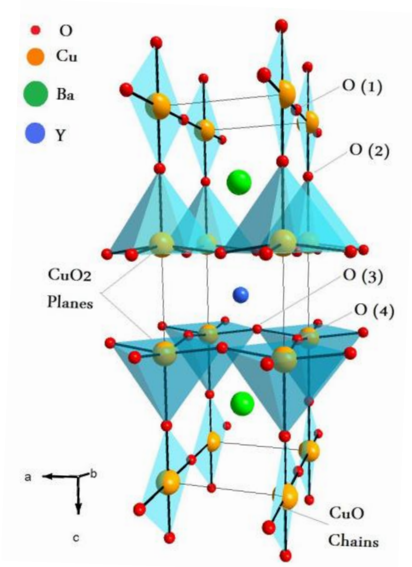

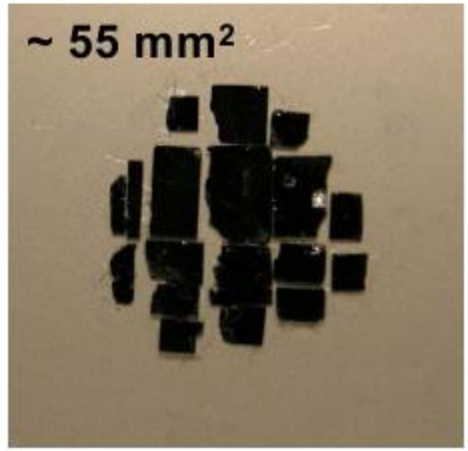

samples produced by
R. Liang, W. Hardy, D. Bonn,
Univ. of British Columbia

Detwinned (>95%) $YBa_2Cu_3O_{6.95}$ crystals optimally doped
(T_c= 94.1 K, $\Delta T_c \leq$ 0.1K)

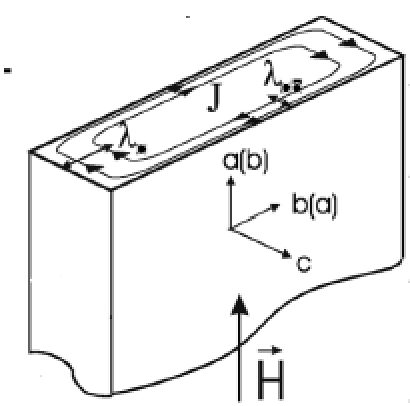

$$\vec{H}_{ext} \parallel \hat{a}\text{-axis} \rightarrow \lambda_b$$

$$\vec{H}_{ext} \parallel \hat{b}\text{-axis} \rightarrow \lambda_a$$

$$\lambda(T) \propto \sqrt{\frac{m^*}{n_S(T)}}$$

← **effective mass**
← **superfluid density**

Allows to measure the temperature dependence of n_S (T), and hence, i.e. the gap symmetry.

R.F. Kiefl *et al.*, PRB **81**, 180502(R), (2010).

Measure Meissner Screening with LEM
YBCO as an Example – Anisotropy

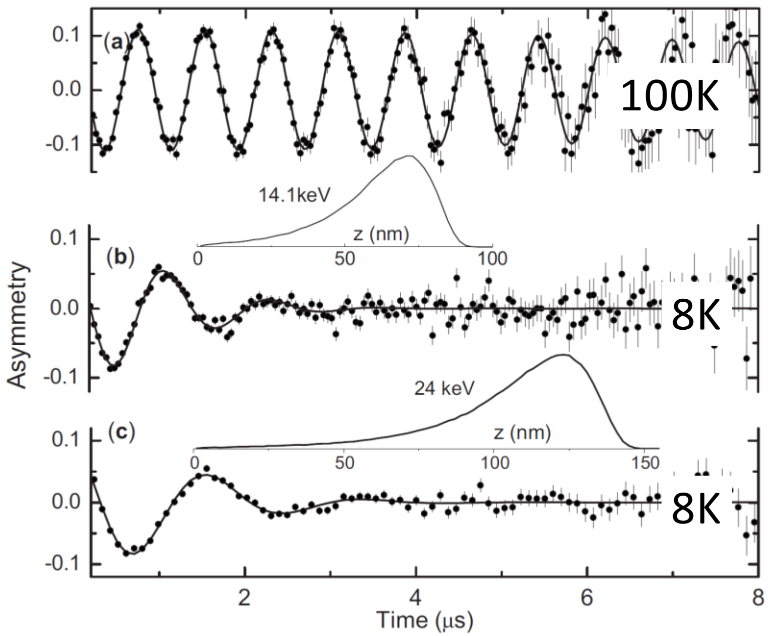

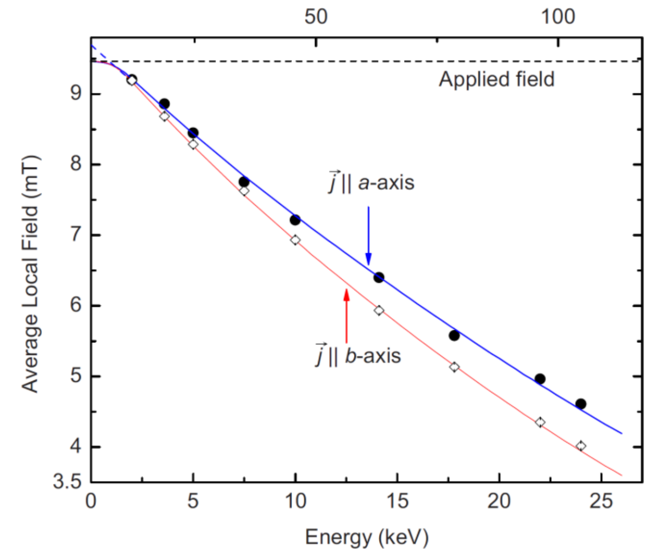

μ^+ stopping distribution

$B(z)$ model, e.g. exponential

$$B(z) = \begin{cases} B_0 \exp[-(z-d)/\lambda_{a,b}] & z \geq d \\ B_0 & z < d, \end{cases}$$

$$\mathcal{A}(t) = A\,\exp[-\sigma^2 t^2/2]\int \rho(z)\cos[\gamma_\mu B(z)t + \phi]dz$$

λ_a = 126(1.2)nm, λ_b = 105.5(1.0) nm, λ_a/λ_b =1.19(1)

d-wave superconductor

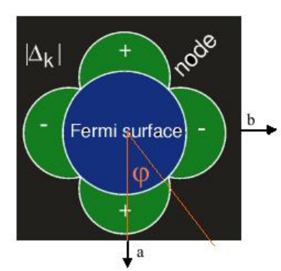

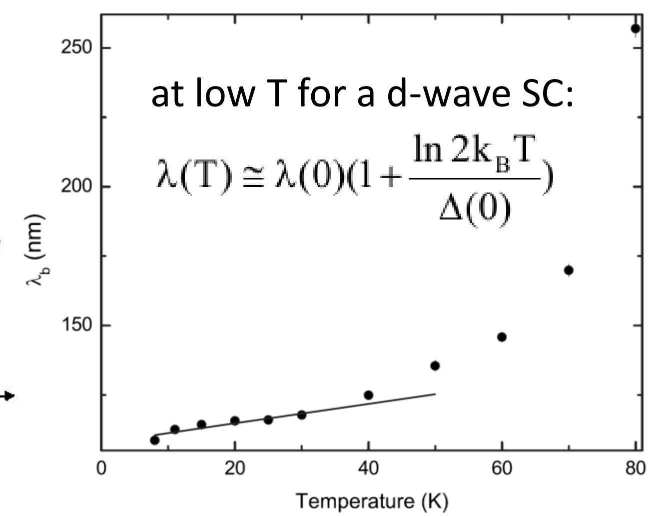

R.F. Kiefl *et al.*, PRB **81**, 180502(R), (2010).

Dimensionality Control of Electronic Phase Transitions

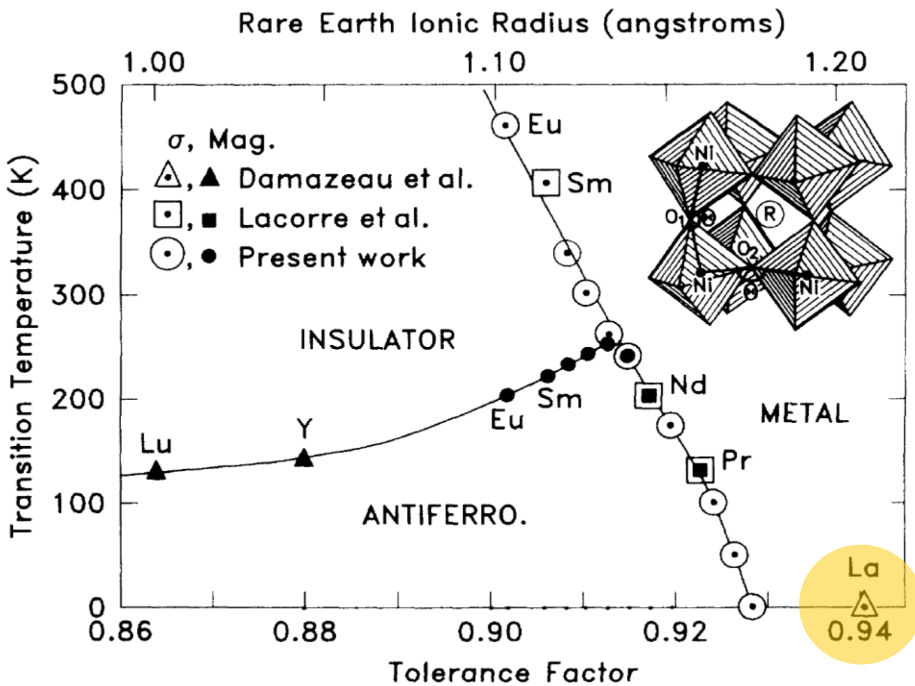

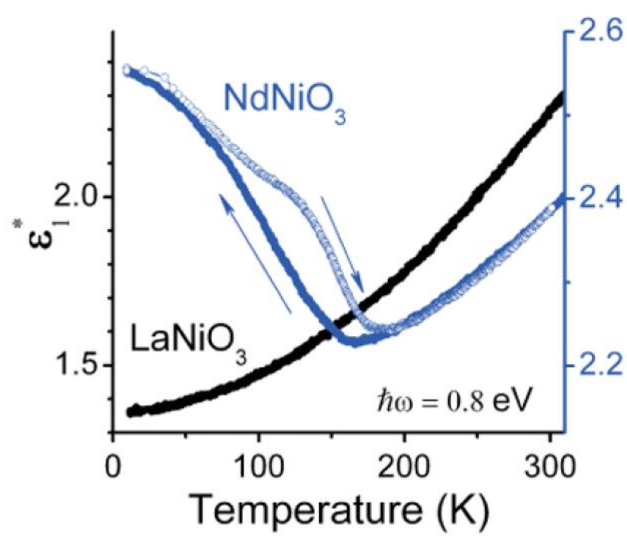

$RNiO_3$

Orthorhombic distortion decreases with increasing rare earth ion radius.

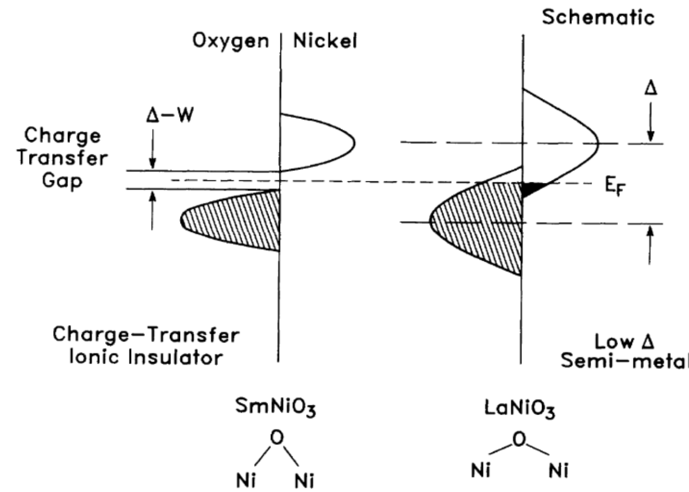

J.B. Torrance, *et al.*, PRB **45**, 8209R (92).
A.V. Boris, *et al.*, Science **332**, 937 (11).

Dimensionality Control of Electronic Phase Transitions

Motivation

- Dimensional tuning of collective electronic phases in order to stabilize new phases.
- $LaNiO_3$ is a correlated metallic paramagnet down to the lowest temperatures, whereas $RNiO_3$ are typically showing a metal-insulator transition, accompanied by a magnetic phase transition, e.g. $NdNiO_3$. Hence $LaNiO_3$ is an interesting case.

$LaNiO_3/LaAlO_3$ SL

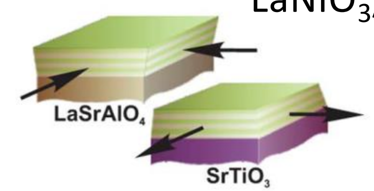

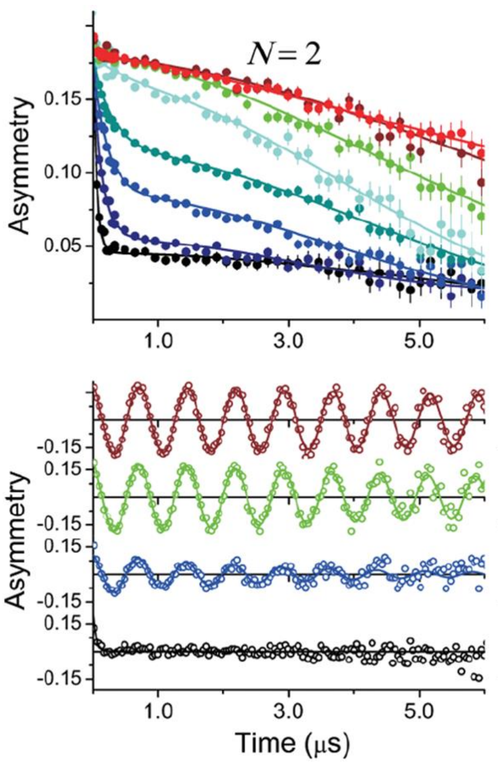

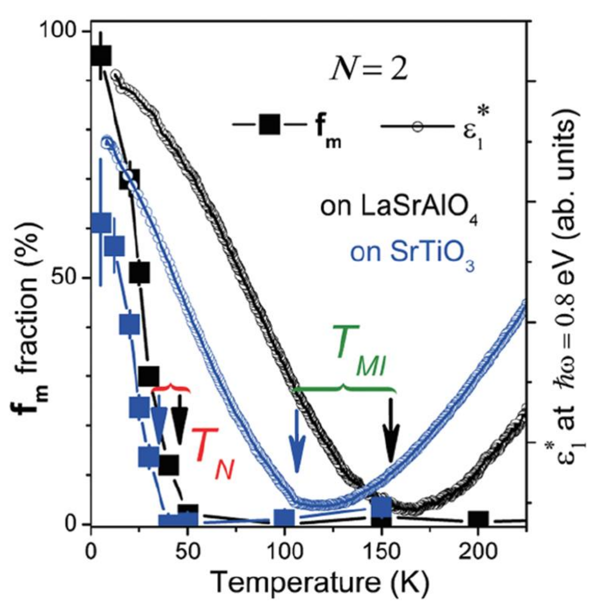

Results

- $LaNiO_3/LaAlO_3$ *N*=4 superlattices are similar to $LaNiO_3$ bulk.
- $LaNiO_3/LaAlO_3$ *N*=2 superlattices show a metal-insulator transition, and at lower temperature a magnetic phase transition (likely to be antiferromagnetic).
- Contrary to bulk, $T_{MI} \neq T_N$.
- Strain is NOT the driving mechanism since both superlattices grown on $LaSrAlO_4$ or $SrTiO_3$ substrates show a similar behaviour.

A.V. Boris, *et al.*, Science **332**, 937 (11).

PAUL SCHERRER INSTITUT PSI

Semiconductors – μ^+ to Measure Charge Carrier Profiles
Example 1: p-doped Ge

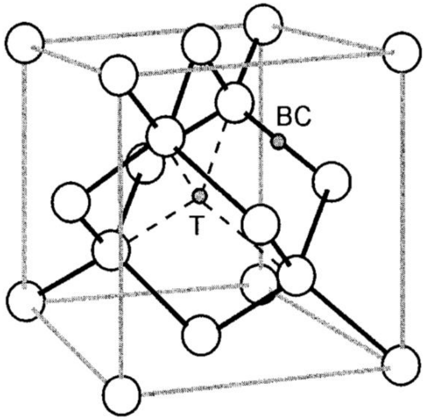

Possible muon charge states:

- "bare" $\mu^+ = Mu^+$ (diamagnetic)
- $\mu^+ + e^- = Mu^0$ (paramagnetic)
- $\mu^+ + 2\ e^- = Mu^-$ (diamagnetic)

Muon sites:

- Bond centered (BC): $Mu_{BC}^{(+,0)}$
- Tetrahedral interstitial size (T): $Mu_T^{(0,-)}$

Ge: Low Temperature

doping	Mu_T^-	Mu_T^0	Mu_{BC}^0
undoped	$\sim 10\%$	$\sim 75\%$	$10-20\%$
$n \sim 2 \times 10^{18}(cm^{-3})$	$\sim 30\%$	$\sim 55\%$	
$n \sim 2 \times 10^{19}(cm^{-3})$	$\sim 80\%$	$\sim 0\%$	

➡ Muon charge state fractions depend strongly on the doping

B.D. Patterson, RMP **60**, 69 (88).
S.F.J. Cox, Reports on Progress in Physics **72**, 116501 (09).

Semiconductors – μ^+ to Measure Charge Carrier Profiles

Example 1: p-doped Ge

Measurements performed at T=220K:

- Mu_{BC}^{0} fully transformed to Mu_{BC}^{+}
- Mu_{T} is used as sensor for free hole carriers.

Charge-Exchange Cylces

$$\mathrm{Mu_T^0} \rightleftharpoons \mathrm{Mu_T^-} + \mathrm{h}$$

$$\mathrm{Mu_T^0} \rightarrow \mathrm{Mu_T^-} : \ \Lambda_\mathrm{i}(T) = \Lambda_0 \exp(-E_\mathrm{A}/(k_\mathrm{B}T))$$

$$\mathrm{Mu_T^-} \rightarrow \mathrm{Mu_T^0} : \ \Lambda_\mathrm{c}(T) = p \cdot (v_h \sigma_c^h)(T)$$

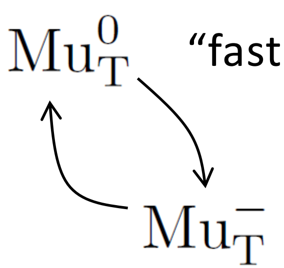

"fast" precession

"slow" precession
= $\gamma_\mu B_{ext}$

Simulation of TF measurements (B=10mT)

$$A(t) = A_\mathrm{D} e^{-\lambda t} \cos(\gamma_\mu B t + \phi)$$

$E_\mathrm{A} = 154\,\mathrm{meV}$
$\Lambda_0 = 3.2 \cdot 10^{13}\,\mathrm{s}^{-1}$

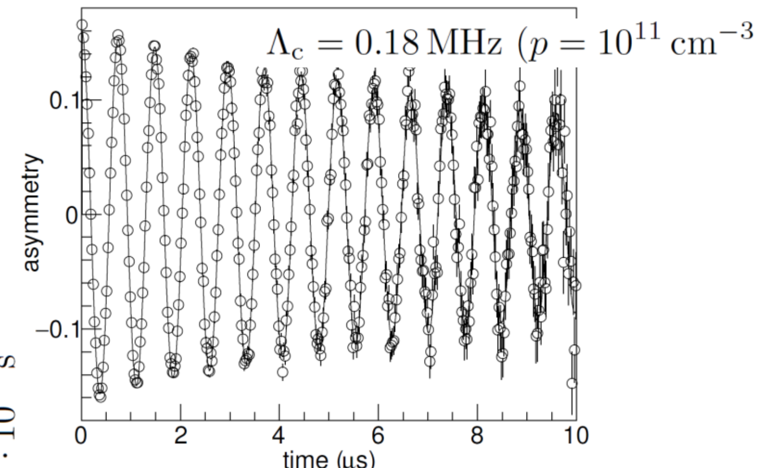

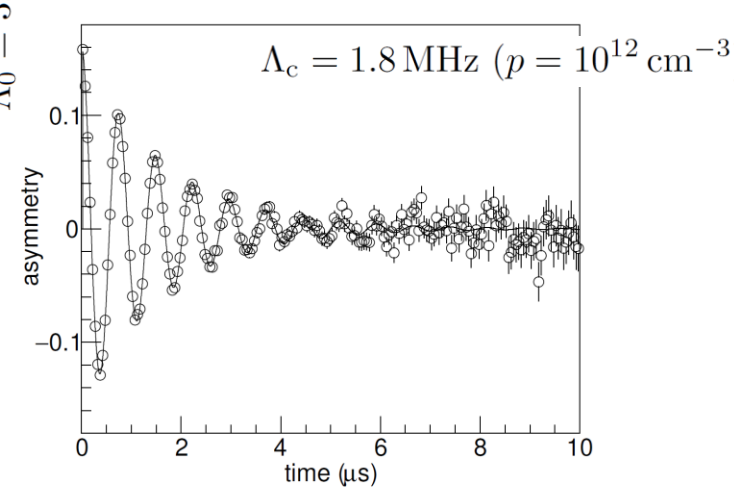

T. Prokscha, *et al.* in preparation.

Semiconductors – μ⁺ to Measure Charge Carrier Profiles

Example 1: p-doped Ge

Data imply following p profile:

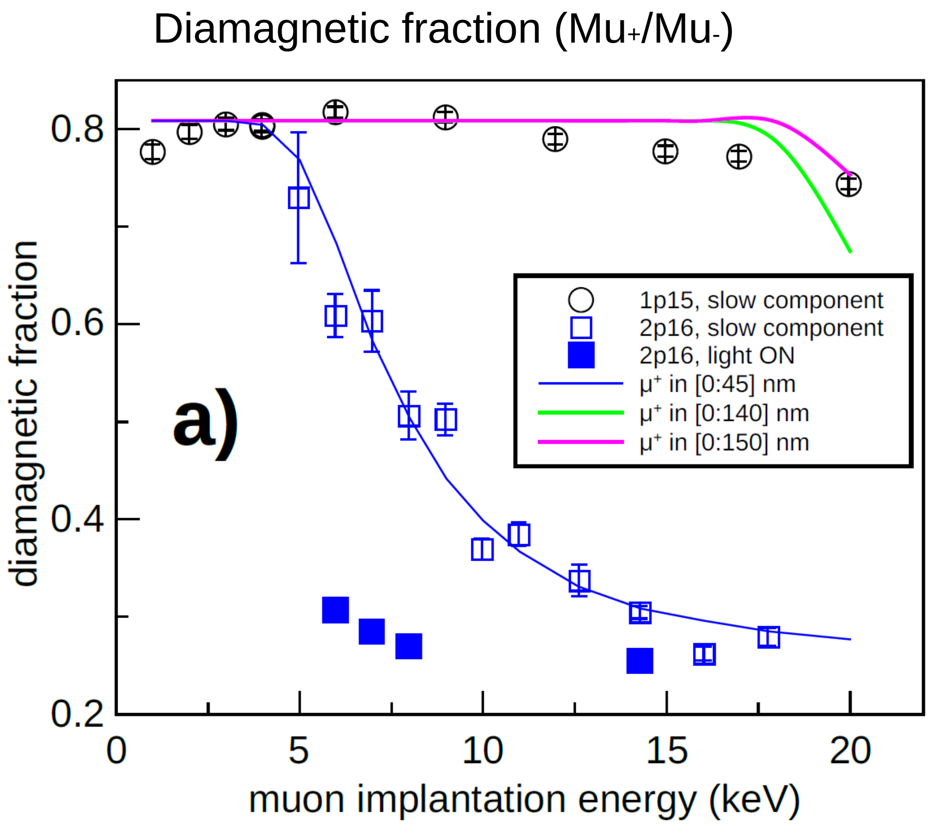

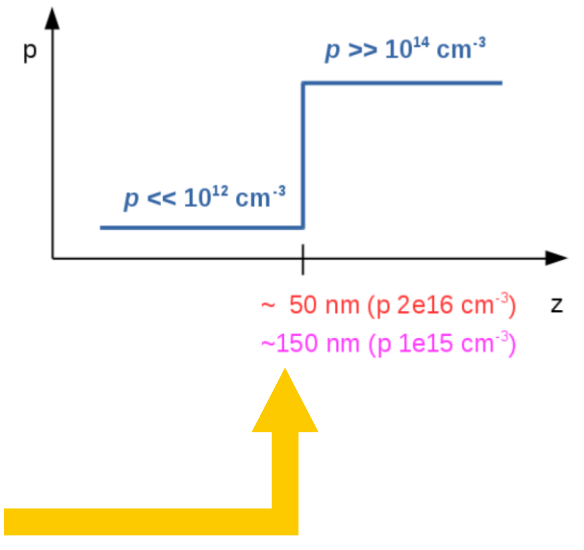

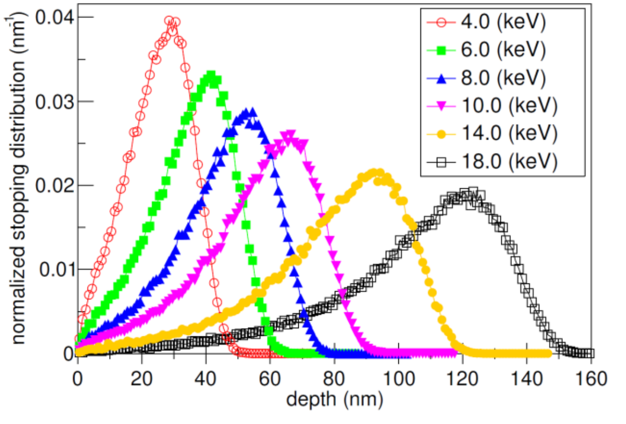

T. Prokscha, *et al.* in preparation.

Semiconductors – μ^+ to Measure Charge Carrier Profiles
Example 2: GaAs quantum well structure preliminary

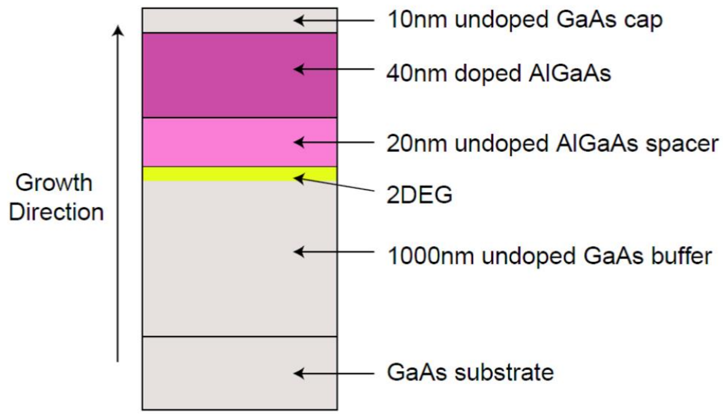

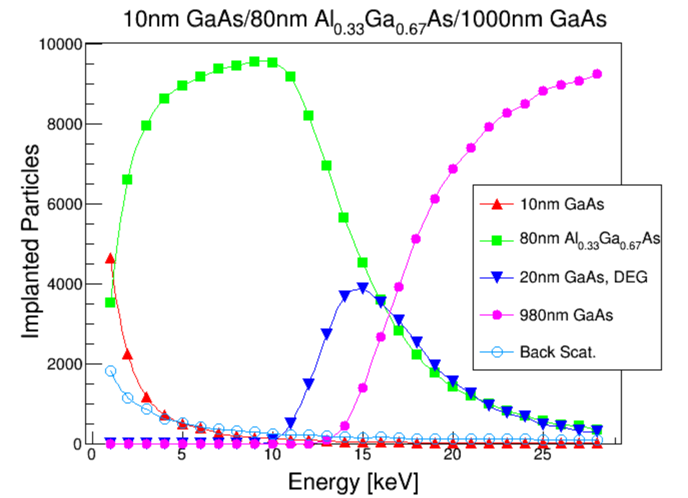

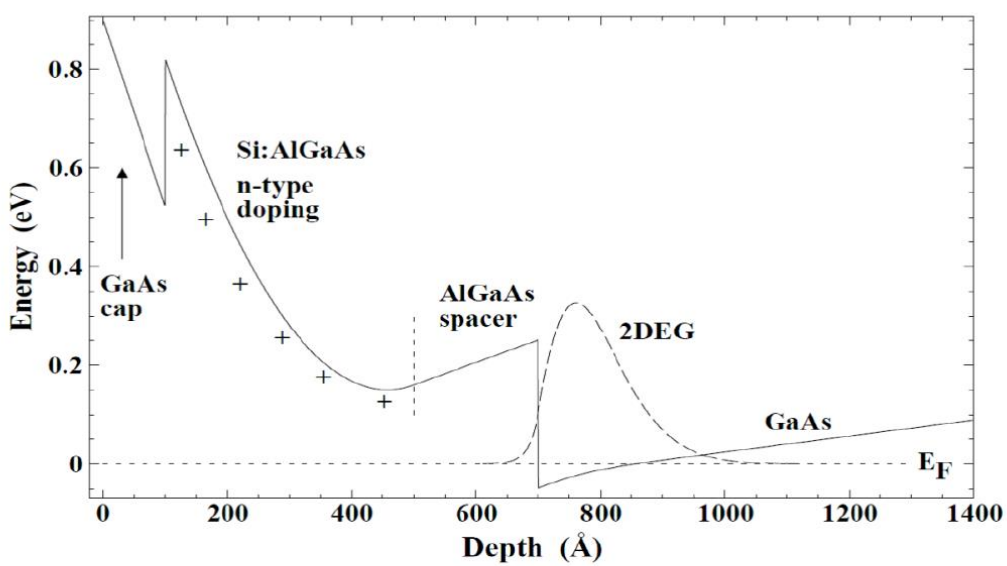

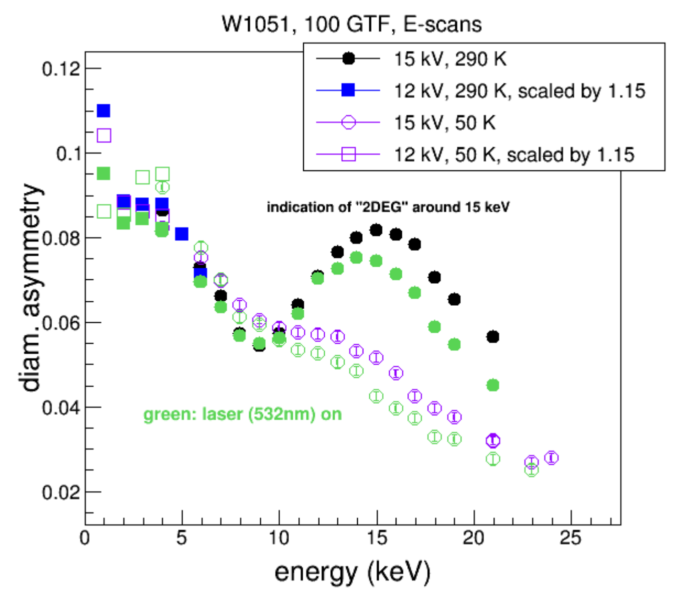

T. Prokscha, *et al.* – Samples MBE grown in the Semiconductor Physics Group, Cavendish Laboratory, U Cambridge

Spatially homogeneous ferromagnetism of (Ga,Mn)As

- Mn-doped GaAs has the potential as a "spintronics" material
- Great interest in fundamental research: evolution from a paramagnetic insulator to ferromagnetic metal

Potential Problem: solubility of Mn in GaAs

Mn tends to cluster in GaAs which would result in a spatially inhomogeneous state, rendering the material useless.

What information LE-μSR can provide other methods cannot?

- Magnetic volume fraction information obtained from weak transverse and zero field measurements.

S.R. Dunsiger, *et al.,* Nature Materials **9**, 299 (2010).

Spatially homogeneous ferromagnetism of (Ga,Mn)As

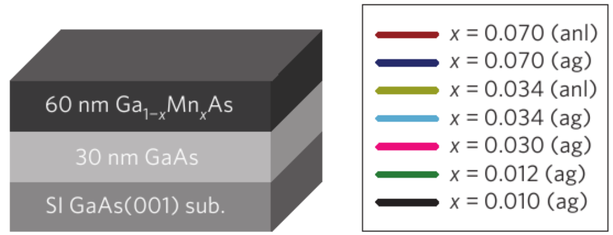

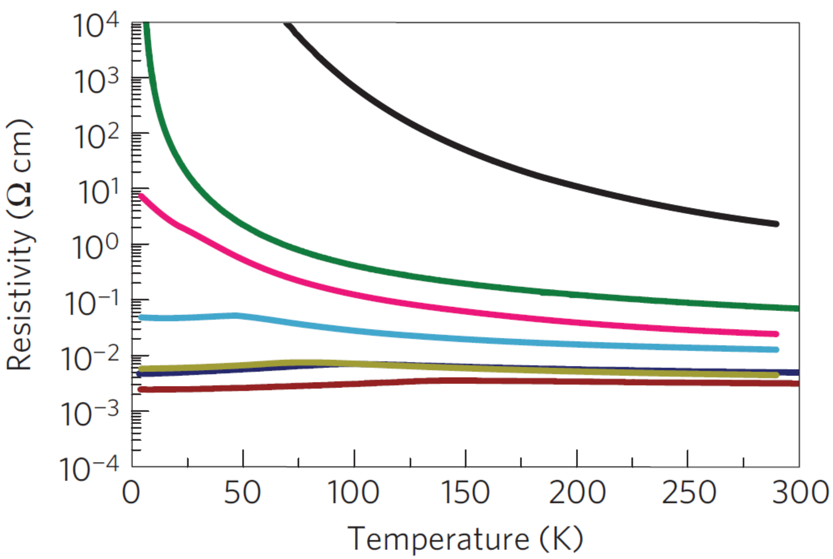

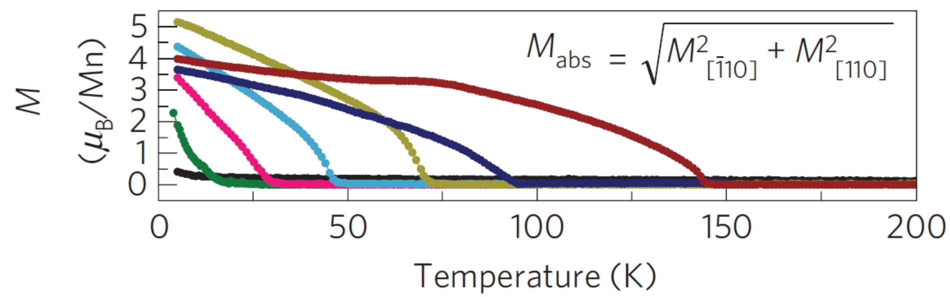

Metal-insulator transition found as function of Mn doping.

Is the MI transition essential to drive the system magnetic?

S.R. Dunsiger, *et al.*, Nature Materials **9**, 299 (2010).

Note to Weak Transfers Field Measurements

Purely static state:

$$P(t) = \int \left\{ \left(\frac{B_{\parallel}}{B}\right)^2 + \left(\frac{B_{\perp}}{B}\right)^2 \cos(\gamma_\mu B t) \right\} d^3 B \qquad B_{\parallel}^2 + B_{\perp}^2 = B^2$$

TF in a paramagnet

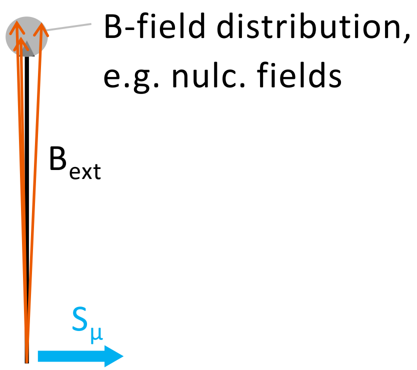

weakly damped asymmetry

ZF in simple AF

B_{int} isotropic

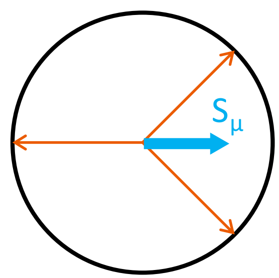

$P(t) = P_1 + P_2 \cos(\gamma_\mu B_{int}\, t)$

Weak TF in simple magnet

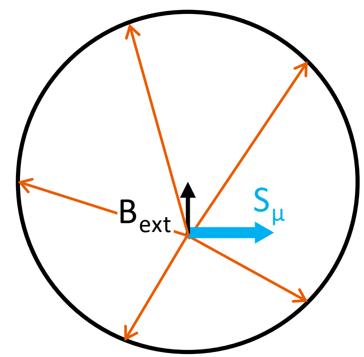

heavily damped or wiped out asymmetry

Spatially homogeneous ferromagnetism of (Ga,Mn)As

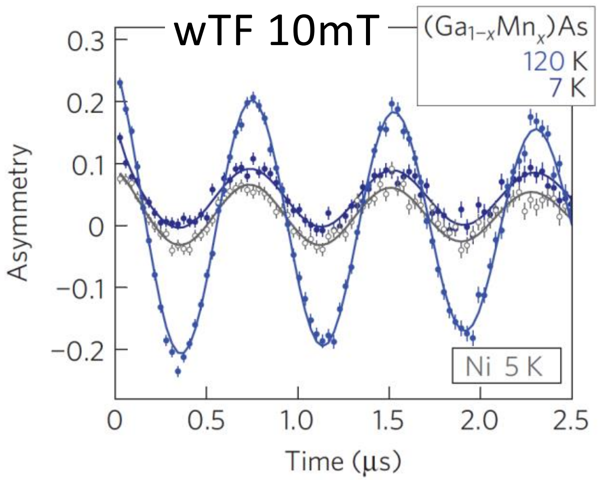

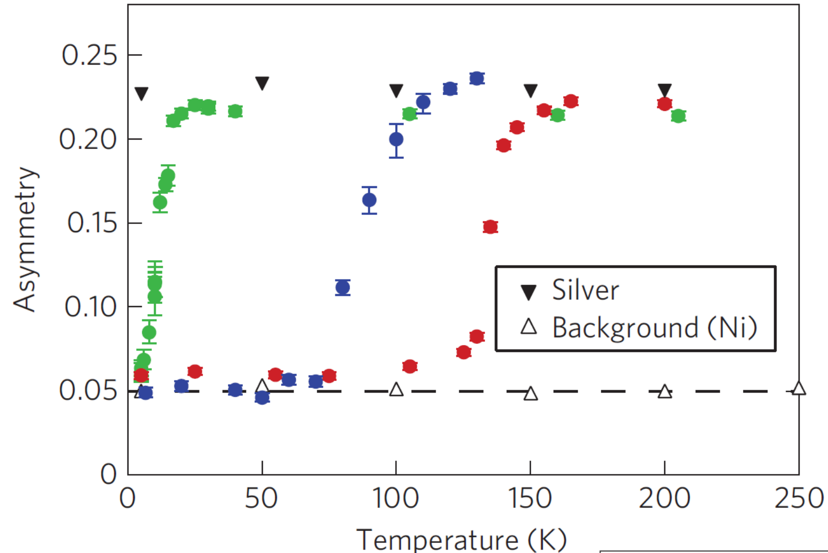

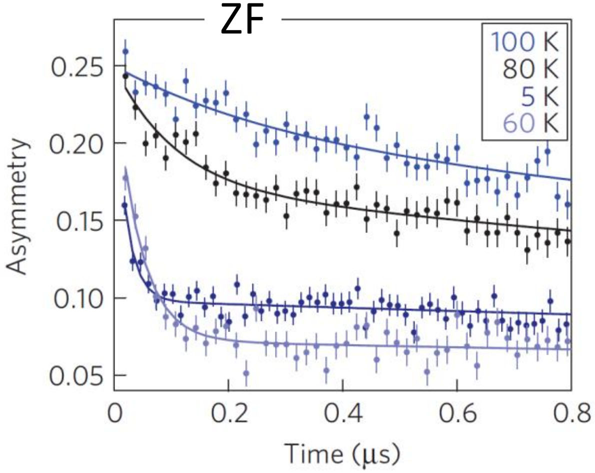

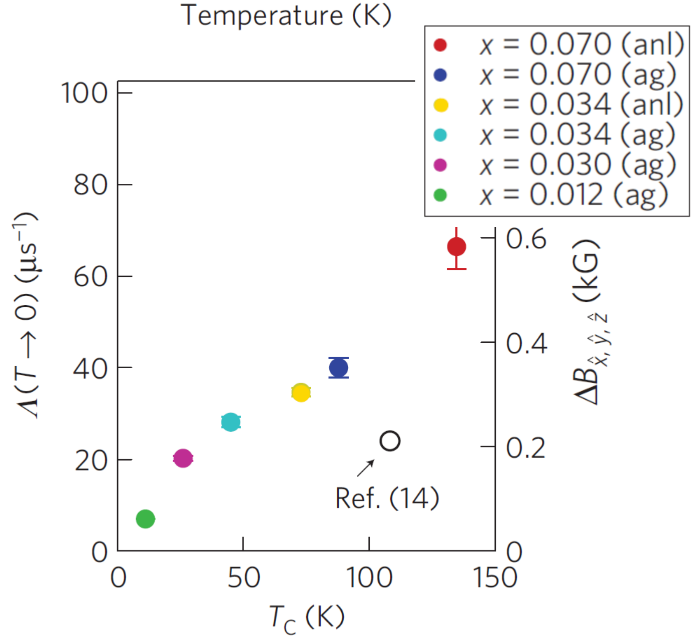

S.R. Dunsiger, *et al.,* Nature Materials **9**, 299 (2010).

Spatially homogeneous ferromagnetism of (Ga,Mn)As

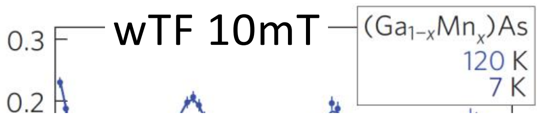

Low-energy µSR (in combination with conductivity and DC/AC mag.) **results**:

- sharp onset of FM order, developing homogeneously in the full volume fraction, in both insulating and metallic films.
- smooth evolution of ordered moment size across metal-insulator transition at x ~ 0.03
- FM coupling between Mn before full emergence of itinerant hole carriers

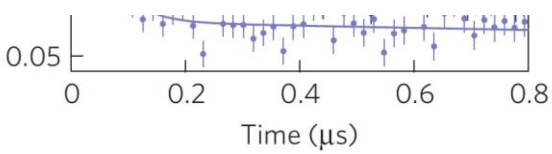

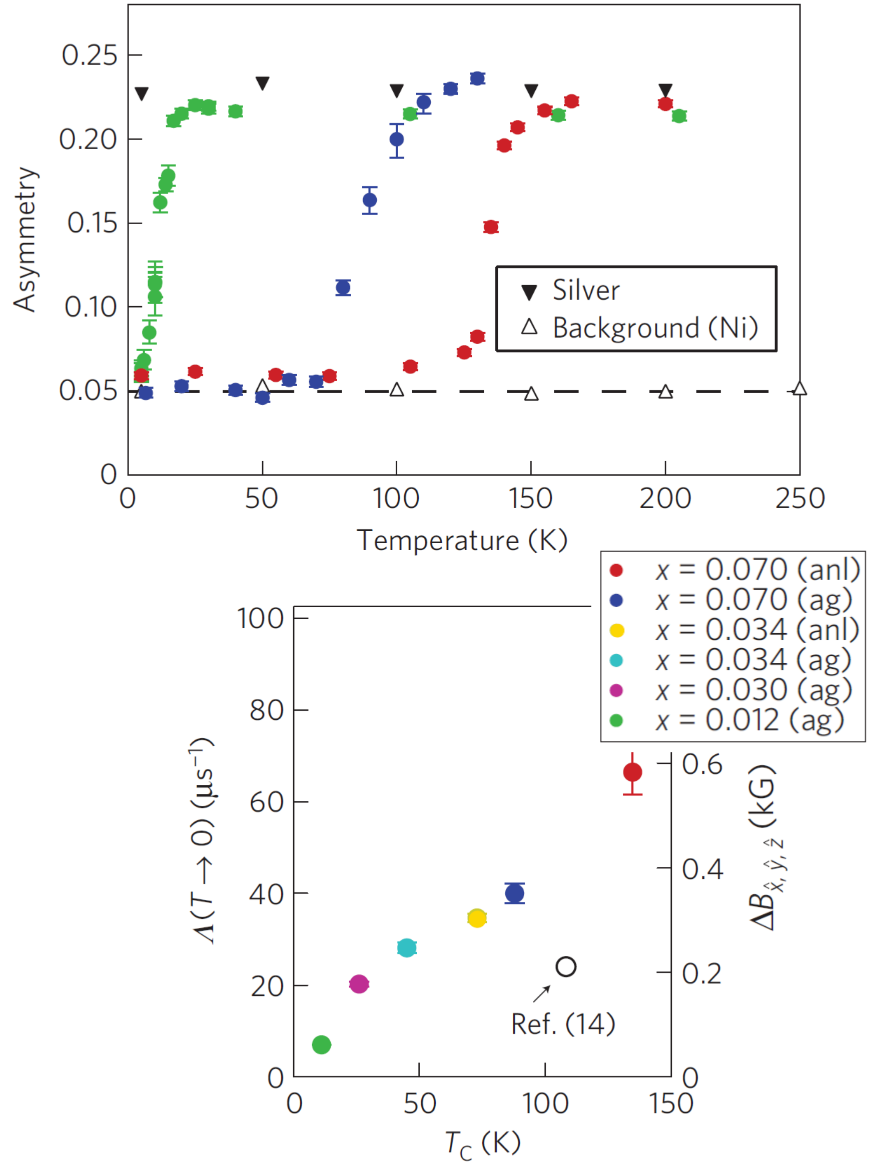

S.R. Dunsiger, *et al.*, Nature Materials **9**, 299 (2010).

δ-doped La_2CuO_4 – a Material which doesn't Exist in Bulk

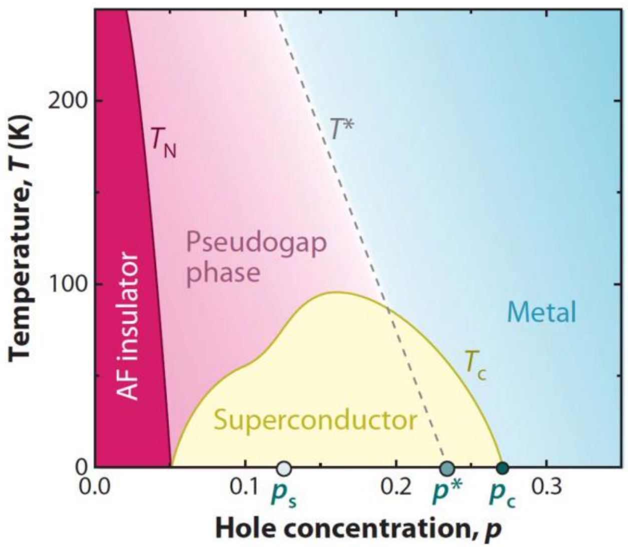

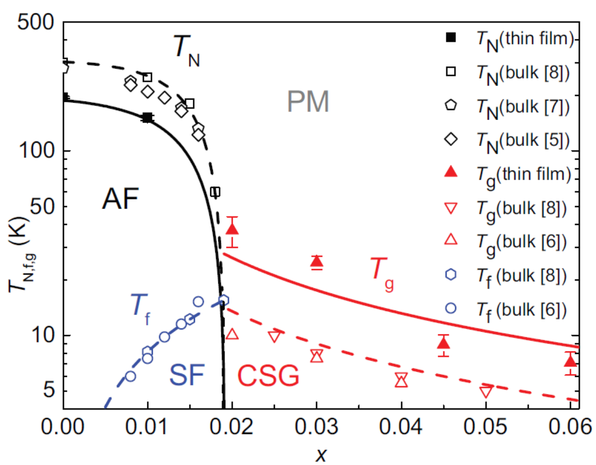

E. Stilp, *et al.* PRB **88**, 064419 (13).

Disorder has a strong impact on the ground state of the Cuprates:

- Zn doping strongly suppresses T_c and leads to a magnetic „bubble“ around the dopant.
- Eu, Nd doping of $La_{2-x}Sr_xCuO_4$ induces strip phases.

Dopant induced disorder on Cuprates can tweak the ground state, especially on the underdoped side:

- Formation of quasi-static SDW order in $YBa_2Cu_3O_{6+x}$.
- Light induced reordering of the chains in $YBa_2Cu_3O_{6+x}$ increases T_c.
- Sr disorder in $La_{2-x}Sr_xCuO_4$ is probably responsible for static long range spin correlations even at high doping levels.
- Oxygen doping of $La_2CuO_{4+\delta}$ is leading to complex phases.

What do we mean by δ-doped LCO?

$La_{2-x}Sr_xCuO4$

a

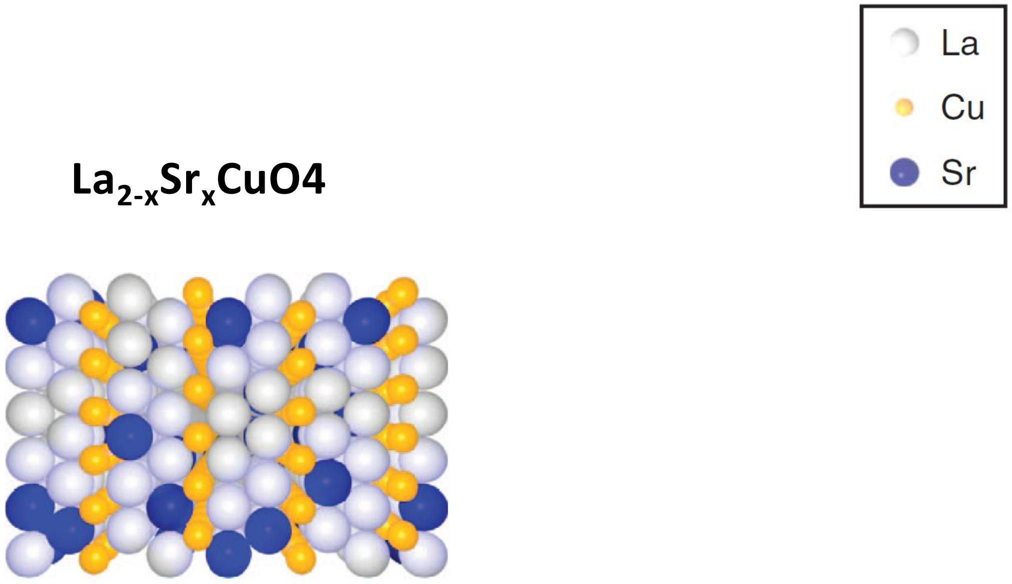

What do we mean by δ-doped LCO?

$$R \times [(LaO\text{-}SrO\text{-}CuO2) + N \times \underbrace{(LaO\text{-}LaO\text{-}CuO2)}_{La_2CuO_4}] \equiv \delta\text{-}LCO_N$$

e.g. δ-LCO_7 #75

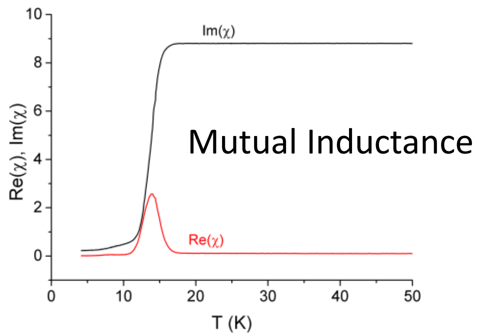

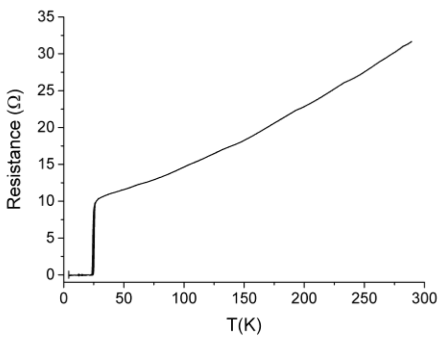

$La_{2-x}Sr_xCuO4$

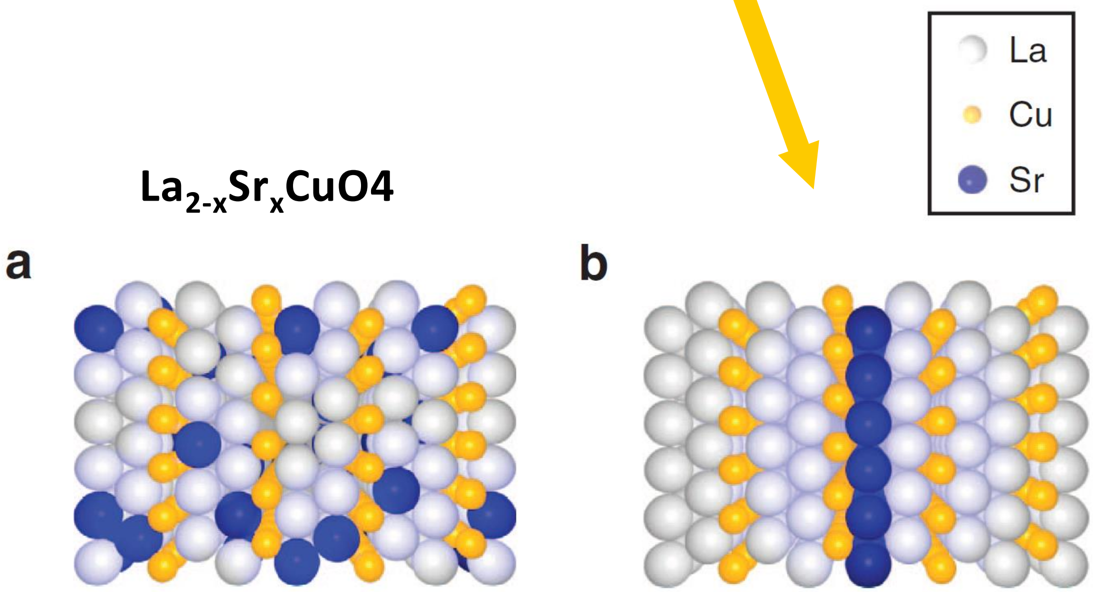

PAUL SCHERRER INSTITUT PSI

How well can such a structure be controlled?

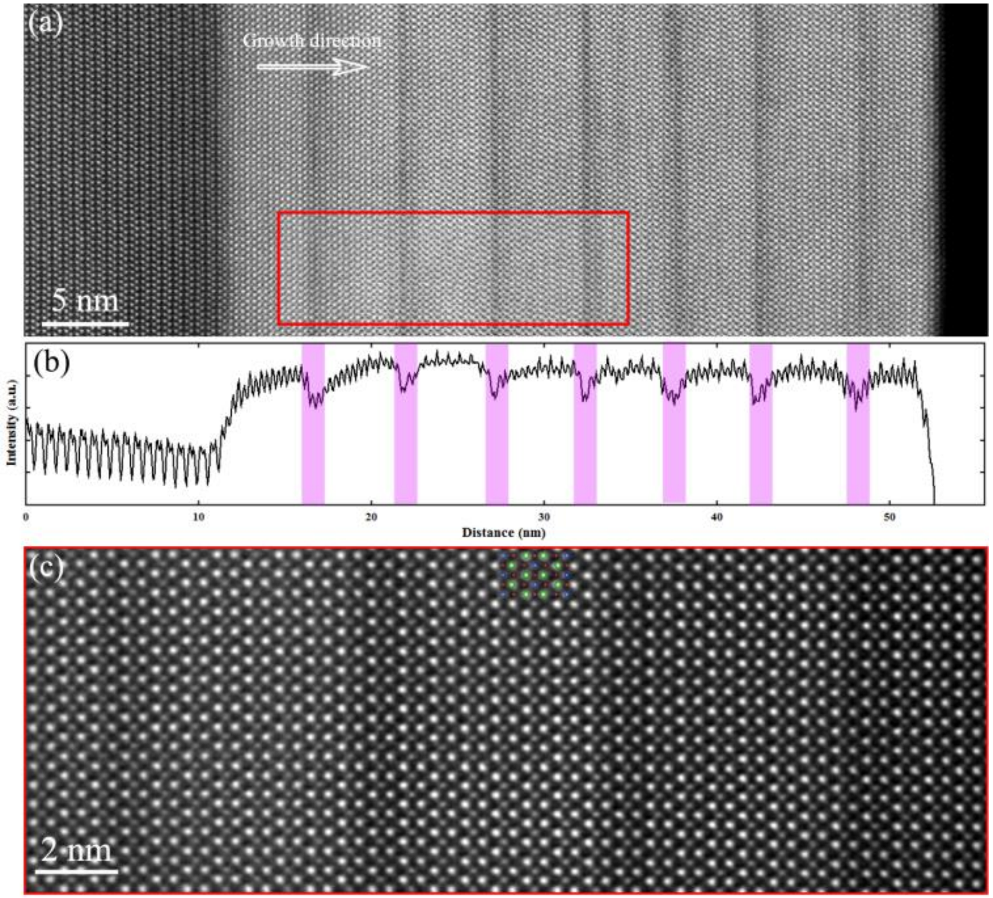

HAADF imaging

- Structure is perfectly epitaxial, free from outgrows and undesired defects.
- Dopant is spread **asymmetrically across the interface**, mainly in the growth direction.
- The structure can be resolved down to the atomic level.

HAADF: high-angle annular dark-field micrography

MPI Stuttgart: F. Baiutti, *et al.* Nat. Commun. DOI: 10.1038/ncomms9586

Sr- and Charge Distribution in δ-LCO_N

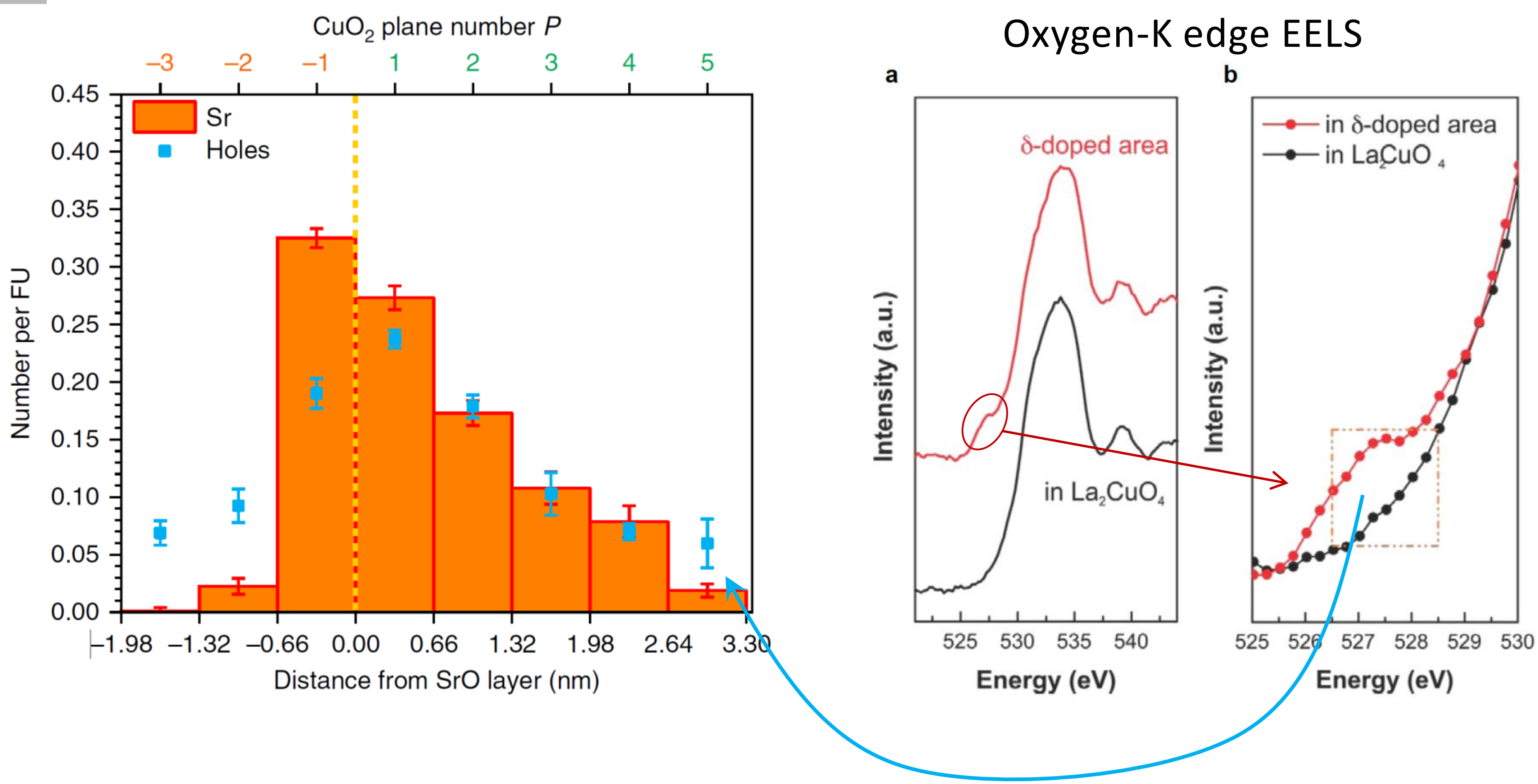

MPI Stuttgart: F. Baiutti, *et al.* Nat. Commun. DOI: 10.1038/ncomms9586

μ^+ stopping profile and La_2CuO_4 structure

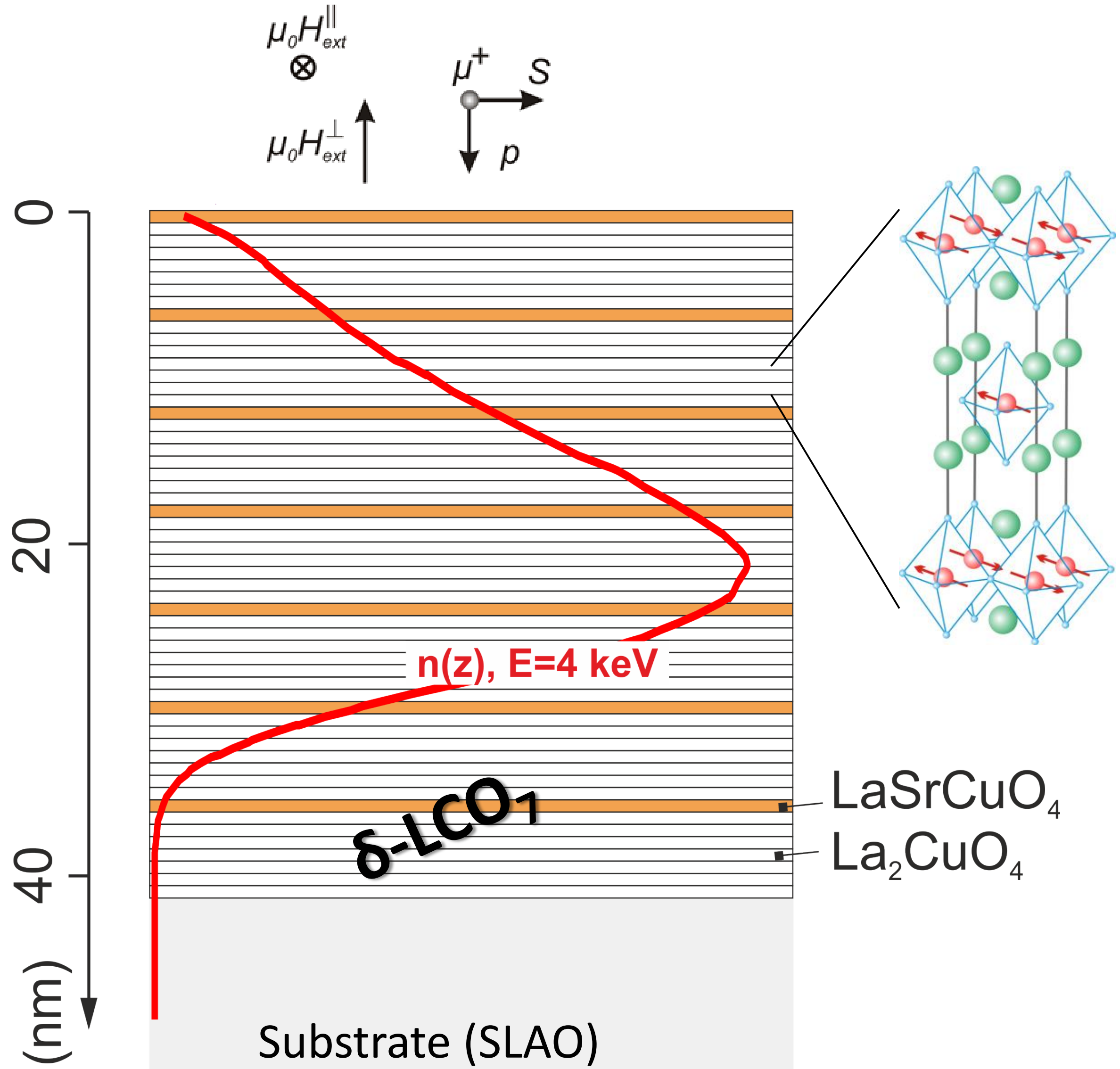

A. Suter, *et al.* PRB **97**, 134522 (18).

Zero Field Time Spectra at Short Times of δ-LCO_{11}

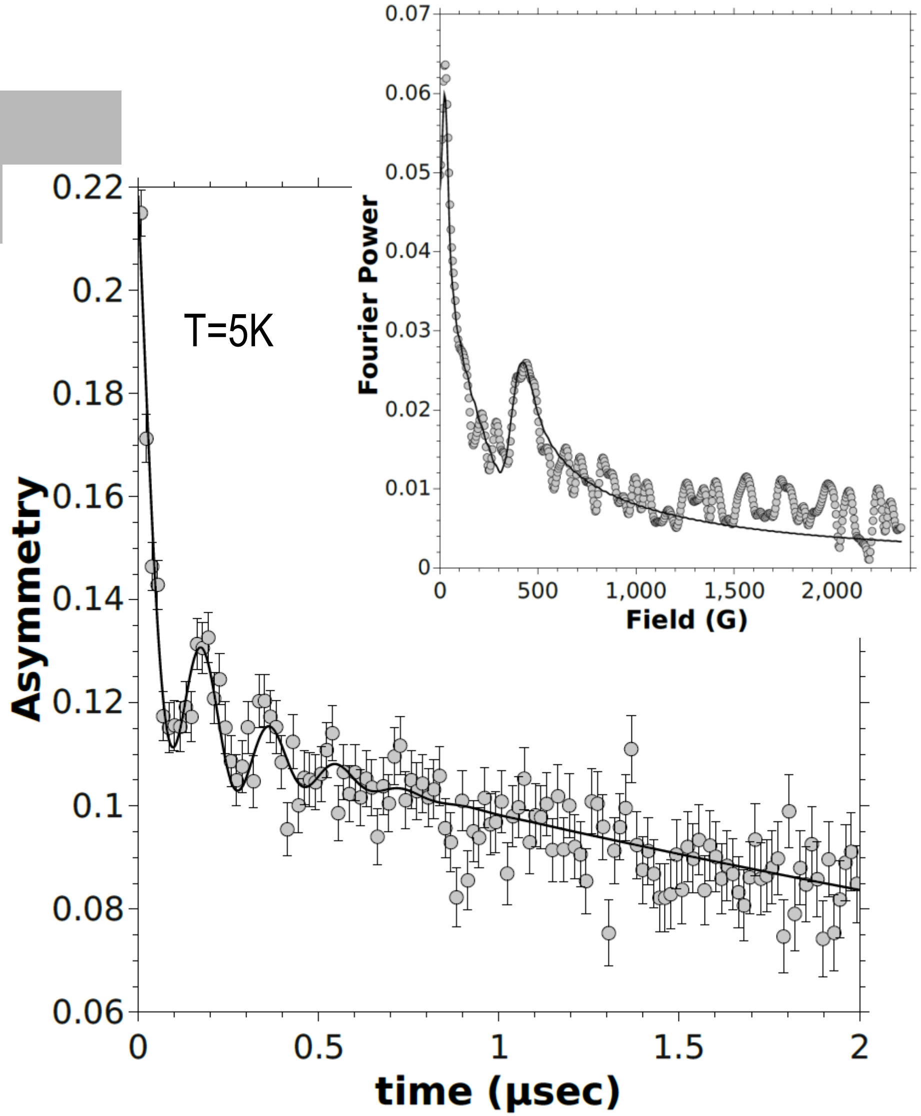

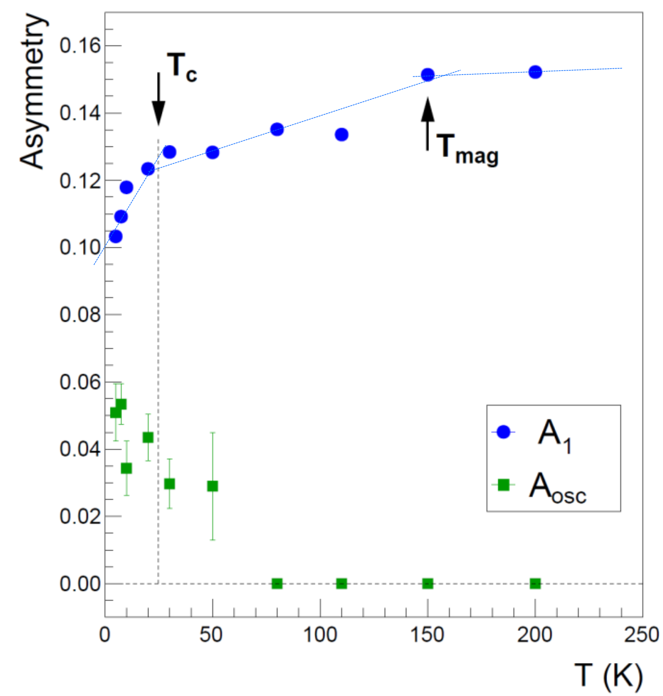

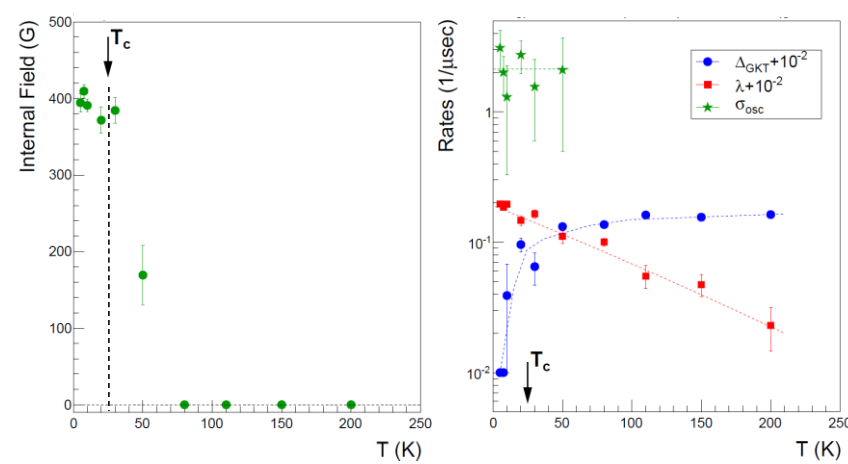

A. Suter, *et al.* PRB **97**, 134522 (18).

Zero Field Time Spectra at Short Times of δ-LCO$_{11}$

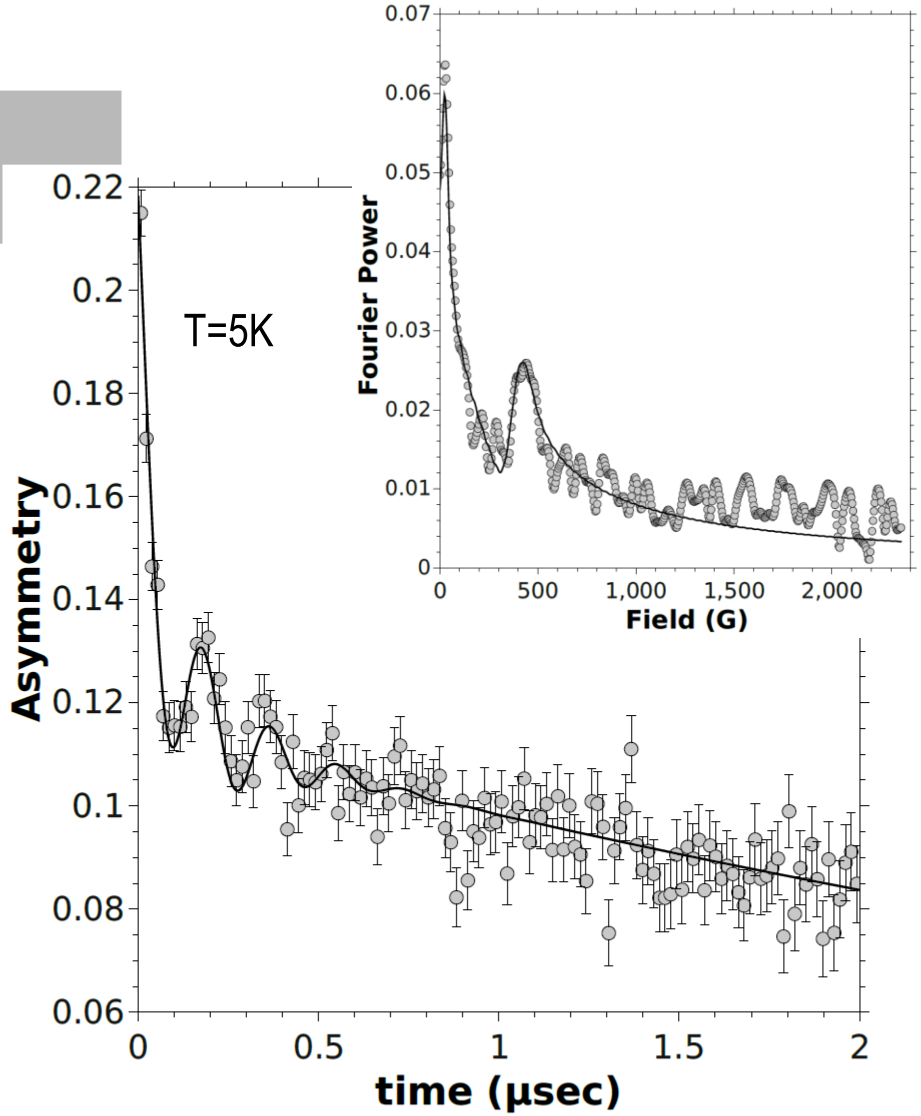

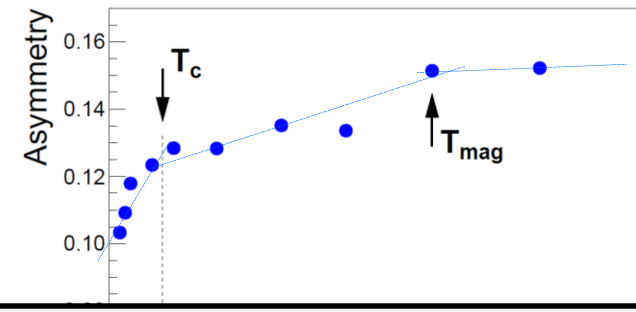

1. At T=5K: B_{loc} = 406(10)G, i.e. the full elec. moment is present!

2. From the A_{osc} the mag. volume fraction can be estimated to 50-75%, depending if one assumes a 1/3- or 1/2-tail.
→ a superconducting layer thickness < 2-4nm.

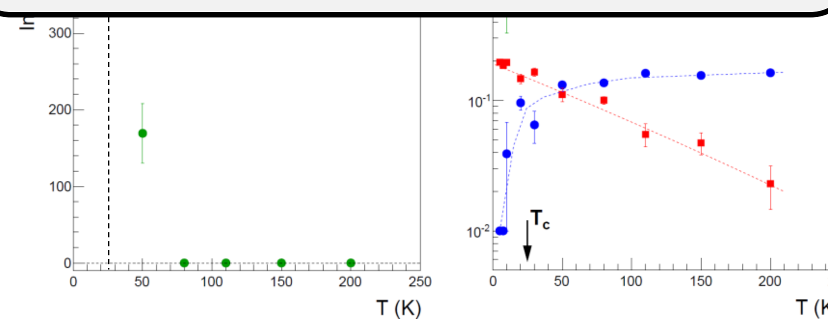

A. Suter, *et al.* PRB **97**, 134522 (18).

Magnetic Volume Fractions of δ-LCO_N

δ-LCO_3

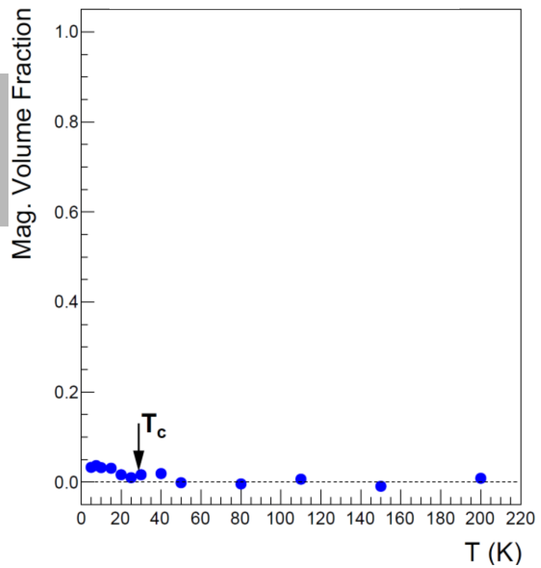

δ-LCO_7

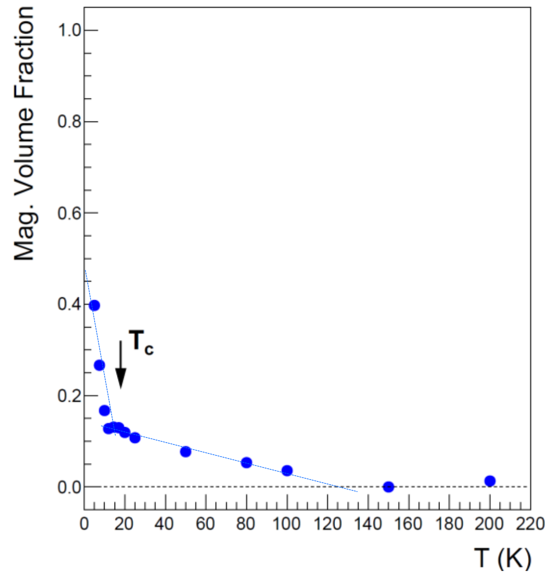

δ-LCO_8

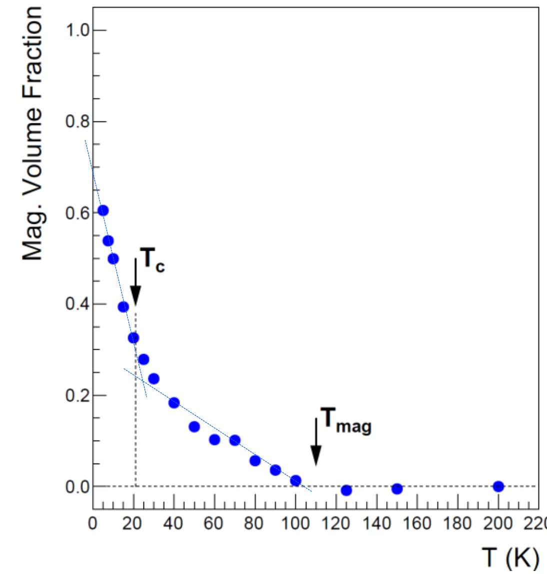

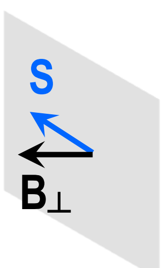

δ-LCO_9

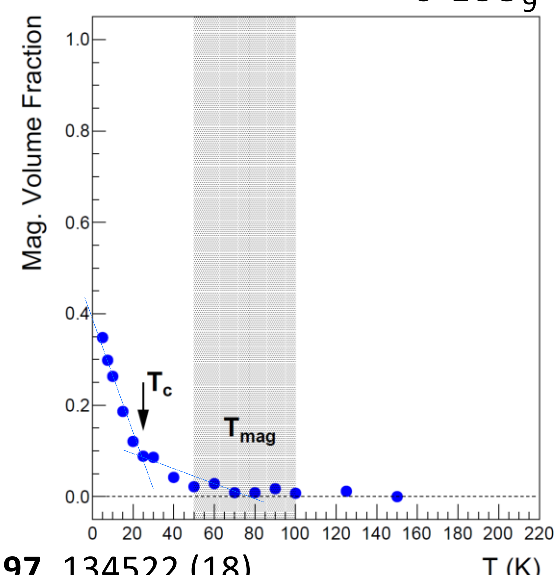

δ-LCO_{11}

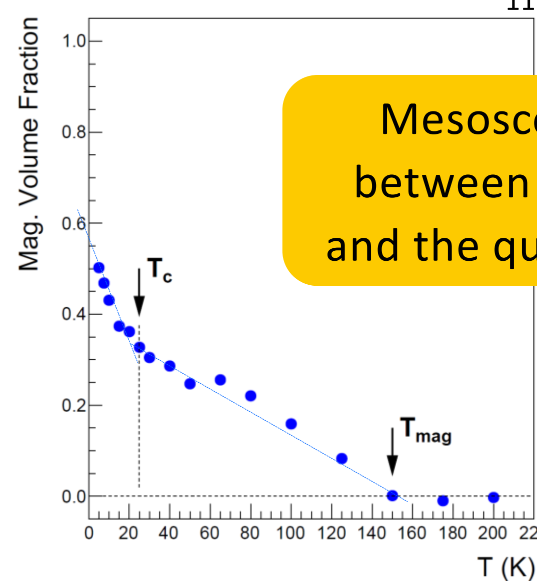

Mesoscopic coupling between the AFM state and the quasi-2D SC state

A. Suter, *et al.* PRB **97**, 134522 (18).

Frustrate Magnetic Metamaterial

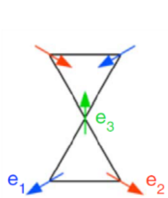

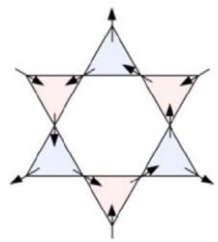

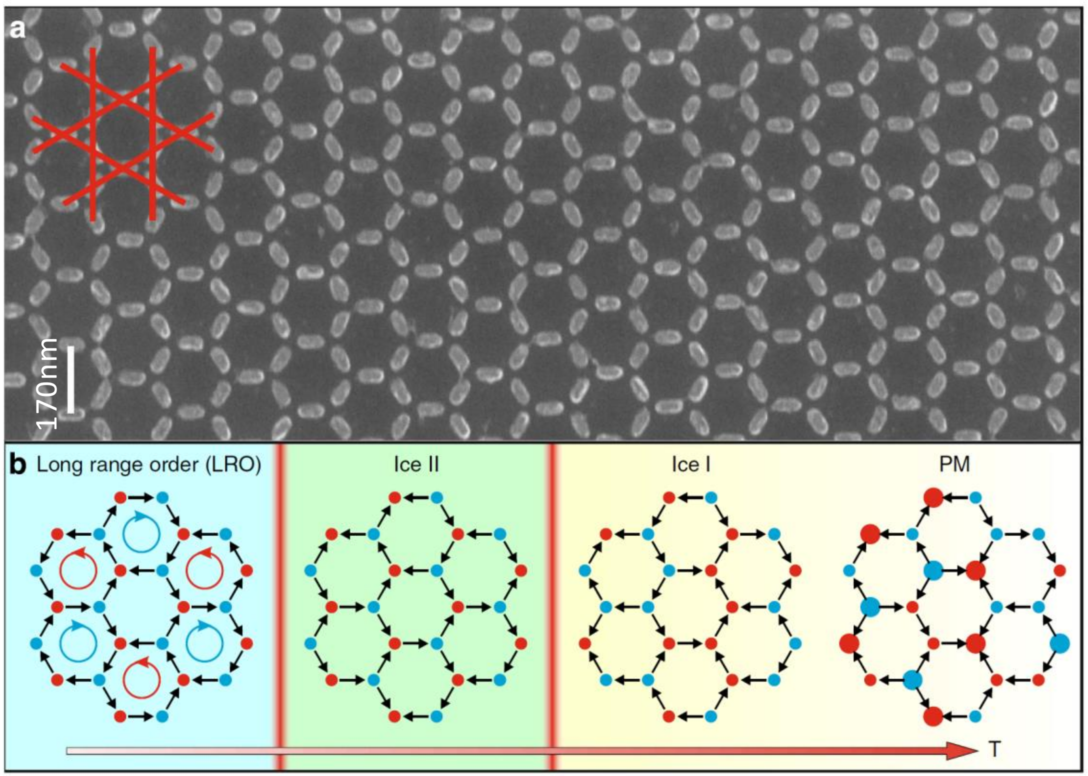

Theoretical Prediction

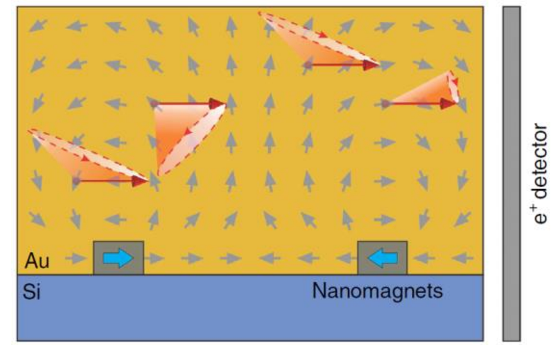

Zero Field Measurements

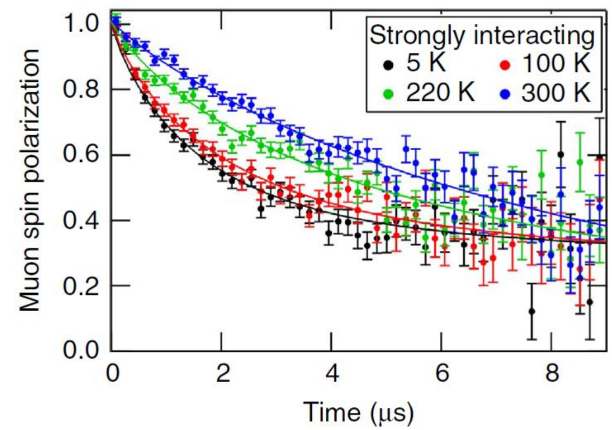

$$P(t) = \frac{2}{3}\exp\left[-(\lambda_{\mathrm{T}}t)^{\beta}\right] + \frac{1}{3}\exp(-\lambda_{\mathrm{L}}t)$$

$$\beta = 0.83 \ldots 1.0$$

L. Anghinolfi, *et al.* Nat. Commun. **6**, 8278 (2015).

Frustrate Magnetic Metamaterial

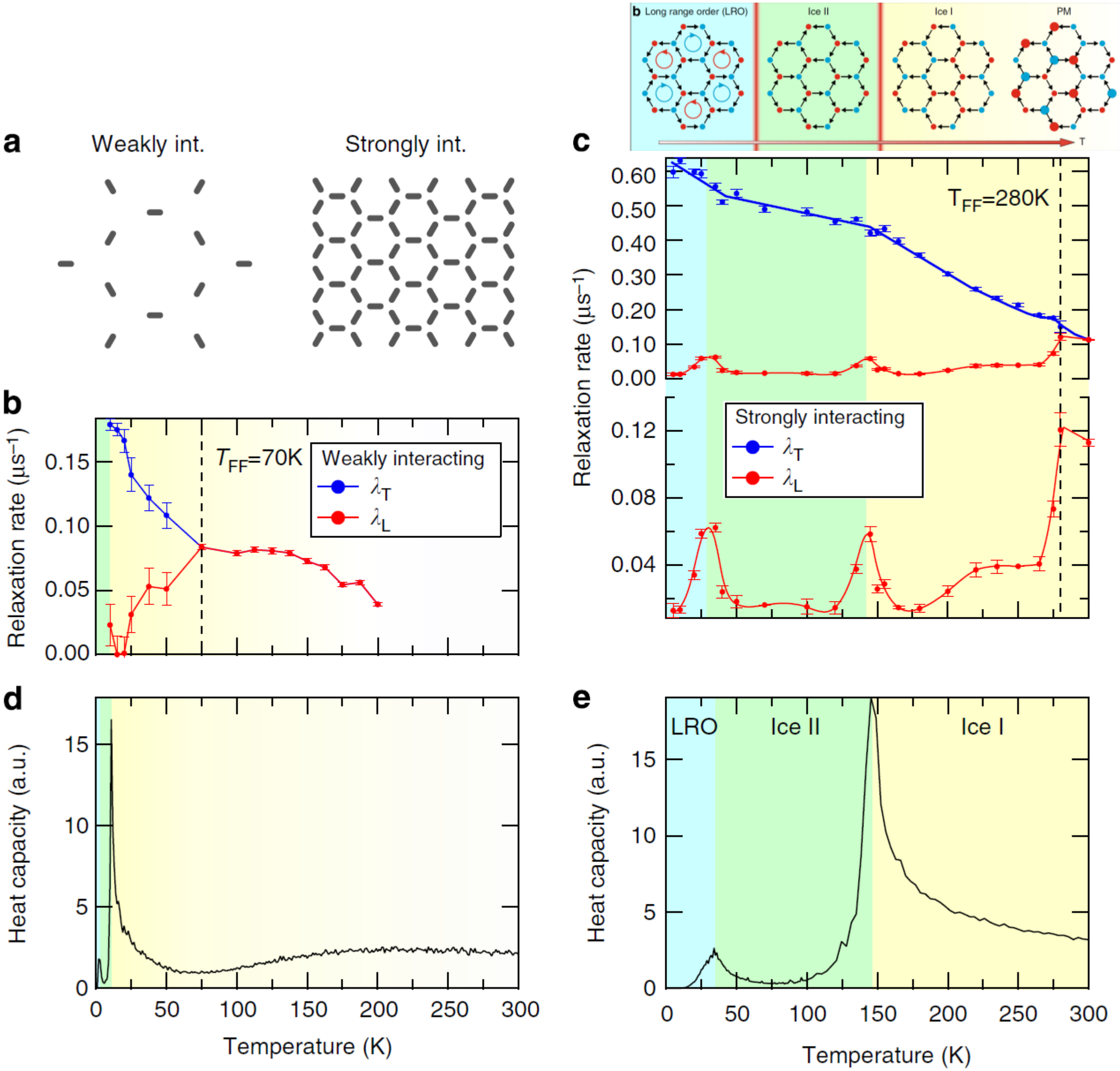

This example shows that it is possible to engineer potentially very interesting meta materials which might help to bridge the gap between theory and more complex bulk materials.

L. Anghinolfi, *et al.* Nat. Commun. **6**, 8278 (2015).

Meissner Effect within the London Theory

Revisited

1st London Eq.: $$\frac{\mathrm{d}\mathbf{j}}{\mathrm{d}t} = \frac{n_S e^2}{m}\mathbf{E}$$

2nd London Eq.: $$\nabla \wedge \mathbf{j} = -\frac{n_S e^2}{mc}\mathbf{B}$$

$$\nabla \wedge \mathbf{B} = \frac{4\pi}{c}\mathbf{j}$$

$$\nabla \wedge \nabla \wedge \mathbf{B} = 4\pi \frac{n_S e^2}{mc^2}\mathbf{B} = \frac{1}{\lambda_L^2}\mathbf{B}$$

Boundaries:
Half plane
+
$B(0) = B_0$

$$B_z(z) = B_0 \exp(-z/\lambda_L)$$

Boundaries:
film with
thickness $2t$
+
$B(0) = B_0 = B(2t)$

$$B_z(z) = B_0 \frac{\cosh\left[(t-z)/\lambda_L\right]}{\cosh(t/\lambda_L)}$$

Electromagnetic Response of a SC for ω→0

$$\nabla \wedge \nabla \wedge \mathbf{A} = \nabla \wedge \mathbf{B} = \frac{4\pi}{c}\mathbf{j}_{\text{total}} = \frac{4\pi}{c}(\mathbf{j}_{\text{ext}} + \mathbf{j}_{\text{med}})$$

↓ q^{th} Fourier component

$$q^2\mathbf{a}(q) = \frac{4\pi}{c}\mathbf{j}_{\text{ext}(q)} - K(q)\mathbf{a}(q)$$

$$\mathbf{a}(q) = \frac{4\pi}{c}\frac{\mathbf{j}_{\text{ext}}(q)}{K(q)+q^2}$$

$$B_z(z) = B_0 \exp(-z/\lambda_{\mathrm{L}})$$

$$j_{x,\text{ext}} = -\frac{c}{2\pi}B_{\text{ext}}\,\delta(z)$$

$$K(q) = \frac{1}{\lambda_{\mathrm{L}}^2}$$

$$B(z) = B_{\text{ext}}\frac{2}{\pi}\int_0^\infty \frac{q}{K(q)+q^2}\sin(qz)\,\mathrm{d}q$$

M. Tinkham, “Introduction to Superconductivity”, Dover (96).
J.R. Schrieffer, “Theory of Superconductivity”, Westview Press (99).

What's wrong with the London Theory?

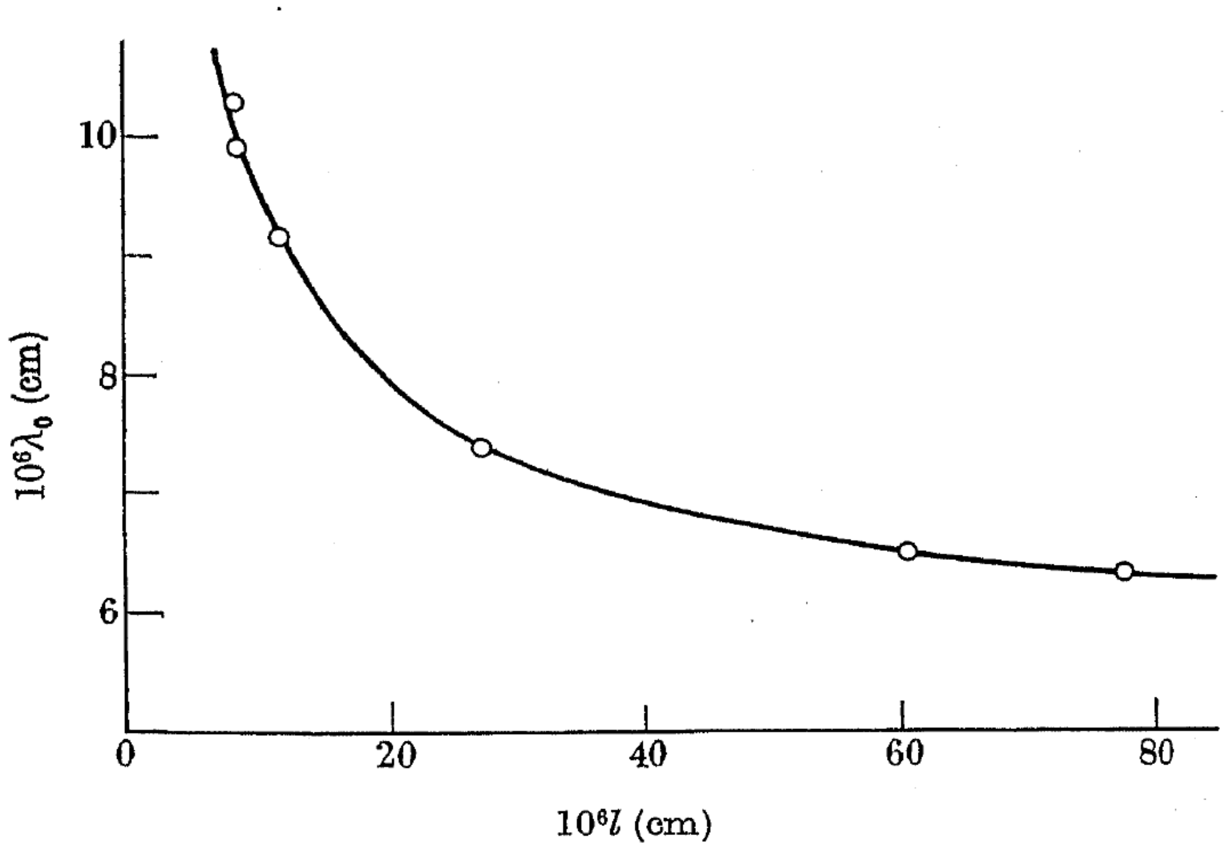

FIGURE 1. Variation of λ_0 with l.

Pippard, Proc.Roy.Soc. (London) **A216**, 547 (1953)

Pippard Kernel

$$B(z) = B_{\rm ext}\,\frac{2}{\pi}\int_0^\infty \frac{q}{K(q)+q^2}\,\sin(qz)\,\mathrm{d}q$$

$$K_{\rm P}(q\xi,T,\ell) = \frac{1}{\lambda^2(T)}\,\frac{\xi_{\rm P}(T,\ell)}{\xi_{\rm P}(0,\ell)}\left[\frac{3}{2}\,\frac{1}{x^3}\left\{\left(1+x^2\right)\arctan(x) - x\right\}\right]$$

$$x = q\xi_{\rm P}(T,\ell)$$

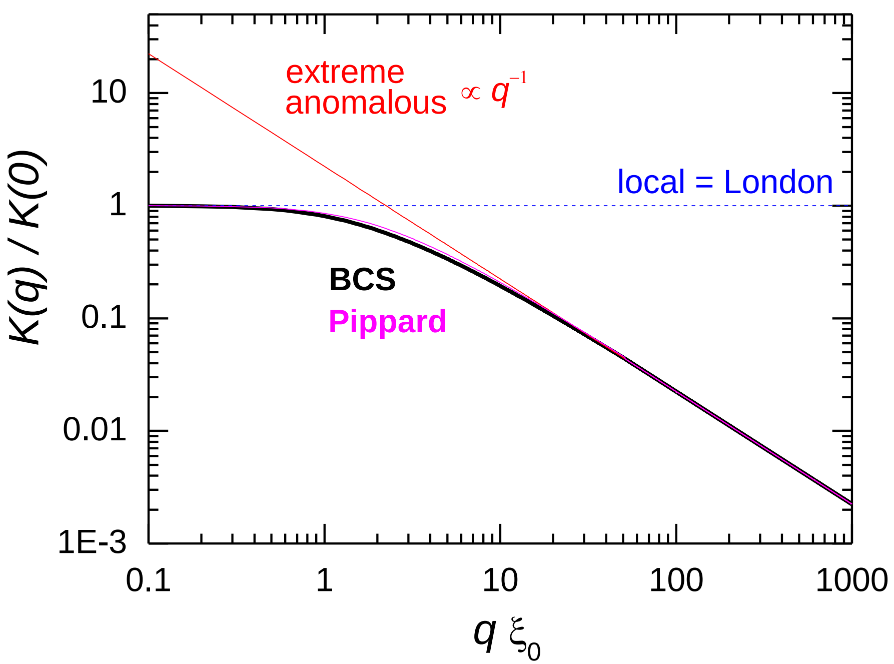

Pippard, Proc.Roy.Soc. (London) **A216**, 547 (1953)

Extreme Nonlocal SC Aluminum (Theory)

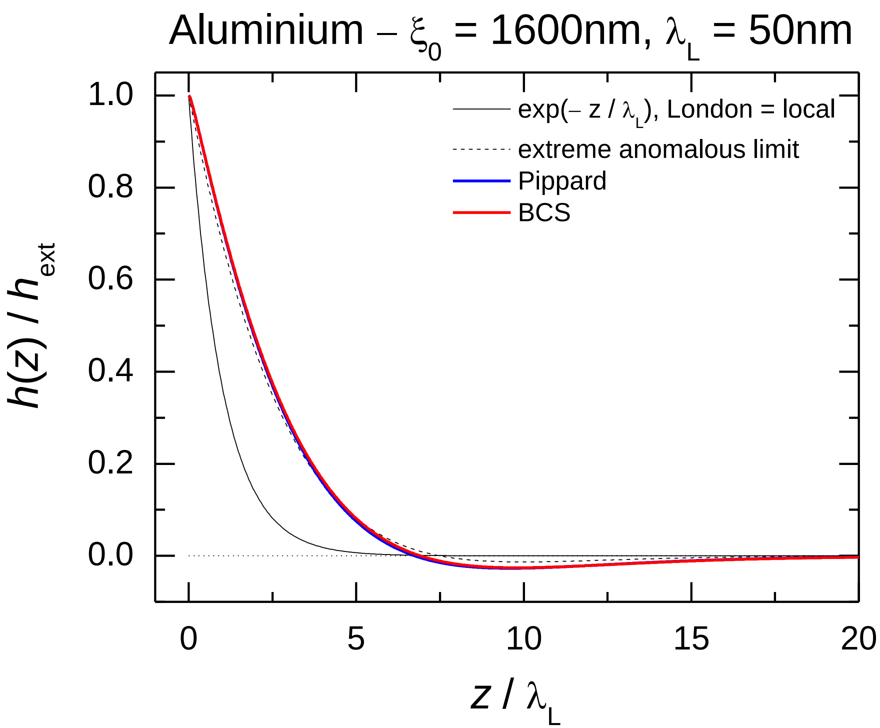

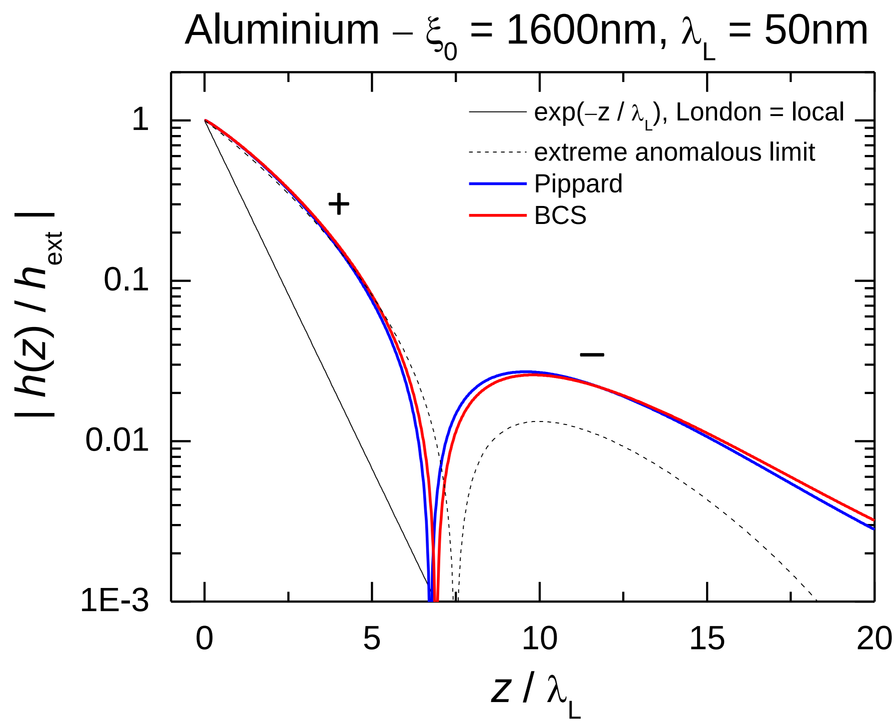

Nonlocal SC Reality

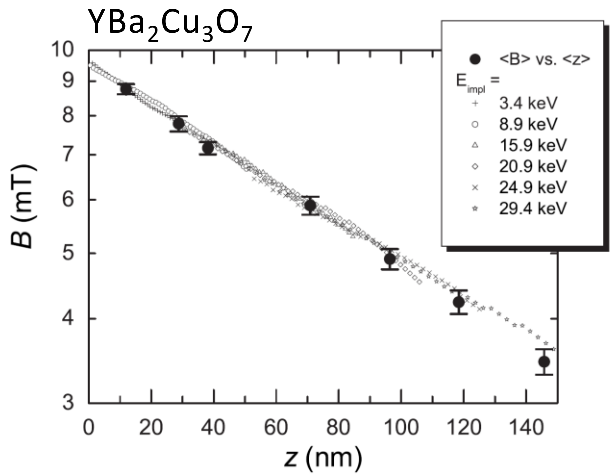

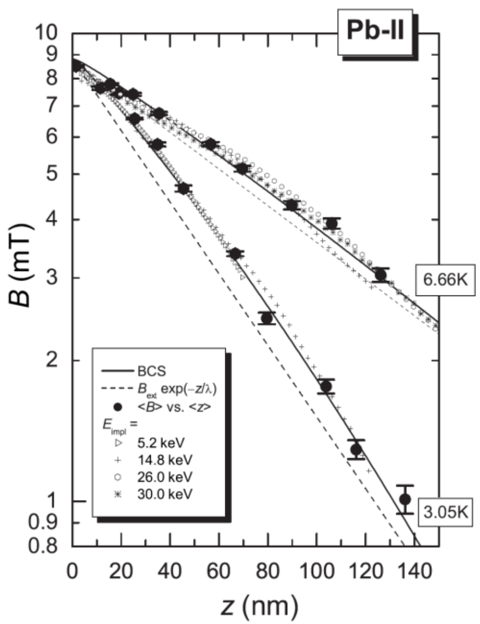

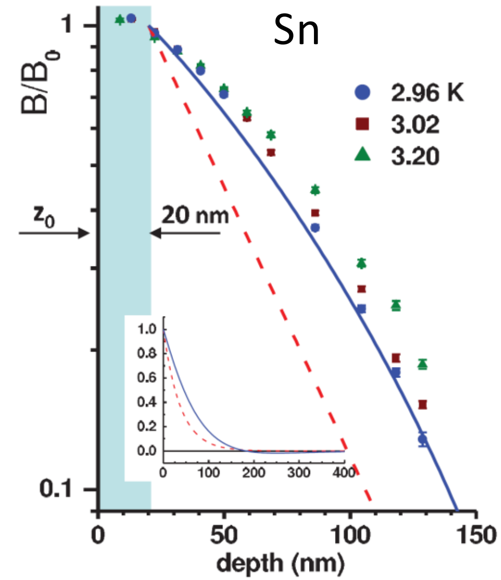

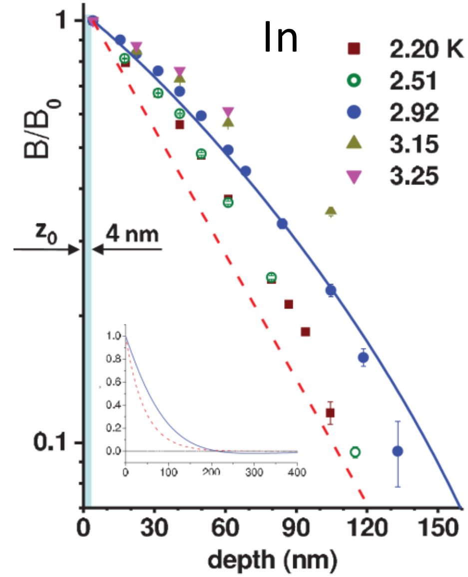

A. Suter, *et al.* PRL **92**, 087001 (04), PRB 72, 024506 (05).
V. Kozhevnikov, *et al.* PRB **87**, 104508 (13).

PAUL SCHERRER INSTITUT

The Superconducting Niobium RF-Cavity Problem

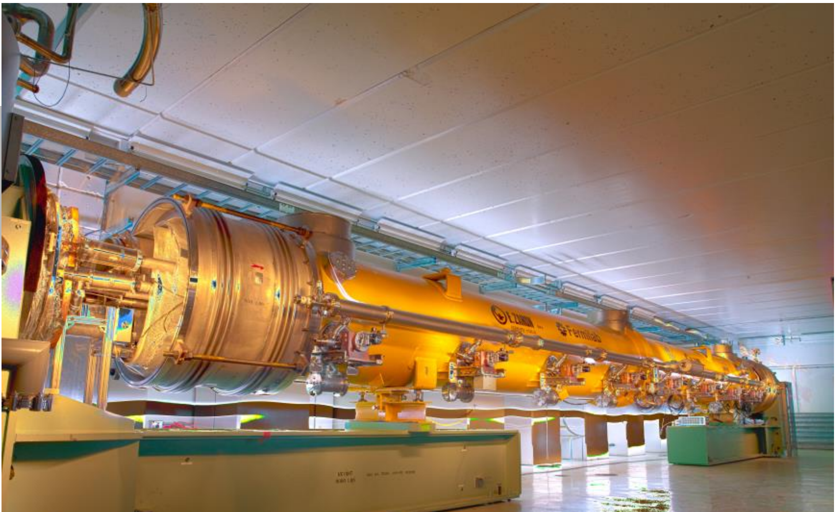

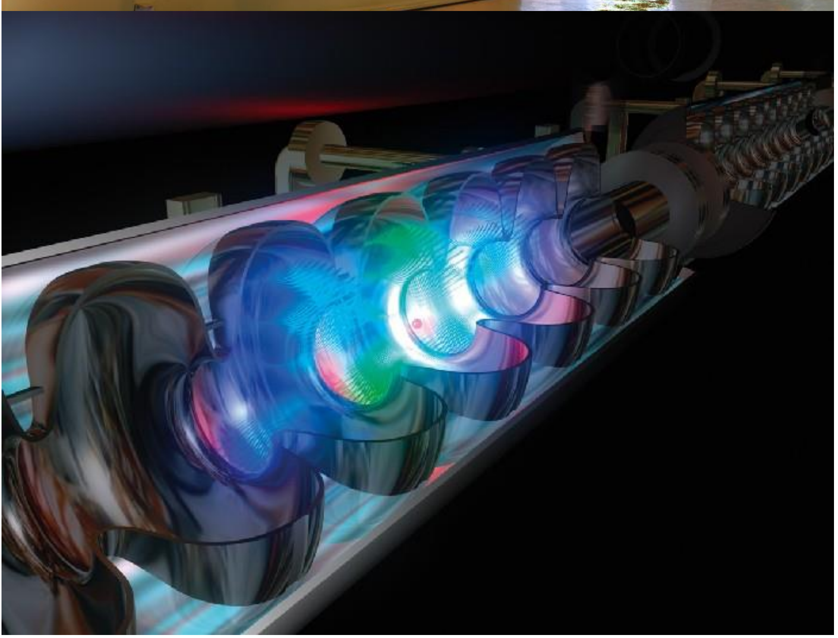

The Goal: highest possible acceleration,
i.e. highest possible electro-magnetic fields.

The Problem: the quality factor, Q_0, breaks down at higher fields (here for an electro-polished SRFC).

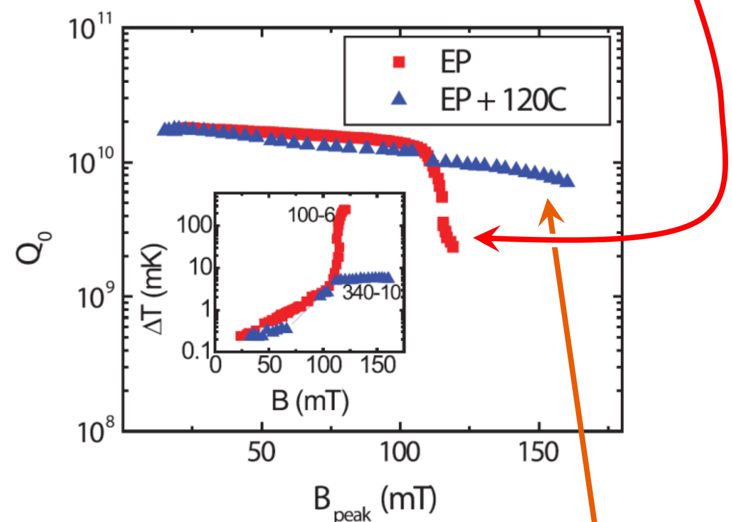

Backing the SRFC at 120˚C, recovers Q_0 at higher fields, but it was not clear why!

Possible Explanations:

- Oxygen intake, surface defects or mag. impurities
- Hydrogen related effects (interstitials, hydrides)

A. Romanenko *et al.*, Applied Physics Letters **104**, 072601 (2014).

The Superconducting Niobium RF-Cavity Problem

Measured Magnetic Screening Profile

(Meissner Screening)

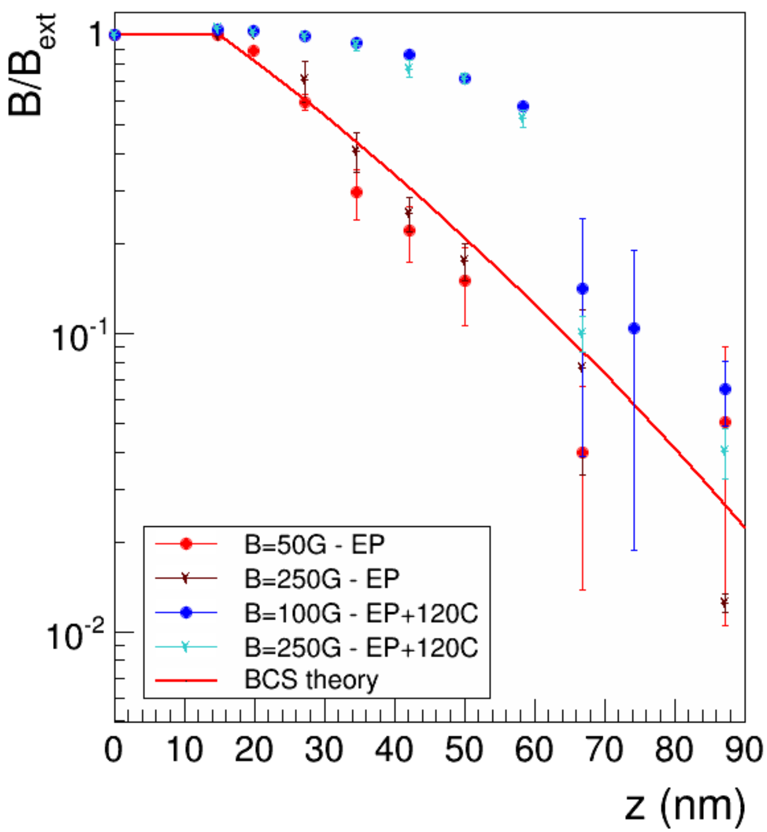

$$B(z) = B_{\mathrm{ext}} \frac{2}{\pi} \int \frac{q}{q^2 + K(q\xi, T, \ell)} \sin(qz) \mathrm{d}q$$

Typical Nb cutout from an operational Cavity.

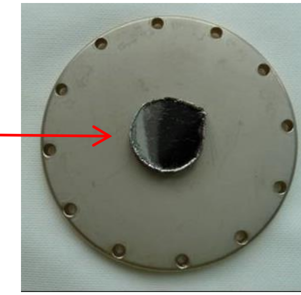

- Red: “good” superconductor but “bad” cavity (Q_0 drop)
- Blue: “bad” superconductor but “good” cavity (no Q_0 drop)

The analysis shows: the 120˚C backing results in an extreme shortening of the mean free path, ℓ, close to the surface. This is only compatible with the decomposition of Nb hydride complexes.

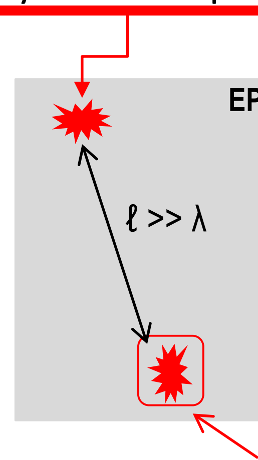

Decomposed Nb hydride complexes are superconducting

→ **no RF losses**

Normal conducting → **RF losses**

A. Romanenko *et al.*, Applied Physics Letters **104**, 072601 (2014).

The Superconducting Niobium RF-Cavity Problem

Measured Magnetic Screening Profile (Meissner Screening)

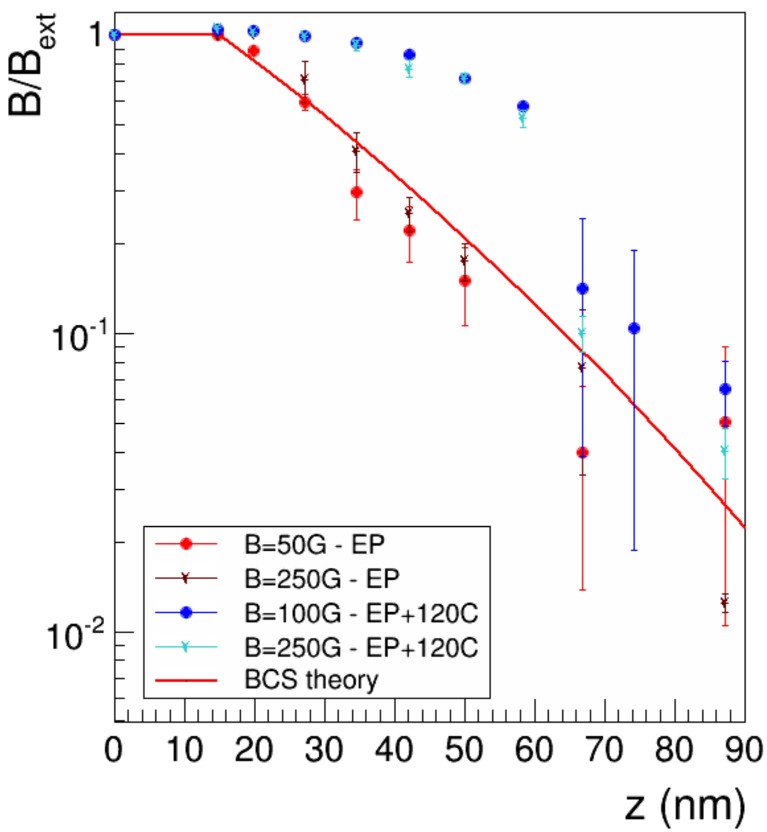

$$B(z) = B_{\mathrm{ext}} \frac{2}{\pi} \int \frac{q}{q^2 + K(q\xi, T, \ell)} \sin(qz)\mathrm{d}q$$

This knowledge directly led to the conclusion that high temperature nitrogen doping should lead to a much better performance.

This is already established by now with a Q_0 increase by a factor of two, without Q_0 slop break.

- Red: "good" superconductor but "bad" cavity (Q_0 drop)
- Blue: "bad" superconductor but "good" cavity (no Q_0 drop)

The analysis shows: the 120˚C backing results in an extreme shortening of the mean free path, ℓ, close to the surface. This is only compatible with the decomposition of Nb hydride complexes.

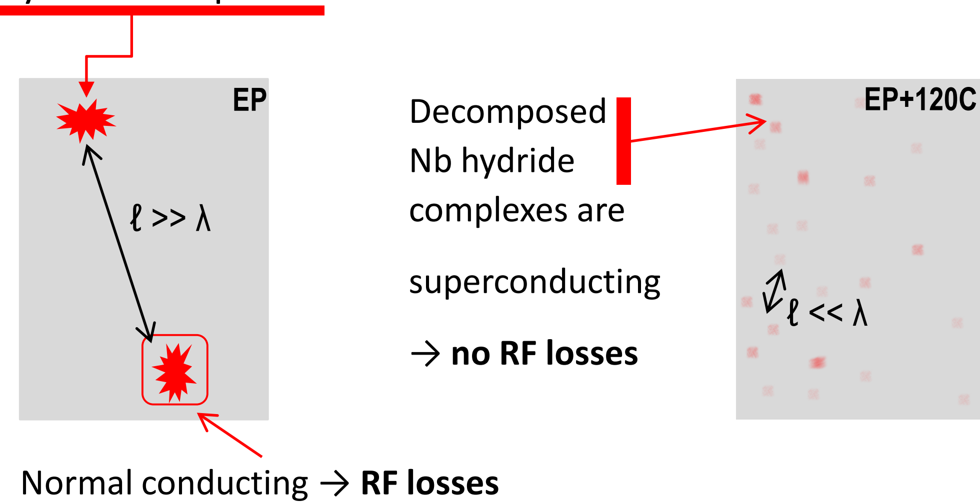

A. Romanenko *et al.*, Applied Physics Letters **104**, 072601 (2014).

Single Molecule Magnets (SMMs)

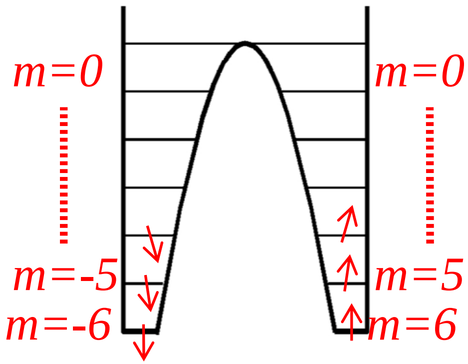

$TbPc_2$

J=6

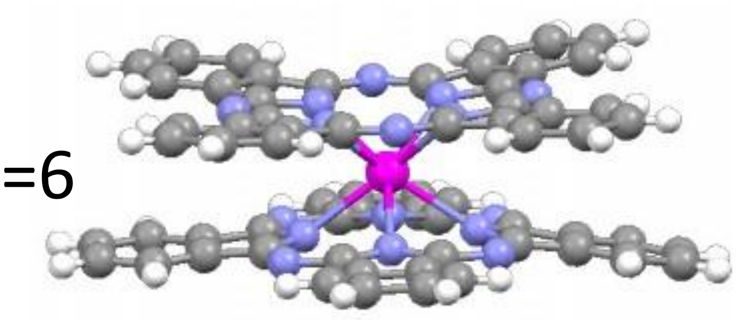

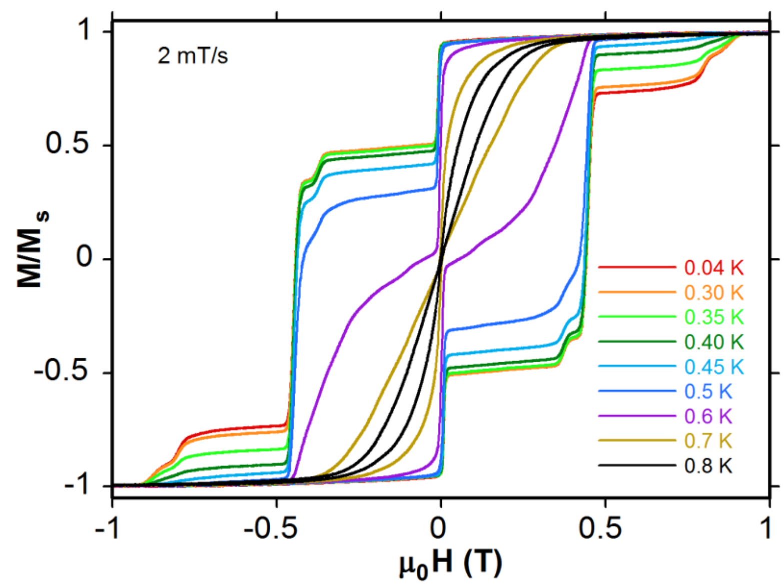

Questions:

- Differences/Similarities between bulk and films.
- Effect of interfaces on spin
- Effect of environment on spin dynamics

Single Molecule Magnets (SMMs)

TbPc$_2$:
$Tb(C_{32}H_{16}N_8)_2$

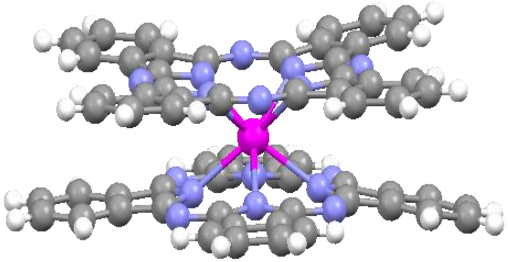

[DyPyNO]$_2$:
$[Dy(hfac)_3(PyNO)]_2$

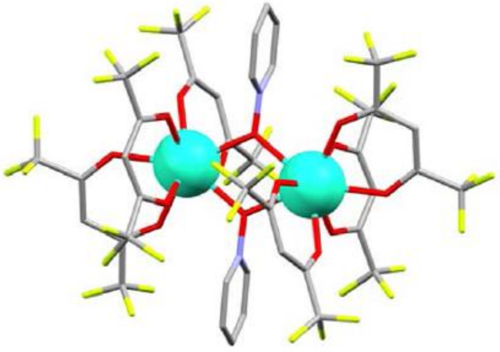

Dytta :
$[Dy(tta)_3(L)]\cdot C_6H_{14}$

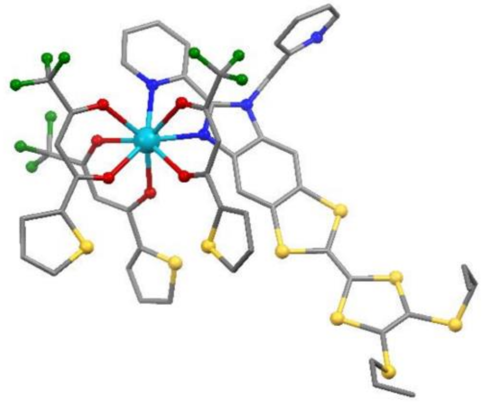

Typical ZF Spectra of SMM

$TbPc_2$

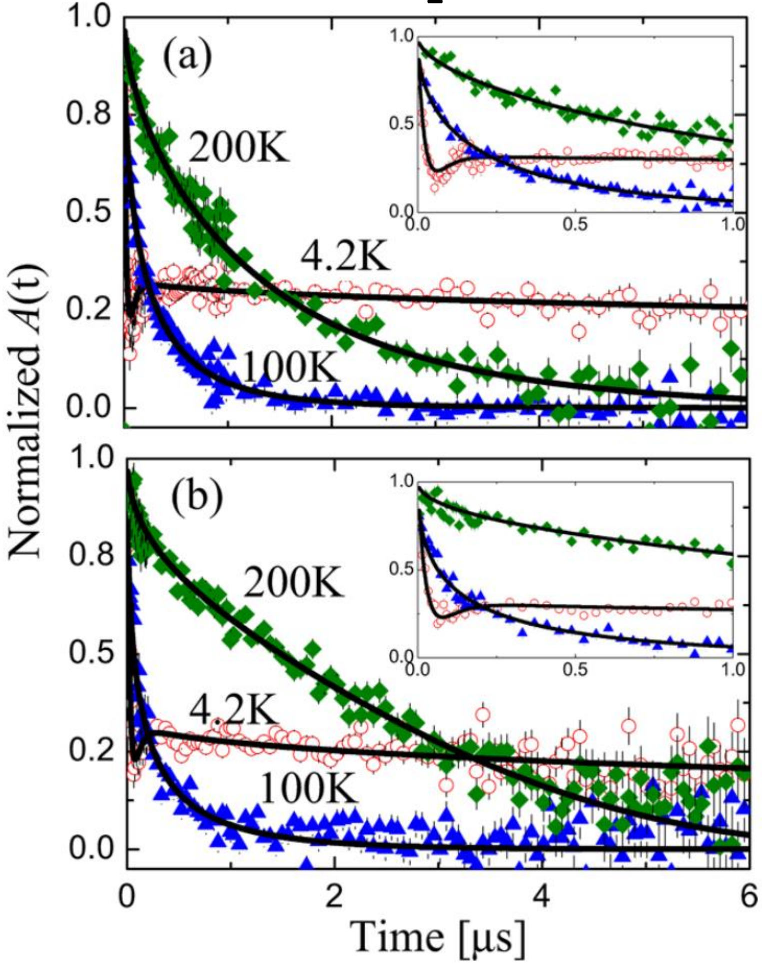

- Dynamic relaxation at high temperatures (exponential)
- Slowing down of the dynamics (down to 100K)
- Freezing – appearance of static magnetic fields (T<100 K)

A. Hoffman *et al.*, ACS Nano **6**, 8390 (2012).

Comparison – $TbPc_2$/Au vs. $TbPc_2$/STO

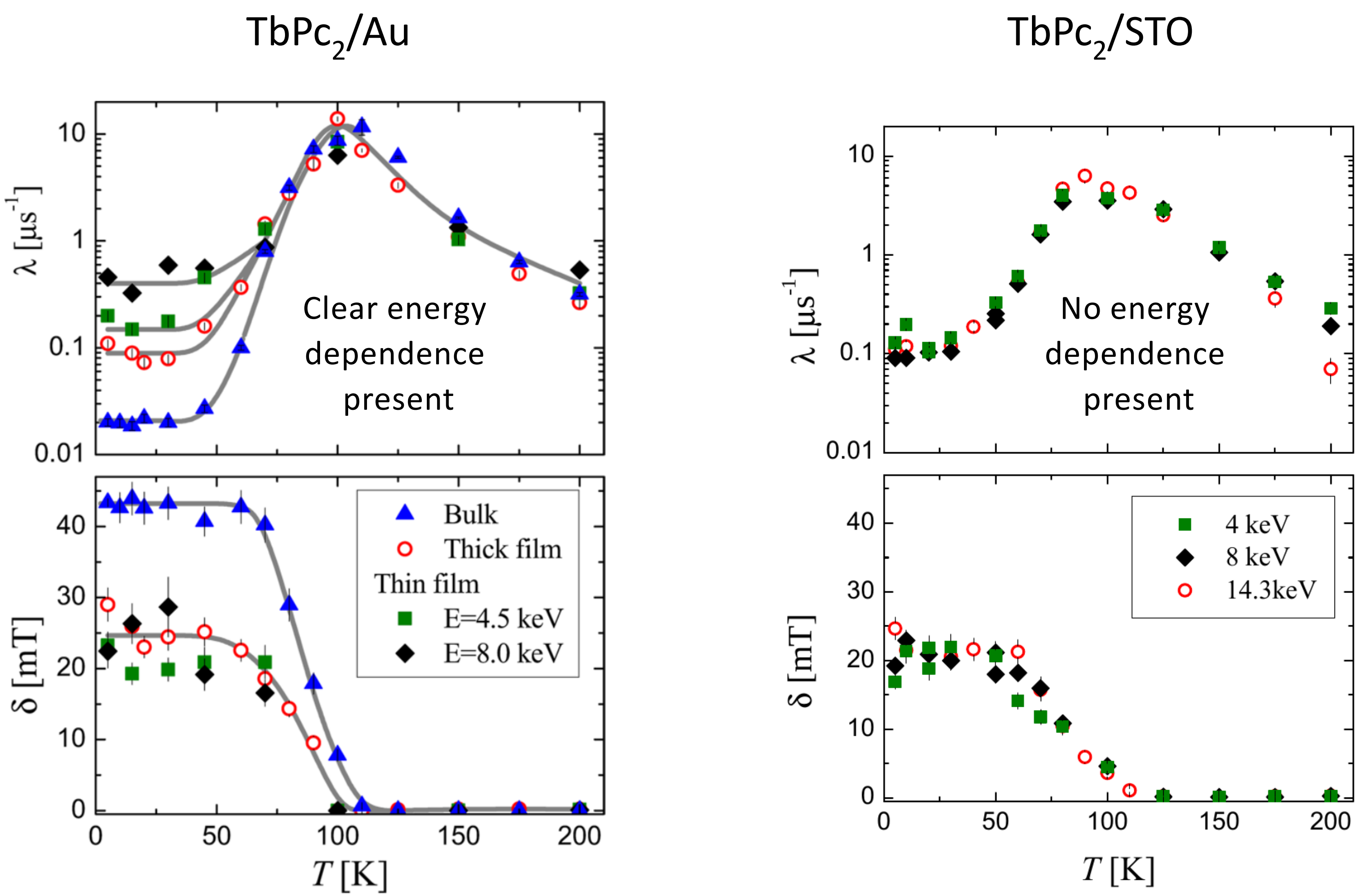

$$A(t) = \frac{A_0}{3}\left[1 + 2(1 - \gamma\delta t)\mathrm{e}^{-\gamma\delta t}\right]\mathrm{e}^{-\sqrt{\lambda t}}$$

A. Hoffman *et al.*, ACS Nano **6**, 8390 (2012).

Spin Dynamics as a Function of Depth – TbPc2/Au

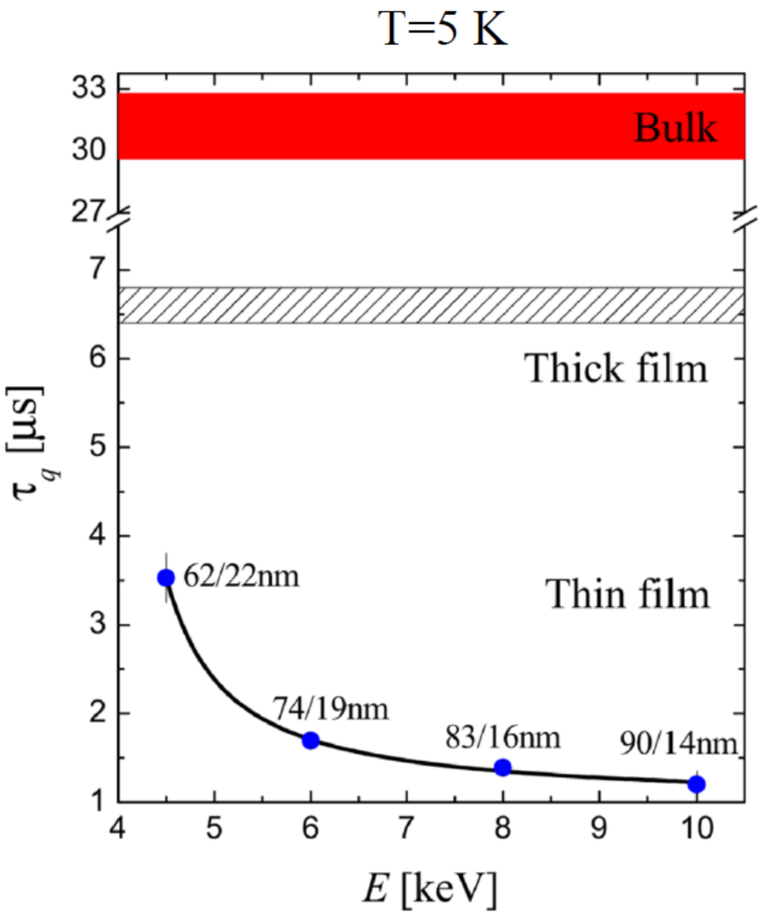

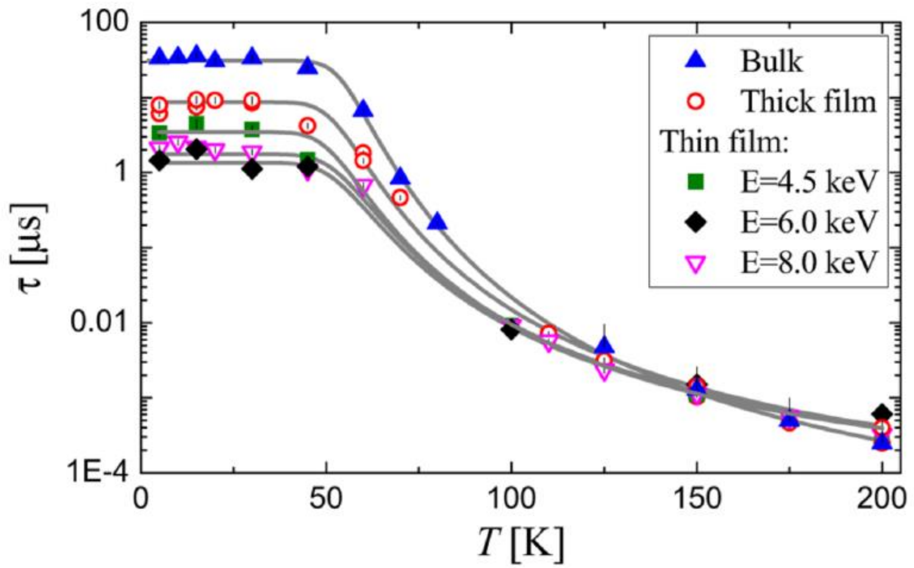

A. Hoffman *et al.*, ACS Nano **6**, 8390 (2012).

Substrate Effect on Packing and Spin Dynamics

On Au:

- Molecules are lying down at the surface
- Gradually change to standing away from the substrate

On $SrTiO_3$:

- Molecules are standing at the surface
- No dramatic change as we go away from the substrate

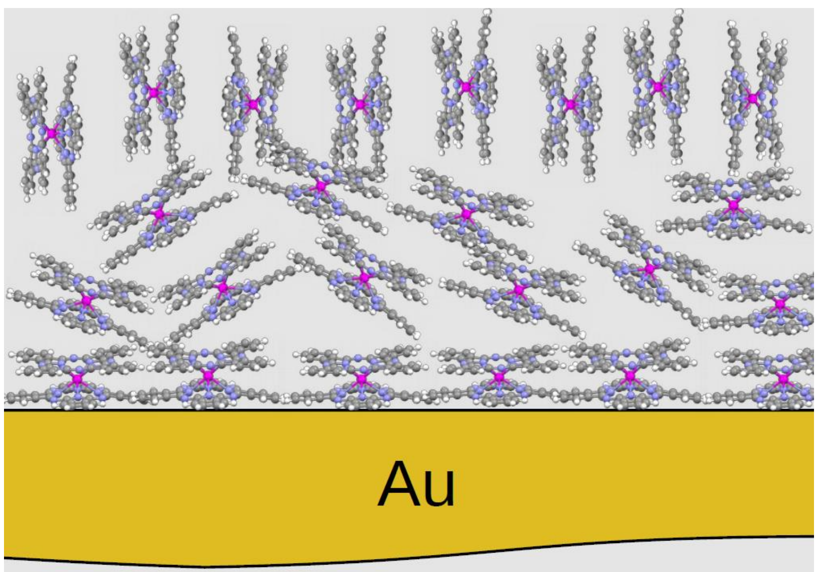

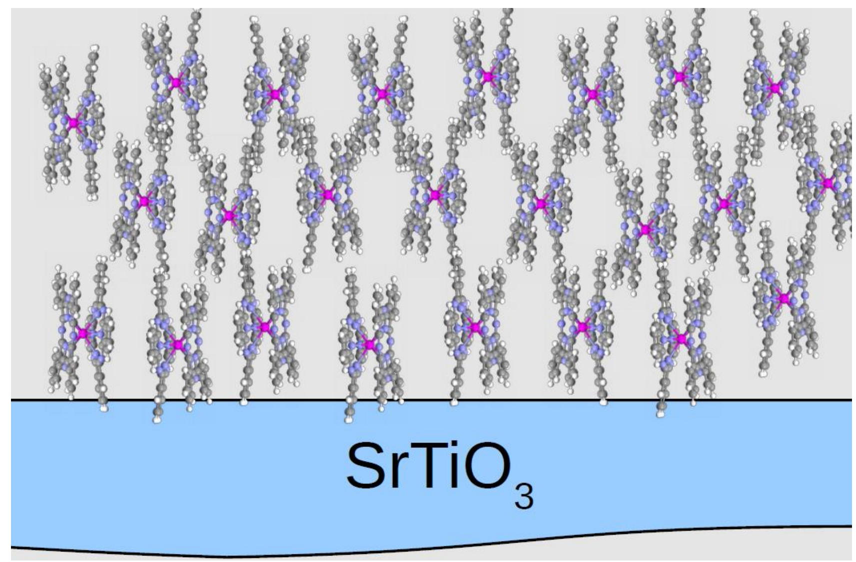

A. Hoffman *et al.*, ACS Nano **6**, 8390 (2012).

Spatial Confinement of Muonium Atoms

Particle Physics meets LEM

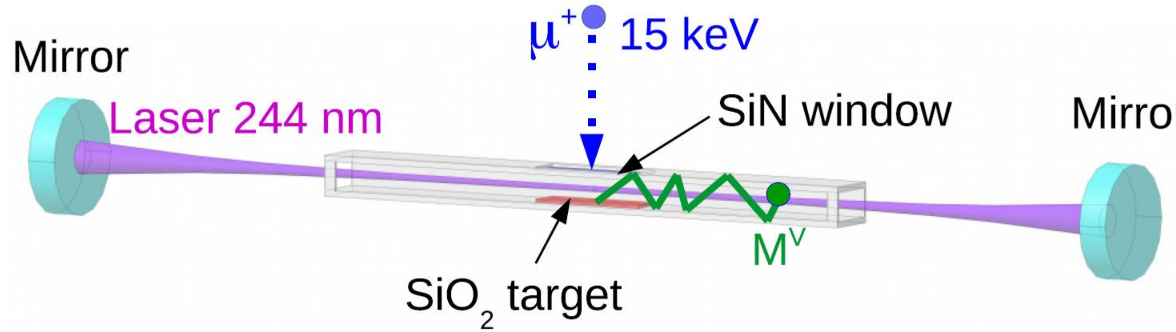

- Atomic Muonium is an ideal system in which to study bound state QED free of finite-size effects and in which hadronic corrections are strongly suppressed compared to hydrogen.
- The Muonium 1s-2s transition offers a clean determination of the muon mass, which in turn is required for a precise interpretation of (g-2) and to determine the weak interaction Fermi coupling constant G_F, and others.

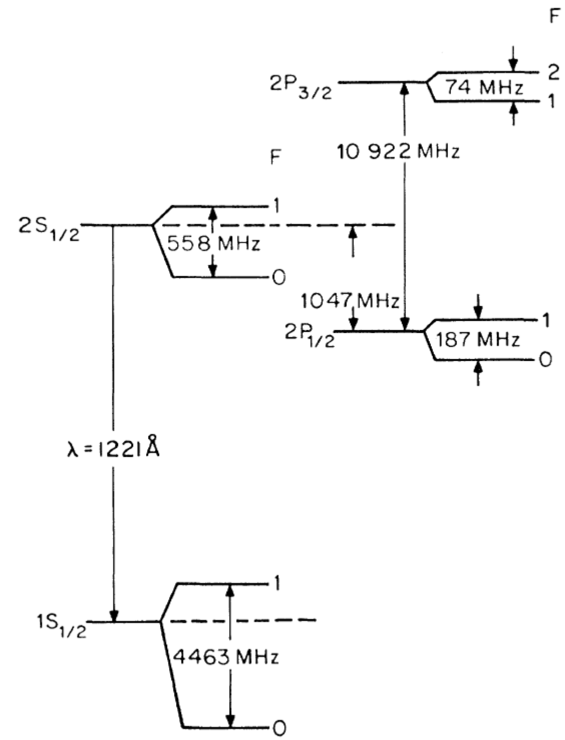

A. Antognini, *et al.* PRL **108**, 143401 (12).
K.S. Khaw, *et al.* PRA **94**, 022716 (16).

Low Energy Muonium Production

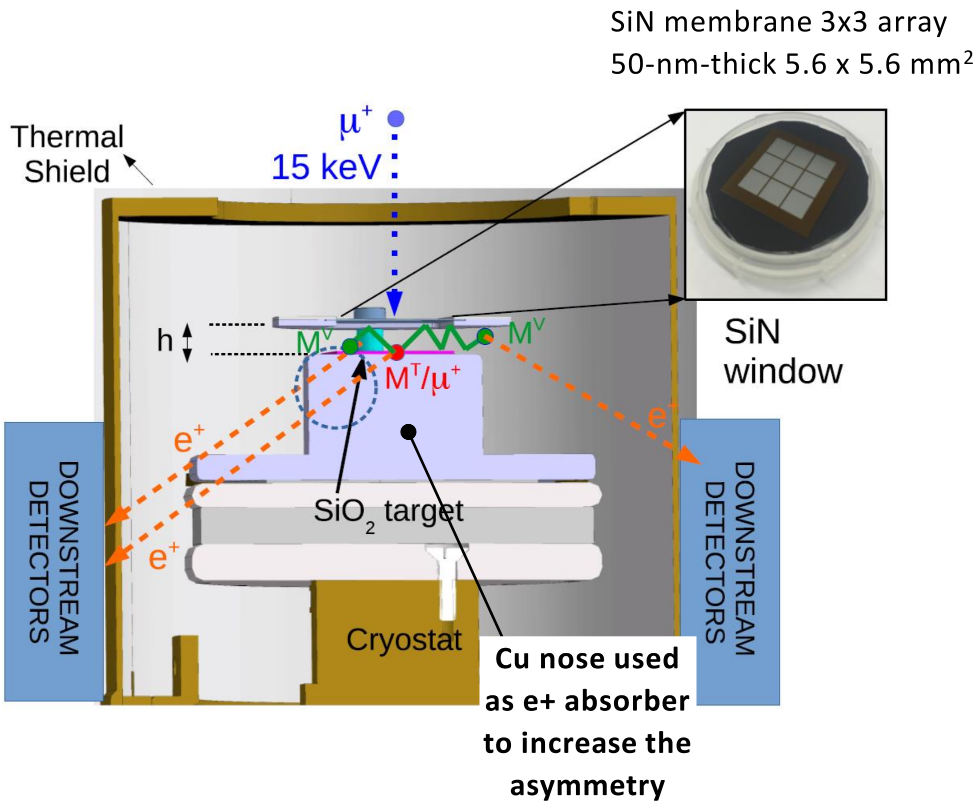

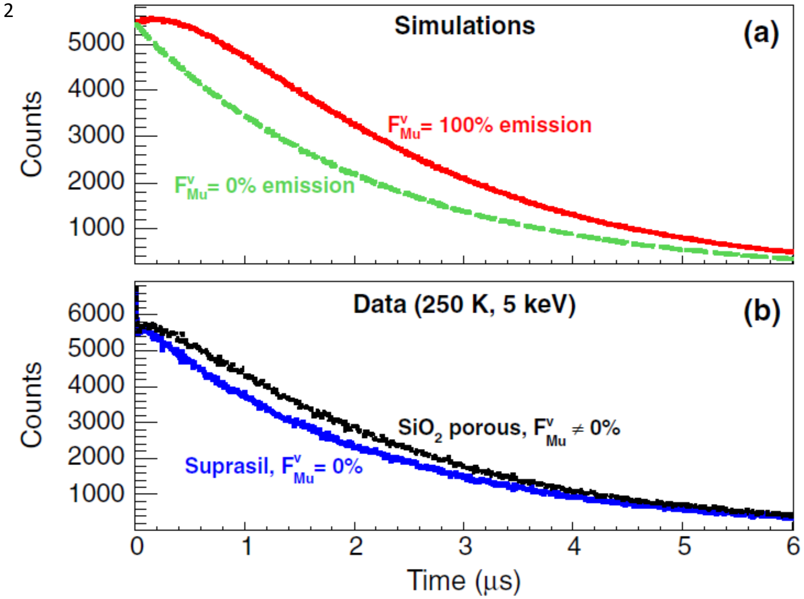

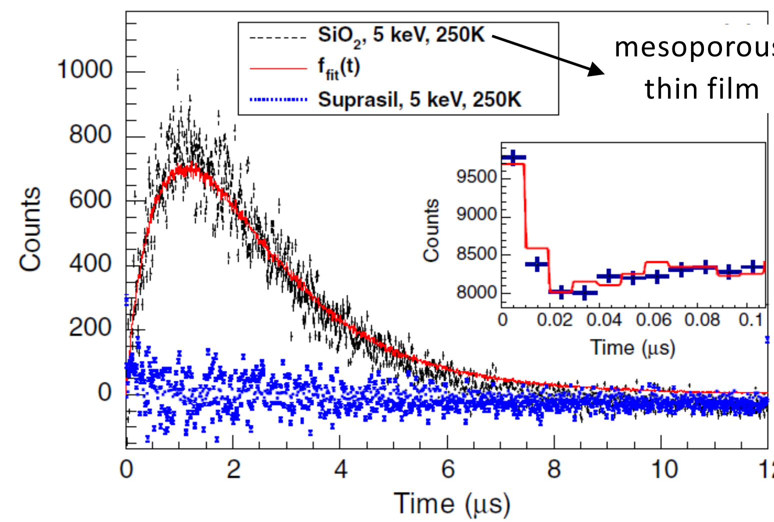

- 2 times higher Mu yield at RT
- High Mu yield also at low-T, important for the 1s-2s experiment

A. Antognini, *et al.* PRL **108**, 143401 (12).
K.S. Khaw, *et al.* PRA **94**, 022716 (16).

Unusual Strong Proximity Effect in PBCO/YBCO Heterostructures

„Classical“ SC/Metal Proximity Effect:

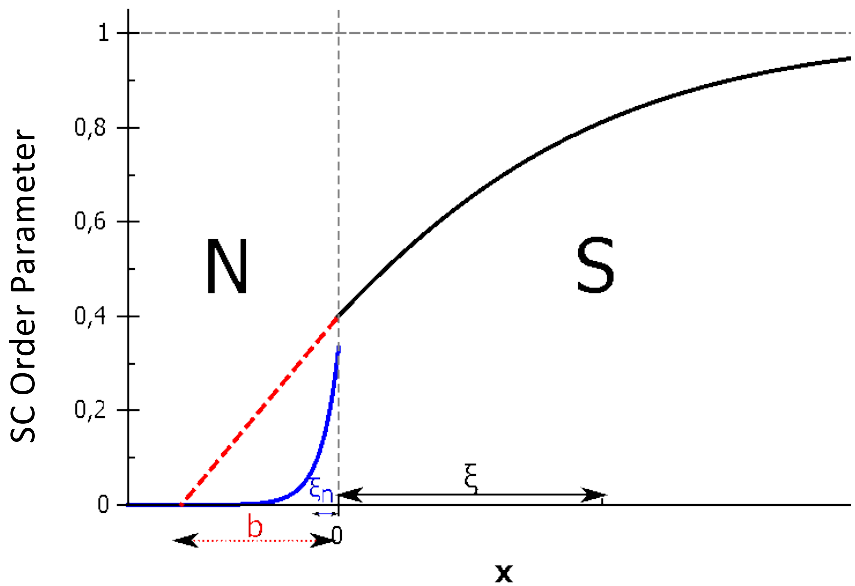

$$l \ll \xi_n$$

$$\xi_n = \sqrt{\frac{\hbar v_F l}{6\pi k_B T}} = \sqrt{\frac{\hbar D}{2\pi k_B T}}$$

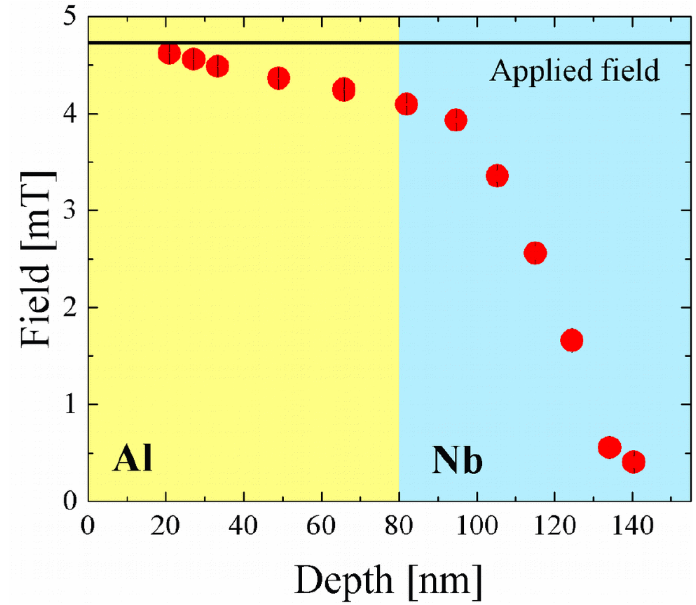

- Nearly linear decrease of the field due to the proximity effect.
- The field shift is always diamagnetic.

P.G. De Gennes, Rev. Mod. Phys. **36**, 225 (1964).

E. Morenzoni, *et al.* unpublished

Unusual Strong Proximity Effect in PBCO/YBCO Heterostructures

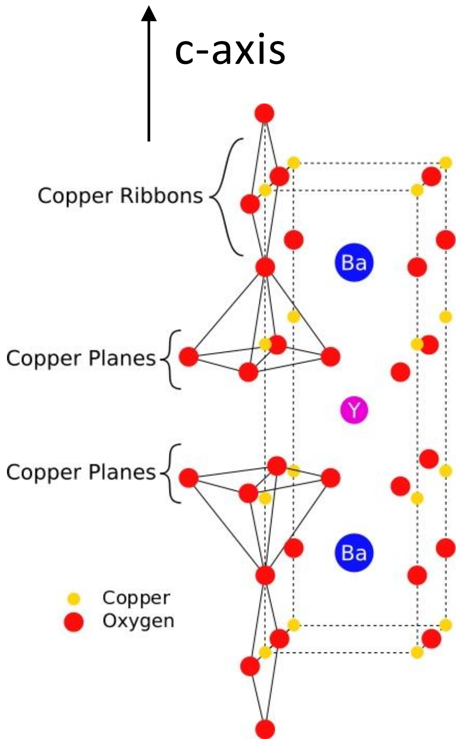

$YBa_2Cu_3O_7$: Superconductor $T_c \approx 90K$

$PrBa_2Cu_3O_7$: "Semiconducting" Antiferromagnet $T_N \approx$ RT

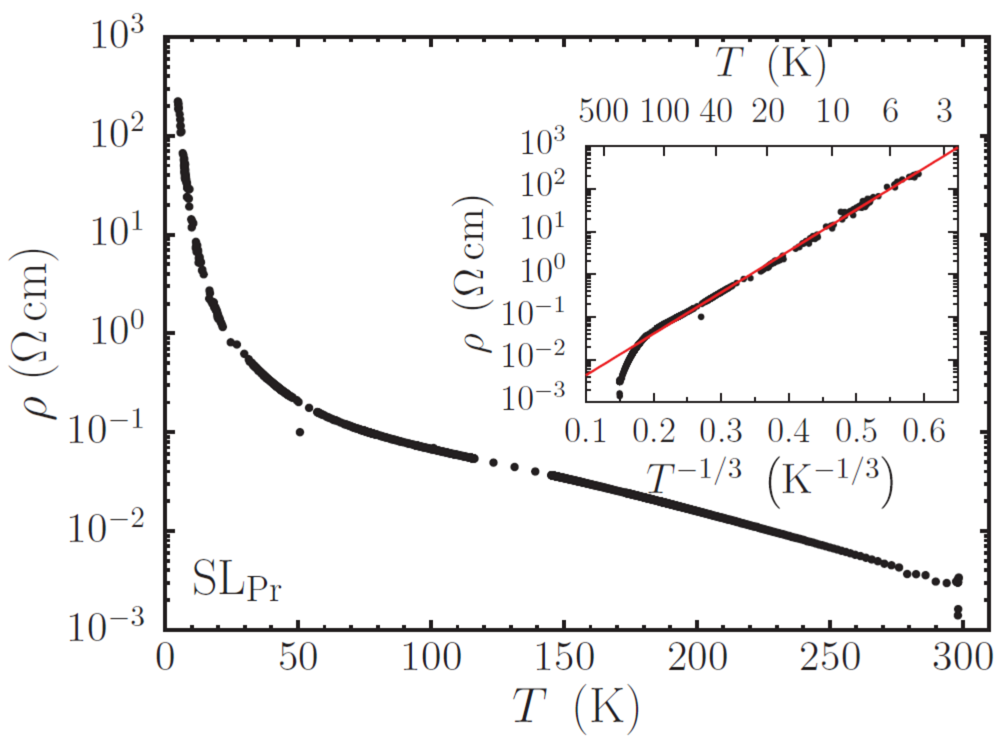

B.M. Wojek, *et al.* PRB **85**, 024505 (12).

PAUL SCHERRER INSTITUT

Unusual Strong Proximity Effect in PBCO/YBCO Heterostructures

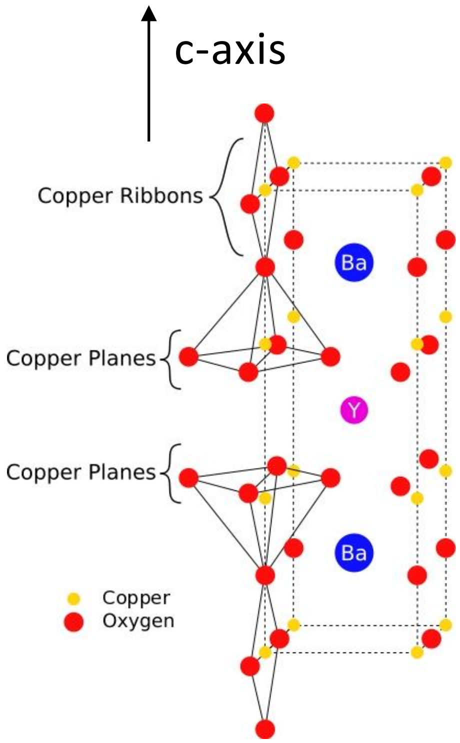

$YBa_2Cu_3O_7$: Superconductor $T_c \approx 90K$

$PrBa_2Cu_3O_7$: “Semiconducting” Antiferromagnet $T_N \approx RT$

Thin film	Constituents	Layer thicknesses (nm)
SL_Y	Au/YBCO	4/200
SL_{Pr}	Au/PBCO	4/45
TL	Au/YBCO/PBCO/YBCO	4/70/45/75
$BL_{Y/Pr}$	YBCO/PBCO	70/75
$BL_{Pr/Y}$	PBCO/YBCO	70/75

B.M. Wojek, *et al.* PRB **85**, 024505 (12).

PBCO Properties

ZF Spectra

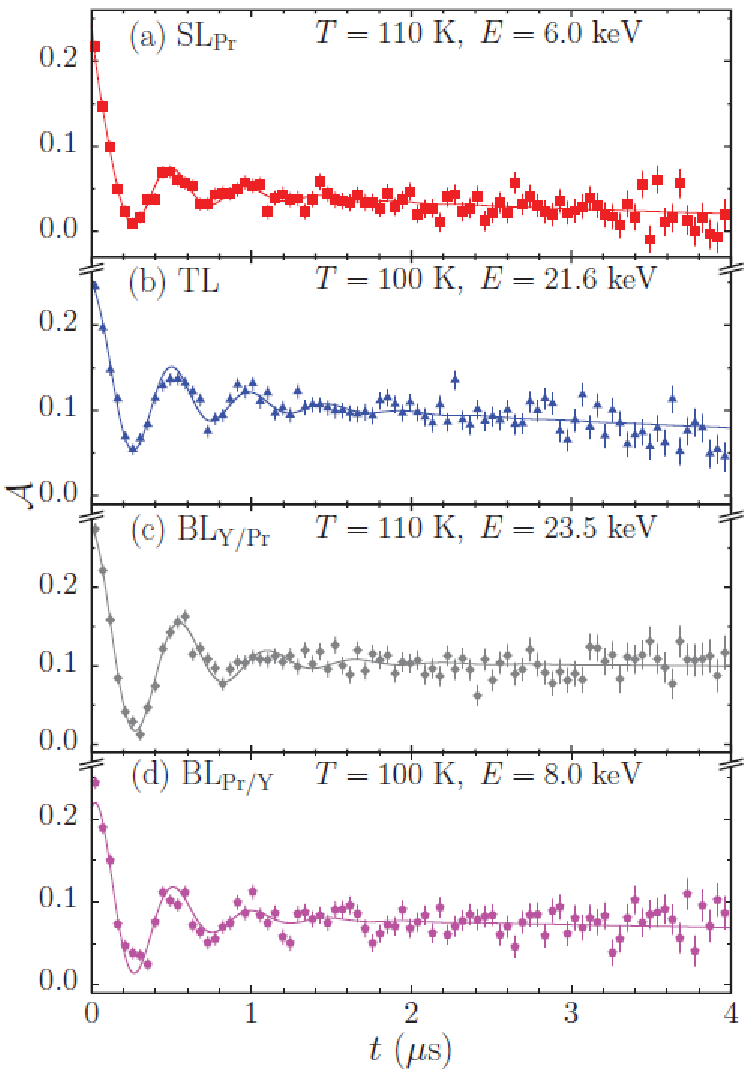

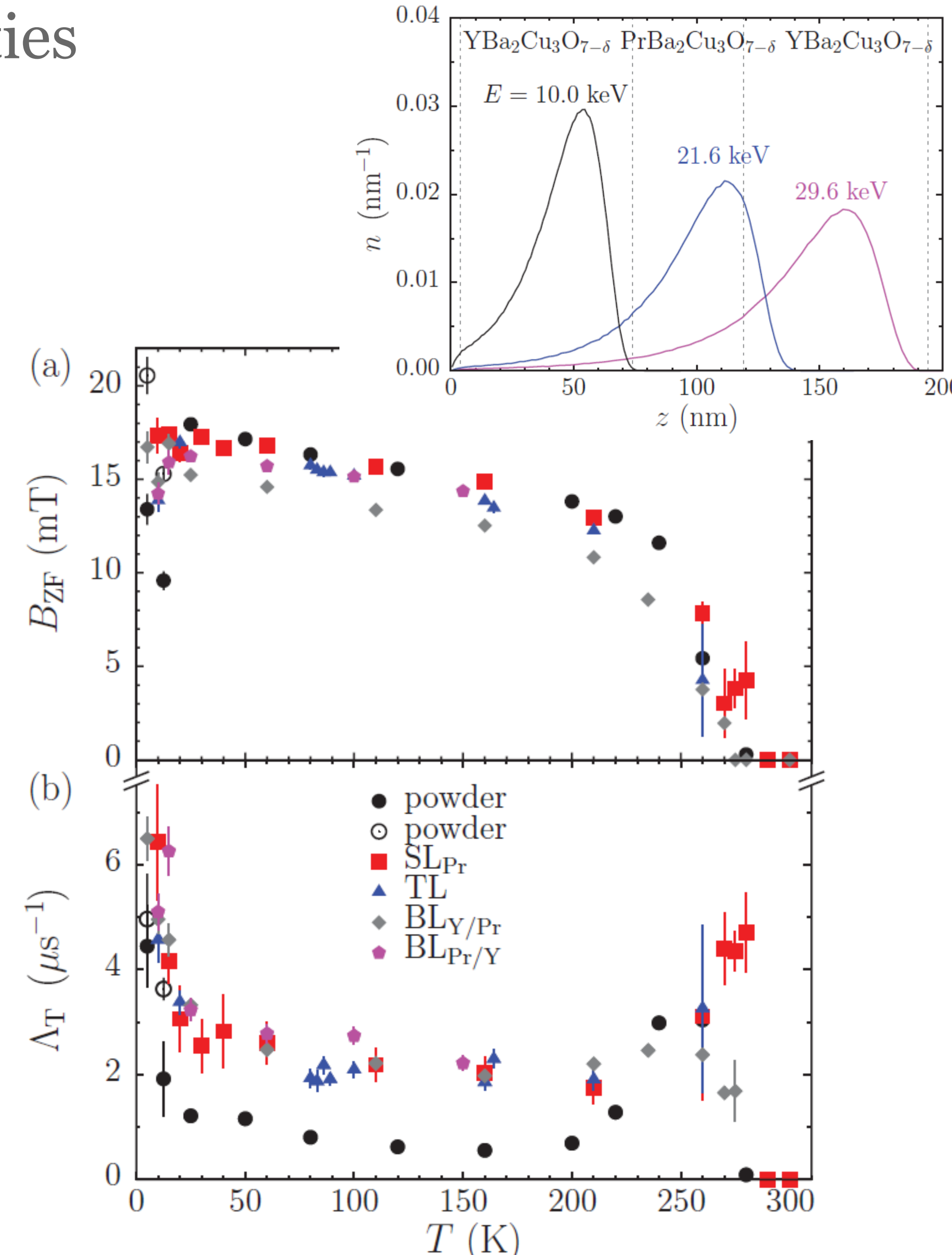

B.M. Wojek, *et al.* PRB **85**, 024505 (12).

PAUL SCHERRER INSTITUT PSI

Unusual Strong Proximity Effect in PBCO/YBCO Heterostructures

PBCO fully insulating

TL
Au/YBCO/PBCO/YBCO
4/70/45/70 nm

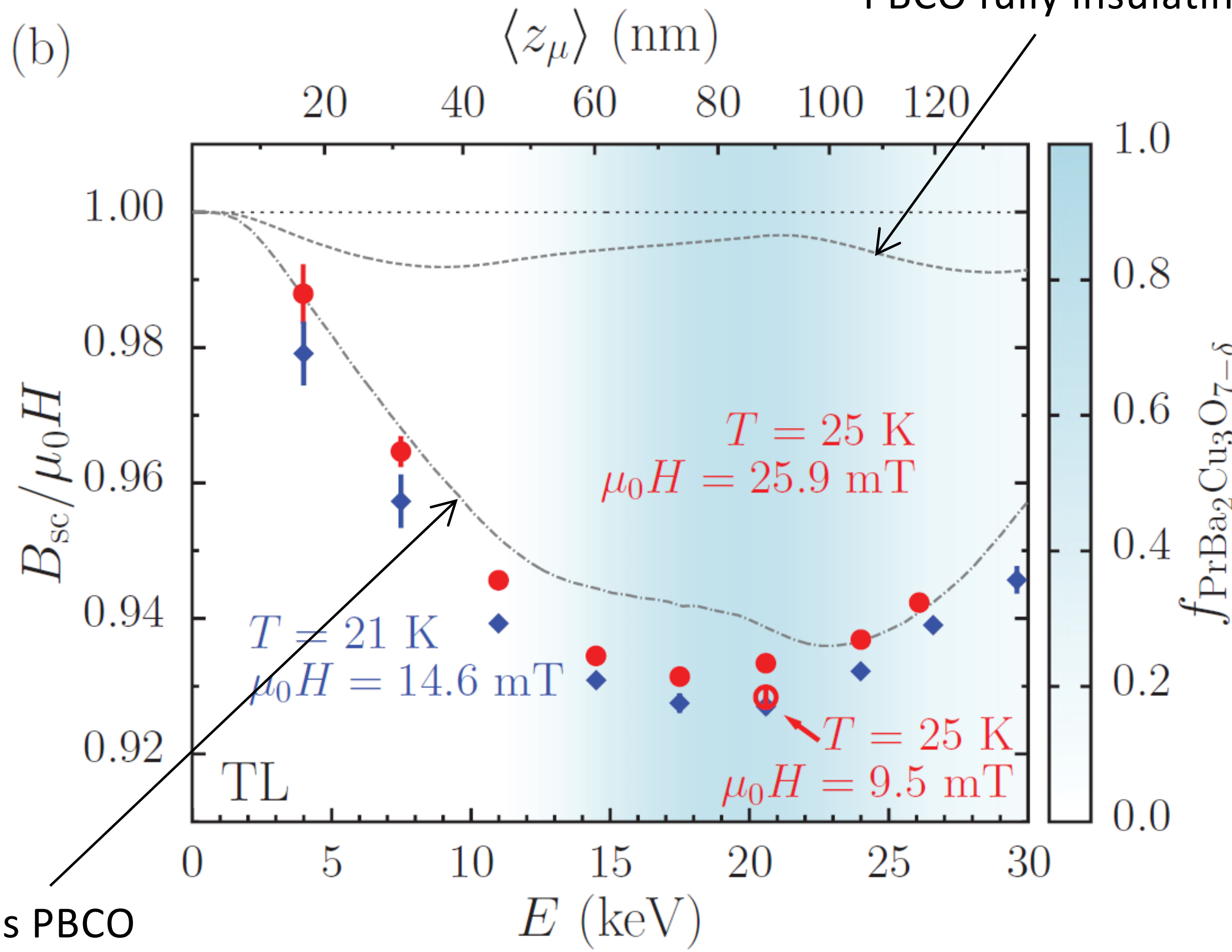

shorts accross PBCO

B.M. Wojek, *et al.* PRB **85**, 024505 (12).

Unusual Strong Proximity Effect in PBCO/YBCO Heterostructures

YBCO only SC:
λ_{YBCO}=160(20)nm

BL
YBCO/PBCO
70/75 nm

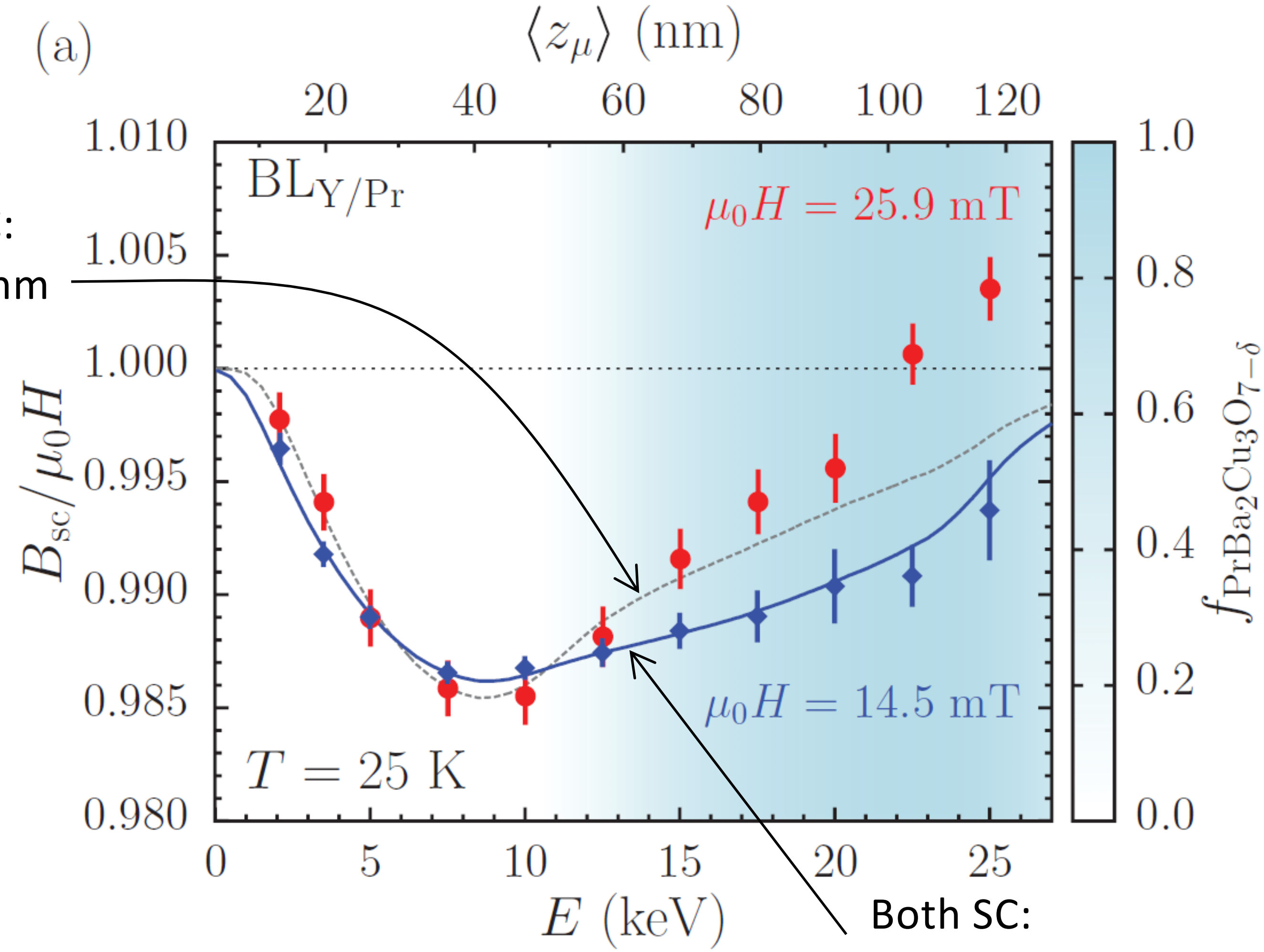

Both SC:
λ_{YBCO}=210(20)nm
λ_{PBCO}=740(50)nm

B.M. Wojek, *et al.* PRB **85**, 024505 (12).